5-2014

DEVELOPMENT OF A MULTI-PURPOSE AUTOMATED SYNTHESIS MODULE FOR PRODUCTION OF NOVEL PET RADIOPHARMACEUTICALS

I Hong Shih

DEVELOPMENT OF A MULTI-PURPOSE AUTOMATED SYNTHESIS MODULE FOR PRODUCTION OF NOVEL PET RADIOPHARMACEUTICALS

by

I Hong Shih, M.S.

APPROVED:

_____

David J Yang, Ph.D.

_____

Franklin C Wong, JD, M.D., Ph.D., MBA

_____

Wendy A. Woodward, M.D., Ph.D.

_____

Zhongxing Liao, M.D.

_____

Osama R Mawlawi, Ph.D.

APPROVED:

_____

Dean, The University of Texas

Graduate School of Biomedical Sciences at Houston

DEVELOPMENT OF A MULTI-PURPOSE AUTOMATED SYNTHESIS MODULE FOR PRODUCTION OF NOVEL PET RADIOPHARMACEUTICALS

A
DISSERTATION

Presented to the Faculty of
The University of Texas
Health Science Center at Houston
and
The University of Texas
MD Anderson Cancer Center
Graduate School of Biomedical Sciences
in Partial Fulfillment
of the Requirements
for the Degree of

DOCTOR OF PHILOSOPHY

by

I Hong Shih, M.S.

Houston, Texas

May 2014

ACKNOWLEDGEMENTS

I would like to acknowledge my advisor, Dr. David J. Yang, for his support and guidance my graduate study over years. Moreover, I have benefited a lot from his mentoring, both professionally and personally. He also introduced me to a group of great people who became my academic committee members, Dr. Osama R Mawlawi, Dr. Franklin C Wong, Dr. Wendy A. Woodward, Dr. Zhongxing Liao, Dr. Edmund E Kim, and Dr. Firas Mourtada. All of these distinguished scientists and physicians provided invaluable advice on my research project and presentation skills. I would like to thank Don Davis and Richard Thornton for the help of the hardware accomplishment, and Dr. Michael A. K. Liebschner who provided his lab in VA hospital for me to manufacture another automated module from the concept to a prototype. Furthermore, I would like to extend my sincere thanks to everyone in Dr. Yang's lab and in our department. Particularly, Dr. Yinhan Zhang and Dr. Mohammad S Ali, who taught me the chemical synthesis of my compounds; Dr. Fanlin Kong and Richard Mendez, who taught me the wet lab techniques; Dong-Fang Yu, who always helped me with my animal studies. In addition, I am greatly appreciative of all the faculty and staff at the University Of Texas Graduate School Of Biomedical Sciences. They are always available and helpful when I need their help.

Last but not least, I would like to thank my parents, Lin-Lin Hong, and Shin-Lin Shih, for the unconditional love and support. I also appreciate all my friends' help and

encouragements alone the way, especially for Wen I Lee, and Allen Shih. Without all of you, I can’t have done this.

DEVELOPMENT OF A MULTI-PURPOSE AUTOMATED SYNTHESIS MODULE FOR PRODUCTION OF NOVEL PET RADIOPHARMACEUTICALS

I Hong Shih, Ph.D.

Advisory Professor: David J. Yang, Ph.D.

Among radiopharmaceuticals of positron emission tomography (PET), ^{18}F-Fluorodeoxyglucose (^{18}F-FDG) made from commercialized automated synthesis module is the most frequently used in tumor diagnoses. But the false positive findings, such as infectious tissues and post-operative surgical conditions, show strong uptake of ^{18}F-FDG in PET scans which requires extra clinical procedures to confirm the results. Moreover, the false negative findings, such as low glycolytic activity tumors, reduce the accuracy of PET scans. Therefore, there will be new PET radiopharmaceuticals to redeem the defects of ^{18}FDG-PET applications.

Current commercialized automated synthesis modules are suitable for clinical use, but researchers are difficult to modify these modules to synthesize their own radiopharmaceuticals. In this study, we developed a multi-purpose automated synthesis module for production of novel PET radiopharmaceuticals, such as gallium-68-ethylenedicysteine-glucosamine (^{68}Ga-ECG), [^{18}F]fluoropropyl-α-methyltyrosine (^{18}F-

FPAMT), and [^{18}F]fluoro-5-propylhydroxy tryptophan (^{18}F-FTP). The specifications of this module are the flexibility for editing synthesis recipes, the stable integration of its hardware and software, the rapid heating process, and the friendly user interface. The synthesis steps of nonradioactive standards for these three radiopharmaceuticals were developed, and the chemical structures and purities of nonradioactive references were confirmed. Then, the manual synthesis recipes of radiopharmaceuticals were followed the synthesis recipes of nonradioactive standards, and the yields and radiochemical purities of these radiopharmaceuticals were demonstrated in an acceptable range. Last, the manual synthesis recipes of these drugs were transformed to the automated synthesis recipes which can be practiced in this multi-purpose automated synthesis module.

The results showed this automated module is capable of synthesizing different radiopharmaceuticals. The pH value and radiochemical purity of automated synthesis are as good as the manual synthesis. Although the yields of automated syntheses are lower than the manual syntheses, the flexible functions of this module provide the opportunity for optimization of automated synthesis methods.

Table of Contents

LIST OF FIGURES

LIST OF TABLES

ABBREVIATIONS

^{11}C	carbon-11
^{13}N	nitrogen-13
^{15}O	oxygen-15
^{18}F	fluorine-18
^{18}F-FDG	[^{18}F]-fluorodeoxyglucose
^{18}F-FLT	[^{18}F]-fluoro-3'-deoxy-3'-L: -fluorothymidine
^{18}F-FMISO	[^{18}F]fluoromisonidazole
^{18}F-FMTEB	[^{18}F]3-fluoro-5-[(2-methyl-1,3-thiazol-4-yl)ethynyl]benzonitrile
^{18}F-FPAMT	[^{18}F]fluoro-propyl-α-methyltyrosine
^{18}F-FTHA	14(R,S)-[^{18}]F-fluoro-6-thia-heptadecanoic acid
^{18}F-FTTP	[^{18}F]fluoro-5-propylhydroxy tryptophan
^{18}F-NaF	[^{18}F] sodium fluoride
6-^{18}F-FDOPA	3,4-dihydroxy-6-[^{18}F]-fluoro-L-phenyl- alanine
^{64}Cu	Copper-64
^{68}Ga	Gallium-68
^{68}Ga-DOTATOC	^{68}Ga-DOTA-D-Phe1-Tyr3-octreotide
^{68}Ga-ECG	gallium-68-ethylenedicysteine-glucosamine
^{68}Ge	Germanium-68
^{82}Rb	rubidium-82
^{82}Sr	strontium-82
$((Boc)_2O$	ditertbutyl dicarbonate

BOC	butoxycarbonyl
cGMP	current Good Manufacturing Practice
CT	computed tomography
DCC	N,N-di-cyclohexylcarbodiimide
DMAP	4-dimethylaminopyridine
DMF	dimethyl formamide
DMSO	dimethyl sulfoxide
DOTATOC	DOTA-D-Phe1-Tyr3-octreotide
ECG	ethylenedicysteine-glucosamine
FDA	Food and Drug Administration
FTP/Boc/Ester	N-Boc-fluoropropoxytryptophan methyl ester
G-$(Ac)_4$	1,3,4,6-tetra-O-acetyl-2-amino-α-D-glucopyranose hydrochloride
HPLC	high-performance liquid chromatography
IUPAC	International Union of Pure and Applied Chemistry
MRI	magnetic resonance imaging
VISA	virtual instrument software architecture
NMR	nuclear magnetic resonance
PET	positron emission tomography
SA	specific activity

SPECT	single-photon emission computed tomography
TEA	triethanolamine
TLC	thin layer chromatography
Tso-PAMT/BOC/Ester	N-t-butoxycarbonyl-O-[3-tosylpropyl]-α-methyl tyrosine ethyl ester
Tso-TP/BOC/Ester	N-Boc-tosylpropoxytryptophan methyl ester
US	ultrasound imaging
VI	virtual Instrument

1 Chapter 1 Introduction

1.1 Introduction of molecular imaging

Molecular imaging is an emerging field which targets to visualize biological and biochemical events in the molecular level of living subjects without invasive methods(1). Molecular imaging, such as positron emission tomography (PET), and single-photon emission computed tomography (SPECT), uses different types of energy and the acquisition equipment for various applications(2-4). Other medical imaging techniques without specific molecular targets, such as magnetic resonance imaging (MRI), ultrasound imaging (US), and computed tomography (CT), can provide better spatial resolution for structural imaging and detect anatomical changes for specific diseases(5-7). The comparisons of medical imaging modalities are listed in Table 1.1. A SPECT scan uses a gamma camera that rotates around the patient to detect the distribution of a radiotracer in the body. SPECT has acceptable penetration depth, but its deficiency is limited in spatial resolution which restricts its usages in molecular imaging(8). A PET scan is a three-dimensional image coming from reconstructing the data of numerous detections of pair photons which are produced from annihilation of radiotracers in the living subject(9). PET is suitable for oncology imaging because of its high sensitivity, sufficient depth penetration and better spatial resolution than SPET. PET and SPECT combined with CT can provide detail information on the anatomy and the function of organs and tissues (10, 11). Other experimental molecular imaging technologies, such as fluorescence imaging, and bioluminescence imaging, can provide high sensitive images

by selection of proper imaging probes, but it is limited in the penetration of tissue depth(1).

Table 1.1 Comparisons of Imaging Technologies

Imaging Technology	Limitation of Spatial Resolution (mm)	Detection Limitation of Tracer/Contrast Material Concentration (mol/kg)
MRI	1.0	10^{-5}
CT	0.3	10^{-3}
US	0.3 (5 MHz)	Difficult quantitative by contrast material
SPECT	7	10^{-8}~10^{-10}
PET	3	10^{-9}~10^{-12}

1.2 Principle of PET radiopharmaceuticals

A radiopharmaceutical is a radiochemical whose chemical substance has radioactive atoms, and it is administrated safely to humans and animals for diagnosis or therapeutic effect by U.S. Food and Drug Administration (FDA) regulations. In oncology, diagnosis radiopharmaceuticals can interact with various biomarkers which can be linked to different biological processes of tumor progression, including cell proliferation,

metabolism, cell migration, receptor expression, hypoxia, and angiogenesis(12-17). The labeling methods of radiopharmaceuticals can be described as the radioisotopic labeling(18) and the structure modifications of its original molecular. The definition of radioisotopic labeling is the replacements of a stable atom in a chemical compound with its radioisotope without modification its original structure. The radioisotopic-labeling chemical is suitable for applications because it shares identical chemical and biological properties of its original molecular. Hydrogen, carbon, nitrogen, oxygen, phosphorus, sulfur, and fluorine are the basic atoms in structures of pharmaceuticals, but radioisotopic-labeling of these atoms is limited to decay-mode, half-life, and synthesis methods(18). Only carbon-11 choline, carbon-14 urea, and fluorine-18 sodium fluoride are FDA-approved radioisotopic labeling radiopharmaceuticals(19). The other synthesis method of radiopharmaceuticals is to label a radioisotope to the target chemicals within modifications of its original structure, and often slightly changes the chemical or biological properties of the original molecular(18). These perturbations may be deleterious or advantageous for applications(20). However, the structure modification method provides more options for synthesis of radiopharmaceuticals. Besides FDA-approved radioisotopic radiophamaceuticals, other FDA-approved radiopharmaceuticals, such as fluorine-18 fluorodeoxyglucose (^{18}F-FDG) and technetium-99m pentetate, are radio-nonisotopic labeling radiopharmaceuticals. FDA-approved PET radiopharmaceuticals and clinical indications are shown in Table 1.2.

Table 1.2 FDA-Approved PET Radiopharmaceuticals

Name	Approved Clinical Indications
Carbon-11 Choline	Carbon-11 choline injection is indicated for PET imaging of patients with suspected prostate cancer recurrence and non-informative bone scintigraphy, CT or MRI. Suspected prostate recurrence is based upon elevated blood prostate specific antigen (PSA) levels following initial therapy.
Fluorine-18 Florbetapir (Amyvid)	Fluorine-18 florbetapir is indicated for PET imaging of the brain to estimate β-amyloid neuritic plaque density in adult patients with cognitive impairment who are being evaluated for Alzheimer's Disease (AD) and other causes of cognitive decline.
Fluorine-18 Sodium Fluoride	Fluorine-18 sodium fluoride is PET bone imaging agent to delineate areas of altered osteogenesis
Fluorine-18 Fludeoxyglucose	Fluorine-18 fludeoxyglucose is indicated in PET imaging for assessment of abnormal glucose metabolism to assist in the evaluation of malignancy in patients with known or suspected abnormalities

	found by other testing modalities, or in patients with an existing diagnosis of cancer.
Nitrogen-13 Ammonia	Nitrogen-13 ammonia is indicated for diagnostic PET imaging of the myocardium under rest or pharmacologic stress conditions to evaluate myocardial perfusion in patients with suspected or existing coronary artery disease.
Rubidium-82 Chloride	Rubidium-82 chloride is PET myocardial perfusion agent that is useful in distinguishing normal from abnormal myocardium in patients with suspected myocardial infarction.

1.2.1 The selection of PET radioisotopes

A nuclide is a combination of protons, neutrons, and its nuclear energy in a nucleus of an atom. Unstable nuclides, called radionuclides, transform to nuclides by emitting radiations, such as α particles, β- particles, β+ particles, electron capture, and isomeric transition. Radionuclide with an excess proton may have positron decay where the proton is converted into a neutron, a positron (β+ particles), and a neutrino. When a

positron interact an electron of an atom in a matter, both particles will annihilated to produce two 511 keV photons with opposite directions (180°) at the same time. Detection of the two photons in coincidence by detectors is the basis of PET(9).

Commonly used PET imaging radionuclides and their characters are listed in Table 1.3. These radioisotopes can be produced from either a cyclotron, like ^{11}C, ^{13}N, ^{15}O, ^{18}F, and ^{64}Cu or in a generator, like $^{68}Ge/^{68}Ga$ and $^{82}Sr/^{82}Rb$. Because carbon, nitrogen, and oxygen are the major atoms of organic compounds, ^{11}C, ^{13}N, and ^{15}O are ideal radionuclides for radioisotopic labeling. However, the positron path of these radionuclides is longer than the path of ^{18}F (Max: 0.02 cm in water) which is similar to the resolution of current PET camera. In addition, these PET isotopes with particulate short half-life, such as ^{11}C, ^{13}N, and ^{15}O, lose major radioactivity when these isotopes are transferred to remote PET imaging centers without a built-in cyclotron. Generally, radiopharmaceuticals with these radioisotopes are difficult practiced in remote PET imaging centers or research facilities if the transport time is over twice of half-life of these radioisotopes.

Table 1.3 Suitable Radionuclides for PET Imaging

Radionuclide	Source	β+(MeV)	Half-life
^{11}C	cyclotron	0.959	20 minutes
^{13}N	cyclotron	1.197	9.97 minutes

^{15}O	cyclotron	1.738	2.03 minutes
^{18}F	cyclotron	0.635	110 minutes
^{124}I	cyclotron	2.13	4.2 days
^{68}Ga	generator	1.9	68 minutes
^{64}Cu	cyclotron	2.91	12.8 hours
^{82}Rb	generator	3.15	76 seconds

Besides PET radioisotopes produced by a cyclotron, generator-produced radioisotopes, such as $^{68}Ge/^{68}Ga$ and $^{82}Sr/^{82}Rb$, are alternative sources of PET radionuclide for a remote imaging facility because a generator is much cheaper and more compact than a cyclotron. The extra short half-life of ^{82}Rb is not suitable for evaluation of biological events in the living organs. Therefore, ^{18}F and ^{68}Ga were selected as target radionuclides for automated radiopharmaceuticals synthesis in this project.

1.3 Radiochemistry of PET radiopharmaceuticals: Fluorine 18 and Gallium 68

Radiochemistry is defined as "the chemical study of radioactive elements, both natural and artificial, and their use in the study of chemical processes"(21). Other than

chemistry, there is a very unique aspect in radiochemistry, infinitesimal reaction quantities of radioactive elements with high outcomes in applications. For example, the average dosage of ^{18}F-FDG for a patient is 10mCi, and this dose contains only 10^{-10}g of fluorine-18. The reaction rate of chemical process is affected by concentrations of reagents, reaction orders, pressure, temperature, solvent, catalyst, and reaction surface area(22). Among these factors, concentrations of reagents and reaction orders have the major impact on the reaction rate of the radiochemical process because of the infinitesimal reaction quantities of radioactive elements.

For radiochemical procedures, ultra-small quantities of radioisotopes are difficult to manipulate because they are easily lost by adherence to the container wall, and filters. Chemists sometimes use the chemically identical material, the stable form of the radioisotope, which is added into the reaction for decreasing the loss of radioisotope by occupying these spaces. Or chemists use the carrier which can carry radioisotope in the chemical reactions. The definition of carrier in Gold Book of the International Union of Pure and Applied Chemistry (IUPAC) is “A substance in appreciable amount which, when associated with a trace of a specified substance, will carry the trace with it through a chemical or physical process”. In addition, carrier-added radiochemical process can decrease the loss of the radioactivity during synthesis by increasing the reaction rate. Except for the zero order reaction, reaction rates in higher order reactions can rise by increasing concentrations of reagents. However, specific activity (SA) of radiotracers is

lower by these non-radioactive carries which can easily saturate low density target receptors and decrease the sensitivity of applications. The definition of SA in the Gold Book of IUPAC is “For a specified isotope, or mixture of isotopes, the activity of a material divided by the mass of the material”. To avoid the decreasing of SA, no-carrier added methods are developed for radiochemical synthesis.

1.3.1 Radiochemistry of Fluorine-18

By using particular nuclear reactions, target materials, and beam energy, current cyclotrons can produce two different forms of fluorine-18, $[^{18}F]F_2$(23) and $[^{18}F]F^-$(24). $[^{18}F]F_2$ is the gas phase which is used for electrophilic substitution(25); $[^{18}F]F^-$ is in the liquid phase which is used for nucleophilic substitution(26).

1.3.1.1 Electrophilic Fluorination

Because $[^{18}F]F_2$ is extremely corrosive and reactive gas which causes non-selective reactions, it is difficult to be manipulated correctly in chemical procedures. After adding carriers, such as xenon and ammonium acetate, $[^{18}F]F_2$ is transferred into less reactive and more selective fluorinated agents, like xenon difluoride(27), and acetyhypofluorite(28) (Figure 1.1).

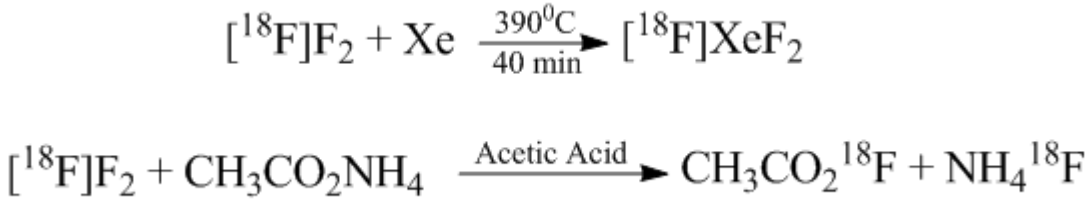

Figure 1.1 Preparations of electrophilic fluorination reagents

These fluorinated-carriers are used to transfer fluorine ions to electron-rich substrates, such as carbanions and aromatic compounds (Figure 1.2) (29), which can't be directly fluorinated by nucleophilic methods. Due to carrier-added reactions, electrophilic fluorination has low specific activity which limited its usage in some applications. In addition, side products are produced during carrier fluorination. To overcome this problem, some reactive groups of the target chemicals are protected from fluorination to improve labeling-efficiency of fluorinated carriers(30).

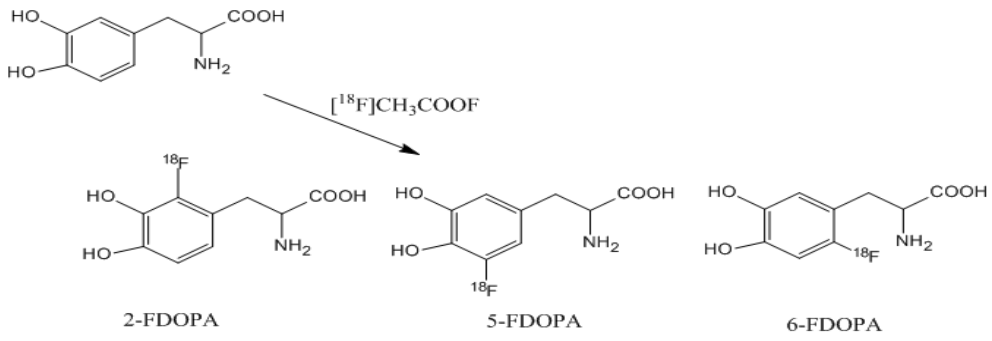

Figure 1.2 Electrophilic syntheses of 6-[^{18}F] FDOPA

1.3.1.2 Nucleophilic Fluorination

Not only production of corrosive F_2 for electrophilic fluorination, a cyclotron can produce radioactive fluoride ions from irradiation of O-18-enriched water for

nucleophilic fluorination which is a no-carrier added synthesis method(31). [^{18}F]F^- is quite unreactive in aqueous form, and it needs certain procedures to increase its nucleophilicity. After irradiation of O-18-enriched water, radioactive fluoride anions are easily to form alkaline metal fluoride (potassium fluoride, cesium fluoride, or silver fluoride), and hydrogen fluoride. In order to remove impurities, the aqueous fluoride solution is loaded through anion exchange resins which can trap fluoride. After that, phase transfer catalysts in aprotic dipolar solvent, such as potassium/Krytofix 222 in acetonitrile or tetraalkylammonium salts in dimethylformamide, are loaded through the resins to capture [^{18}F]fluoride ions. During this procedure, the bases, potassium oxalate or potassium carbonate, are added with phase transfer catalysts in aprotic dipolar solvent to prevent the occurrence of hydrogen fluoride(32). Then, azeotropic distillation with acetonitrile is used several times to remove residual water for obtaining "free" or "naked" form of fluoride ion. Nucleophilic fluorination is frequently carried out because of its easy preparation and high specific activity (33-35). Methods of nucleophilic fluorination range from aromatic and aliphatic substitution.

1.3.1.2.1 Aliphatic nucleophilic substitution

Nucleophilic fluorination of aliphatic compounds is the S_N2 reaction whose reaction rate is affected by two factors, leaving groups and solvents(36). The typical

leaving groups are halogens, triflate, nosylate, tosylate, and mesylate. The typical solvents are polar aprotic solvents, such as acetonitrile, dimethyl sulfoxide, NN-dimethylformamide, NN-dimethylacetamide, tetrahydrofuran, and acetone(37). While aliphatic nucleophilic substitution can often be a one-step reaction, it is often followed by a deprotection step (38)(Figure 1.3). Except for the reaction rate, elimination of side product, such as fluorinated leaving groups, can also improve fluorination efficiency(38).

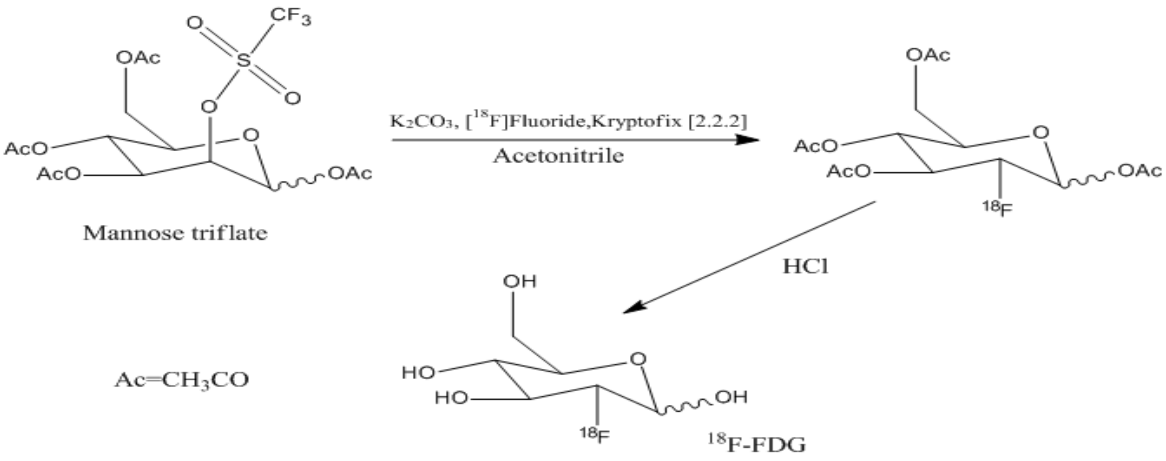

Figure 1.3 Synthesis of [^{18}F]-FDG by aliphatic nucleophilic fluorination

1.3.1.2.2 Aromatic nucleophilic substitution

This reaction requires the leaving group in the aryl ring with one electron-withdrawing group at an ortho position or a para position. The common leaving groups, listed in the order of its leaving ability, are I < Br < Cl < F < NO_2 < N^+Me_3(39). The electron-withdrawing groups, listed in the order of its activating effect, are 3-NO_2 < 4-CH_3CO < 4-CN < 4-NO_2(40). The most common solvents in this reaction are dimethyl sulfoxide, and N, N-dimethylacetamide (Figure 1.4)(41).

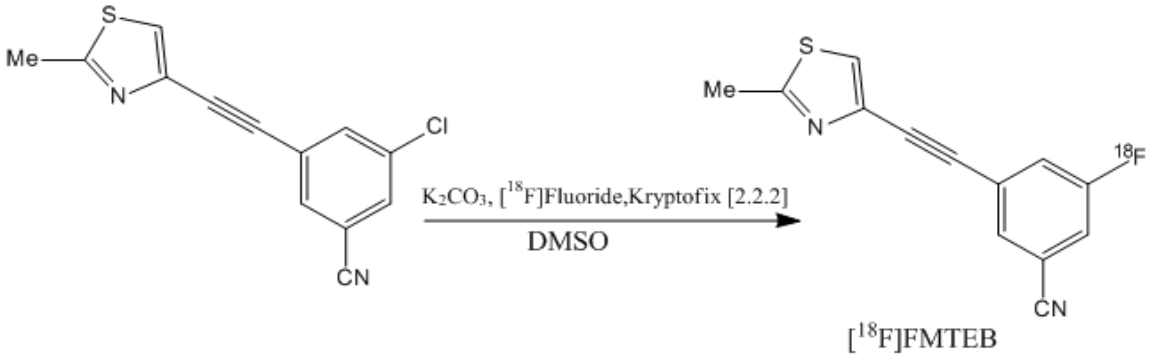

Figure 1.4 Synthesis of [^{18}F]FMTEB by aromatic nucleophilic substitution

For aromatic compounds without electron-withdrawing groups, Balz-Schiemann reaction or Wallach reaction(42) is an option for nucleophilic fluorination. However, these reactions require carriers for the preparation of fluoroboric acid. This reaction is rarely used because its low SA and radiochemical yield. For nucleophilic heteroaromatic fluorination, especially pyridines, even if there are no electron-withdrawing groups in the aromatic ring, the quantitative radiochemical yield is achieved (Figure 1.5)(35).

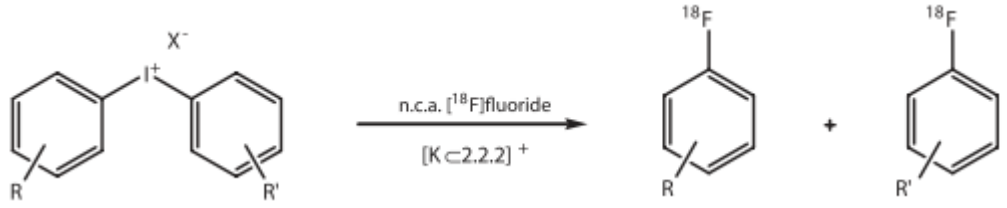

(X=Cl, Br, I, TsO, ClO_4, CF_3SO_3; R, or R′=H, Cl, Br, I, NO_2, CH_3, OCH_3)

Figure 1.5 Synthesis of [^{18}F] pyridine by nucleophilic heteroaromatic fluorination

1.3.2 Radiochemistry of ^{68}Ga

Radionuclide generators have significant research and clinical interest because they allow radioactive studies without an on-site cyclotron. Gallium-68 generators have the following advantages over other positron-emitting radionuclides generators(43). Gallium-68 is high efficiency positron emitter (89%) which is a suitable radionuclide for PET radiopharmaceuticals. In addition, ^{68}Ga has a physical half-life of 68 minutes which provides enough time-window for observing biological events. The parent isotope of ^{68}Ga generator, ^{68}Ge, has long half-life of 271 days, and this feature allows ^{68}Ga generator has long life-cycle and is available for long distance shipment. ^{68}Ga generators have organic or inorganic matrices to separate ^{68}Ge and ^{68}Ga by immobilization ^{68}Ge in the oxidation state IV+. After elution with hydrochloric acid from generators, the +3 oxidation state of ^{68}Ga is the most stable form in the acid solution. Ga^{3+} ion is a hard Lewis acid with coordination number of four to six. Chelators act as Lewis bases which provide at least two pairs of electrons to bond Ga^{3+}. The majority of chelators for Ga^{3+}

are tetradentate, pentadentate, and hexadentate ligands (44). If the chelator, besides binding the metal cation, also provides other functional groups which conjugate a targeting molecular for biological events, it is called a bifunctional chelator(45). DOTA-tris(tBu) is the monoactive bifuntional prochelator, and can be coupled to the somatostatin analogue Tyr^3-Lys^5(BOC)-octreotide. After deprotection in trifluoroacrtic acid with water, DOTA-D-Phe1-Tyr3-octreotide (DOTATOC) was ready to react with ^{68}Ga ions for constituting the coordination complexes, ^{68}Ga-DOTA-D-Phe1-Tyr3-octreotide (^{68}Ga-DOTATOC)(46). ^{68}Ga-DOTATOC demonstrates thermodynamically and kinetically stable in clinical studies, and is an octreotide analogue which can interact with somatostatin receptors for diagnosis of certain types of cancers (47-52).

1.4 Automated synthesis devices

Merrifield and Stewart proposed the first apparatus for automated synthesis of solid phase peptides in 1966(53). Following this successful and pioneer prototype, other automated systems share the same concepts for different applications, including radiosynthesis. For radiochemistry, Wolf et al first synthesized ^{18}F-FDG by electrophilic fluorination in 1976(54), and Barrio et al developed a remote, semiautomated system to synthesize ^{18}F-FDG by electrophilic fluorination in 1981(55). Before popularity and improvement of microprocessor, semiautomated and automated synthesis systems could provide limited functions for radiosynthesis, and the availability of ^{18}F-FDG produced by electrophilic fluorination is limited by its low yield. Until 1986, Hamacher et

al synthesized ^{18}F-FDG by using kryptofix 222 as a phase transfer catalyst, and this nucleophilic fluorination provided short synthesis time and high radiochemical yield(56, 57). This method improved the availability of ^{18}F-FDG, and more ^{18}F-FDG researches were carried out, especially in oncology (58-62). After FDA approvals of clinical usages for ^{18}F-FDG in tumor glucose metabolism in 2000, there are strong demands for the usage of ^{18}F-FDG automated synthesizers in clinics.

Current common commercially available automated synthesis modules for production of ^{18}F-FDG are Explora FDG_4 (Siemens Healthcare, Malvern, PA, USA), FASTlab/TRACERlab (GE Healthcare, Wauwatosa, WI, USA), FDG-Plus Synthesizer/Modular-Lab (Eckert & Ziegler, Valencia, CA, USA), Synthera (IBA Molecular, Dulles, VA, USA), and NanoTek (Advion, Ithaca, NY, USA). All these modules provide the reproducibility and acceptable yield of ^{18}F-FDG, even if design concepts are slightly different. The design concept of Explora FDG_4, TRACERlab, and FDG-Plus Synthesizer are the integration of equipment which is more close to the pioneer prototype made by Merrifield and Stewart(53). There are commercially available ^{18}F-FDG kits for these modules include syringes, vials, tubes, needles, and chemicals. Other modules, like FASTlab, Synthera, and NanoTek, integrate functions of these items into a single-use cassette or a microfluidic chip in order to increase the yield of ^{18}F-FDG and minimize the size of the module. Modular-Lab is a fully user-defined system which is assembled by various valves, sensors and other equipment, and this type of design can increase its flexibility for different methods of radiosynthesis. Besides modules for synthesis of ^{18}F-

FDG by nucleophilic fluorination, these companies developed other modules and kits for electrophilic fluorination, and other radioisotopes, such as ^{11}C, ^{13}N, ^{15}O, and ^{68}Ga. These commercial automated synthesizers are listed in Table 1.4.

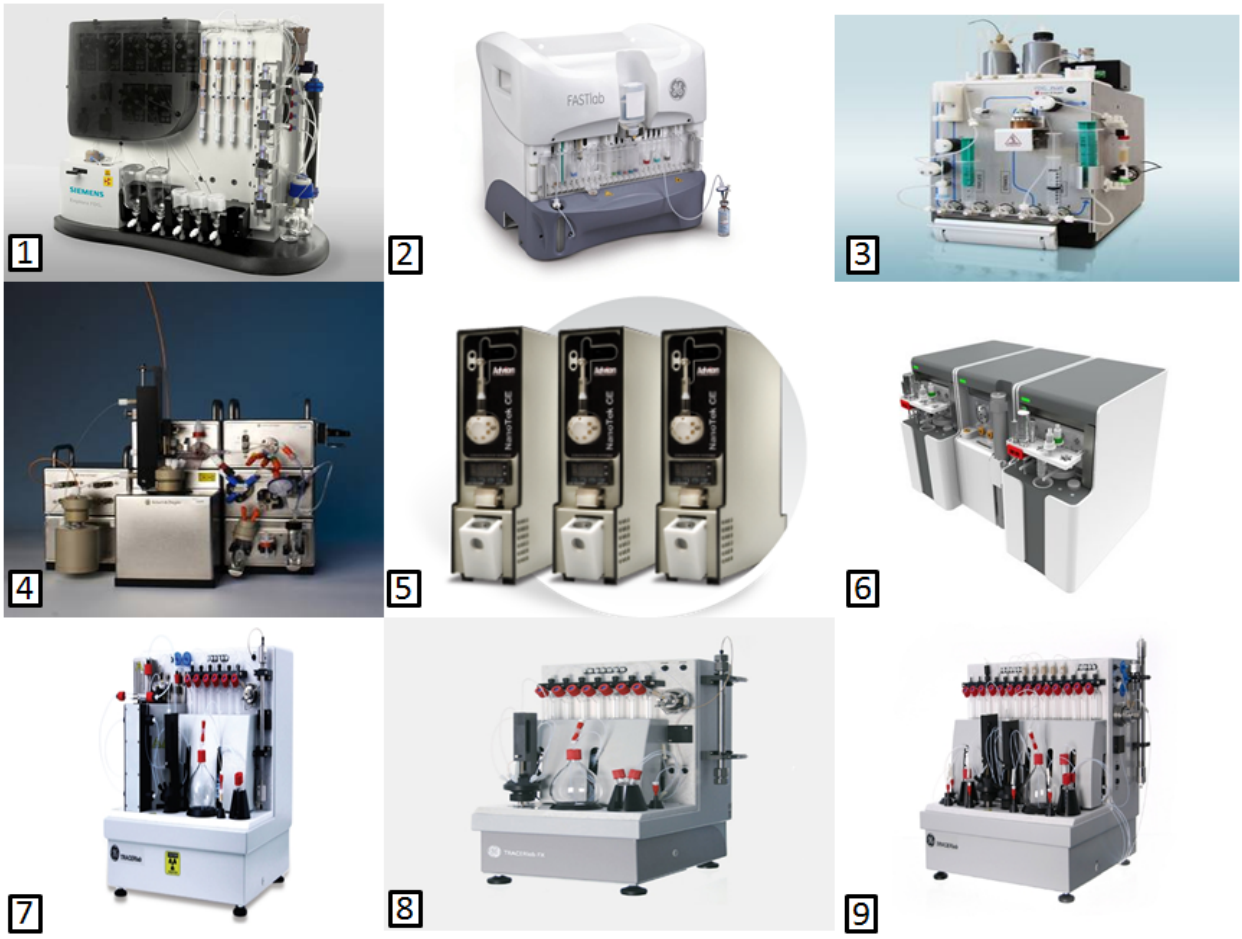

Figure 1.6 Images of common commercialized synthesis modules. 1: Explora FDG_4; 2:Fastlab; 3:FDG-Plus; 4:Modular-lab; 5:NanoTek; 6:Synthera; 7: TRACERlab FX C Pro; 8: TRACERlab FX E Pro; 9: TRACERlab FX N Pro.

Table 1.4 Common Commercialized Automated Radiopharmaceuticals Synthesizer

Module	Manufacture	Comments	Radiopharmaceuticals
FASTlab	GE	Disposable cassette/ No HPLC integrated Size: 41cmx44cmx51 cm (W x H x L)	^{18}F-FDG ^{18}F-NaF ^{18}F-FMISO ^{18}F-FLT
TRACERlab FX N Pro	GE	Production of [^{18}F] tracers via nucleophilic substitution with [^{18}F] F- Fluoride trapped from [^{18}O] water/HPLC integrated Size: 49 cm x 48 cm x 50 cm (W x H x L)	^{18}F-FTHA ^{18}F-Fluoromisonidazole ^{18}F-Methylbenperidol ^{18}F-Methylspiperone ^{18}F-Fluorostradiol ^{18}F-Altanserine ^{18}F-FLT ^{18}F-FDG

TRACERlab FX E Pro	GE	Production of general [^{18}F] tracers via electrophilic substitution with [^{18}F] Fluorine in the form of F_2/ HPLC integrated Size: 29 cm x 48 cm x 35.5cm (W x H x L)	^{18}F-FDOPA ^{18}F-FLT ^{18}F-Fluorouracil
TRACERlab FX C Pro	GE	Production of [^{11}C] labeled tracers by methylation reactions using methyl iodide or methyl triflate produced from either carbon dioxide or methane/HPLC integrated Size: 50cm x 48 cm x 45cm (W x H x L)	^{11}C-Raclopride ^{11}C-Metahydroxyephedrine ^{11}C-Methylspiperone ^{11}C-Methionine ^{11}C-Acetate

Explora FDG_4	Siemens	Disposable cassette /No HPLC integrated Size: 61cm x 14 cm x 36cm (W x H x L)	^{18}F-FDG
FDG-Plus	Eckert & Ziegler	No HPLC integrated Size: 45cm x 25 cm x 50cm (W x H x L)	^{18}F-FDG ^{18}F-NaF ^{18}F-FMISO ^{18}F-FLT
Modular-lab	Eckert & Ziegler	Integrated with various types of actuators, and sensors.	^{68}Ga-Tracers ^{18}F-Tracers ^{11}C-Tracers
Synthera	IBA Molecular	Disposable cassette (Integrated Fluidic Processor) / No HPLC integrated Size: 17cm x 29 cm x	^{18}F-FDG ^{18}F-NaF ^{18}F-FMISO ^{18}F-FLT

		28.5cm (W x H x L)	
NanoTek	Advion	Microreactors & HPLC integrated	^{18}F-Fallypride ^{18}F-FDG ^{11}C-CO

However, the major goal of these modules is for clinical usage. Therefore, scientists have to modify the commercialized modules or to build their own modules for production of specific radiopharmaceuticals (63-77).

In the trend of industry, the basic purpose of automated production is to provide massive and quality product to customers, and the development of automated production is the result of demand for applications. In addition, automated synthesis modules are housed in a lead-shield chamber which is called “hot cell”, and hot cell can reduce the unnecessary radiation exposure to employees. Considering the space usage in a hot cell, the design of appearance of current commercialized modules has a tendency to compact module, and this feature can maximize the utilization of hot cell space.

1.5 Scope of the dissertation

The role of automated radiopharmaceuticals synthesis modules in clinics is to reduce the radiation exposure during the production of radiopharmaceuticals and

provide a consistant amount of radiopharmaceuticals with quality control and quality assurance. In order to achieve the goal, the hardware and software designs have to be optimized for the specific synthesis method, and the size of the module can be housed in the hot cell. In research field, radiochemists want to synthesize novel radiopharmaceuticals for different applications, and to optimize the synthesis methods for good quality radiopharmaceuticals. Therefore, numerous ideas for radiopharmaceuticals synthesis are practiced for these purposes. However, the features of clinical automated synthesis modules limit possibilities for performing these ideas.

In order to bridge the gap between the research interests and clinical demands, a multi-purpose automated synthesis module for production of novel PET radiopharmaceuticals is needed. Our hypothesis is that we can design an automated synthesis module, the hardware configuration and the software design can transform the manual chemical reaction processes into automated synthesis steps, which may allow users to synthesize three different PET pharmaceuticals with quality control by organic or metallic chemical reactions. Three specific aims are addressed to test this hypothesis.

Specific Aim 1: To design, assemble and test the hardware of this module for transforming manual synthesis processes into automated steps.

Specific Aim 2: To develop the software for creating synthesis receipts and recording data, including time, temperature, and flow rate.

Specific Aim 3: To validate the automated synthesis module by producing three different PET radiopharmaceuticals gallium-68-ethylenedicysteine-glucosamine (^{68}Ga-GaECG), [^{18}F]fluoropropyl-α-methyltyrosine (^{18}F-FPAMT), and [^{18}F]fluoro-5-propylhydroxy tryptophan (^{18}F-FHTP), with high radiochemical purity (>90%), acceptable pH range (pH=4.5~8.3).

2 Chapter 2 Hardware design and Setup

2.1 Introduction of hardware design

Traditionally, chemists used graduated cylinders, flasks, beakers, hot plates, thermometers, and other material to complete chemical reactions. Several reaction steps are involved to compose a synthesis method. In order to design the hardware of this module, we spitted each chemical reaction into several simple actions. Each action is controlled by appropriate sensors and actuators(78). Through the customized user-interface and other equipment, users could control sensors and actuators to complete the synthesis.

There are three different levels of the hardware design for this automated synthesis module. First, we defined the basic actions of this automated synthesis module. Secondly, we searched appropriate electrical and mechanical components to complete these basic actions, designed the customized circuit board, and drawed the blueprint of this automated module. Lastly, after completing physical appearance of this module, we assembled each component to complete the hardware of this module.

2.2 Basic actions for chemical reactions

We defined five actions, such as add, purge, heat, transfer, and mix. The definition of “add” is “Inject the solution to the reaction vial”. The definition of “Purge” is “Remove the residual solution from the channels to the reaction vial”. The definition of

“Heat” is “Heat the reaction vial at the specific temperature in a short time”. The definition of “Transfer” is “Transfer the solution in the reaction vial to another reaction vial”. The definition of “Mix” is “Use bubbles to mix the solution inside the reaction vial”.

2.3 Selection of hardware components for the basic actions

Based on the definition of basic actions, we found appropriate components to complete the chemicals reactions. In addition, these components are capable of production of various radiopharmaceuticals in the extreme conditions, such as extra small volumes, higher temperature, high pressure, and radiation exposure.

“Add”

By its definition, the module can transfer certain quantities of chemicals into the reaction vials. In order to control this action, we designed a customized syringe pump by using the stepper motor. Several customized syringe pumps, and different types of valves are used to integrate this action into the multi-purposes synthesis,.

“Purge”

By its definition, the module can purge the residual solution from the flow channel to the reaction vial. We used nitrogen gas as the pressure source to transfer the residual solutions, and a mass flow controller to maintain the nitrogen pressure for

processing this procedure. Concerning integration this action into the multi-purposes synthesis, different types of valves for specifying “purge” affected zone were employed.

“Heat”

Among many options of heating method, we selected the infrared heater due to its rapid heating process. The functions of heating in chemical reactions usually are to speed up the process of the chemical reactions or to evaporate solvents. Therefore, a small vacuum pump is used to increase the evaporation rate. Concerning integration this action into the multi-purposes synthesis, the infrared heater is mounted on the plate which is driven by the stepper motor, and different types of valves can provide the pressure balance inside the module. Consequently, “heat” can work on different reaction vials.

“Transfer”

The definition is very similar between “add” and “transfer”. The difference between these two actions is that “Transfer” use compressed nitrogen gas as the power source of transferring. Concerning integration this action into the multi-purposes synthesis, we used different types of valves to specify the source and the destination of “Transfer”.

“Mix”

We used a vacuum pump to cause the negative pressure inside the reaction vial. Therefore, air can enter the reaction vial, and become bubbles which can mix the solution to increase the chemical reaction rate.

All these basic functions are operated by electrical or mechanical components. In order to control these components, a control system is used to exchange single between these components, and a power supply is needed to provide adequate power to these components. In addition, this control system allows us to design the customized user interface by its operational software. Besides a control system and a power supply, a customized circuit board is designed to manage signal and power for each component.

Our multi-purposes automated synthesis module consists of two parts, the control box and the synthesizer. The main components of this control box are the two power supplies, the one solid state power controller, and the control system. One power supply can provide 24V/5A (PS-12024, Altech Corp., Flemington, NJ, USA), and another power supply can provide 12V/10A (PS-12012, Altech Corp., Flemington, NJ, USA). Both power supplies are connected to the circuit protection devices (Altech Corp., Flemington, NJ, USA). The solid state power controller (DIN-A-MITE Style C, Watlow, St. Louis, Missouri, USA) provides voltage to the infrared heater. The control system consists of five parts, the ethernet/RS232 interface with 4 slot backplane module (cFP-1804, National Instruments, Austin, TX, USA), two digital output modules (cFP-DO-401,

National Instruments, Austin, TX, USA), and two analog input/output modules (cFP-AIO-600, National Instruments, Austin, TX, USA). These digital and analog modules are connected with 4-slot ethernet/serial interface module, and the customized circuit board of the synthesizer. Users can control the synthesizer through ethernet by connecting the network line between the laptop to the 4-slot ethernet/serial interface module. The layout of the control box is shown in Figure 2.1, and the picture of the control box is shown in Figure 2.2.

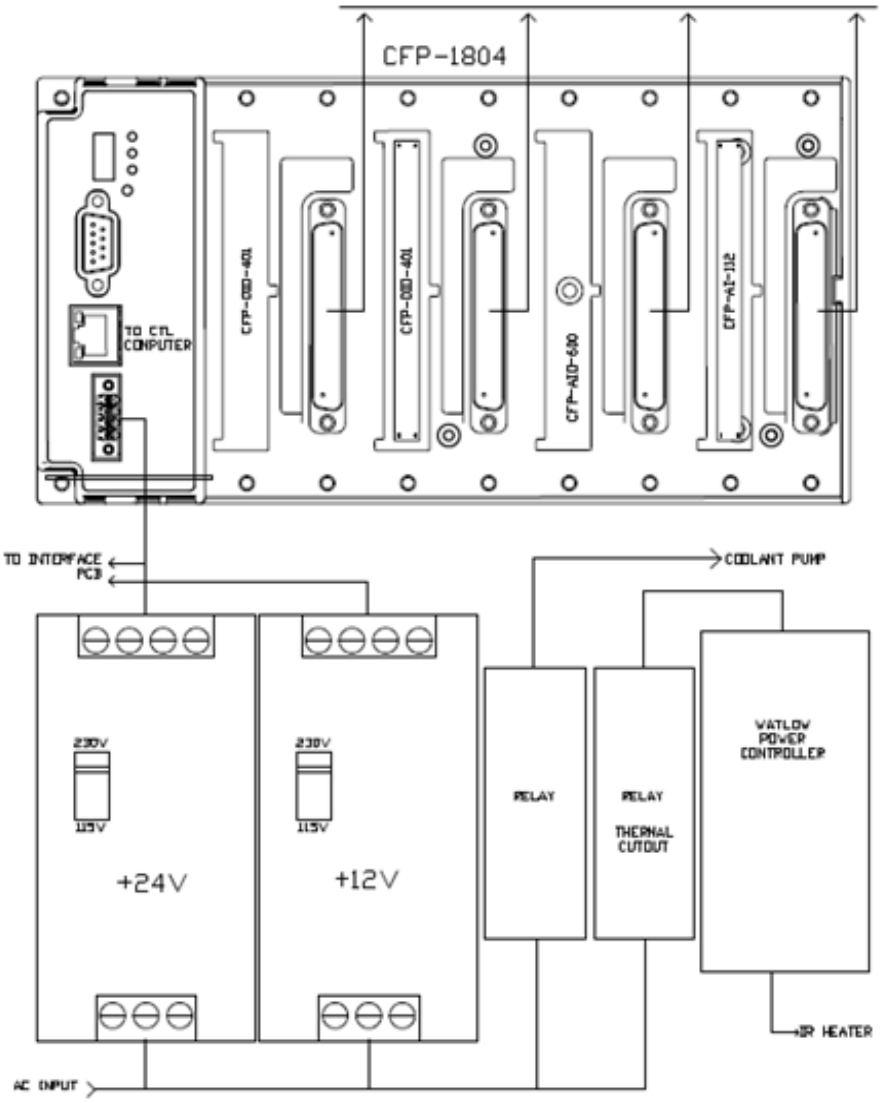

Figure 2.1 The layout of control box

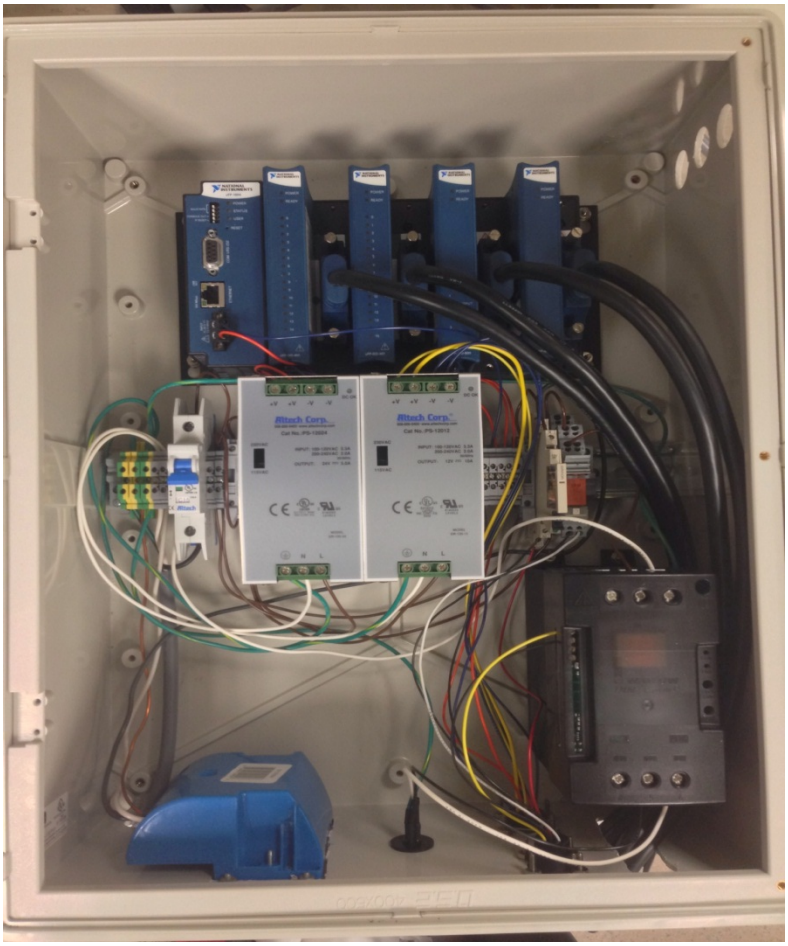

Figure 2.2 The picture of the control box

The synthesizer consists of one mass flow controller (FMA5508, Omega Engineering, Inc., Stamford, CT, USA), one customized circuit board, one USB to RS485 converter (USB485, RMS Technologies, Carson City, NV, USA), one infrared heater (Model 5306, RESEARCH INC., Eden Prairie, NM, USA), four radiation sensors (Si photodiode S8559, Hamamatsu Photonics K.K., Hamamatsu City, Japan), two temperature sensors (RTD-860, Omega Engineering, Inc., Stamford, CT, USA), one vacuum pump (C117H-12, Hargraves Technology Corporation, Mooresville, NC, USA),

two 6-way rotary valves (C65Z-3186I, Valco Instruments Co. Inc., Houston, TX, USA), three 4-way rotary valves (C65Z-3186I, Valco Instruments Co. Inc., Houston, TX, USA), five 3-way solenoid valves (LFRX0500600BE, The Lee Company, Westbrook, CT, USA), five two-way solenoid valves (6126, Bürkert, Charlotte, NC, USA), seven stepper motors (PK223PA-SG18, Oriental Motor, Basingstoke, UK), seven stepper motor controllers (R256, RMS Technologies, Carson City, NV, USA), and various types of HPLC fittings (Valco Instruments Co. Inc., Houston, TX, USA). The figure 2.3 shows the layout of the customized circuit board with joint indicators of the components in the synthesizer. The figure 2.4 is the appearance design drawings of this synthesizer, the top view, the front view, and the side view. The figure 2.5 is the detail appearance design drawing of this synthesizer. The figure 2.6 is the front view picture of the synthesizer.

2.4 Validation of hardware components of this module

After assembling the module, different validation methods were practiced in different components. Voltage transferred from the control box can test the function of valves, and current transferred from the control box can test the function of IR heater. Because the stepper motor connected to the module through USB, the hyperterminal was used to test the function of stepper motors, including forward, backward, and safety issue.

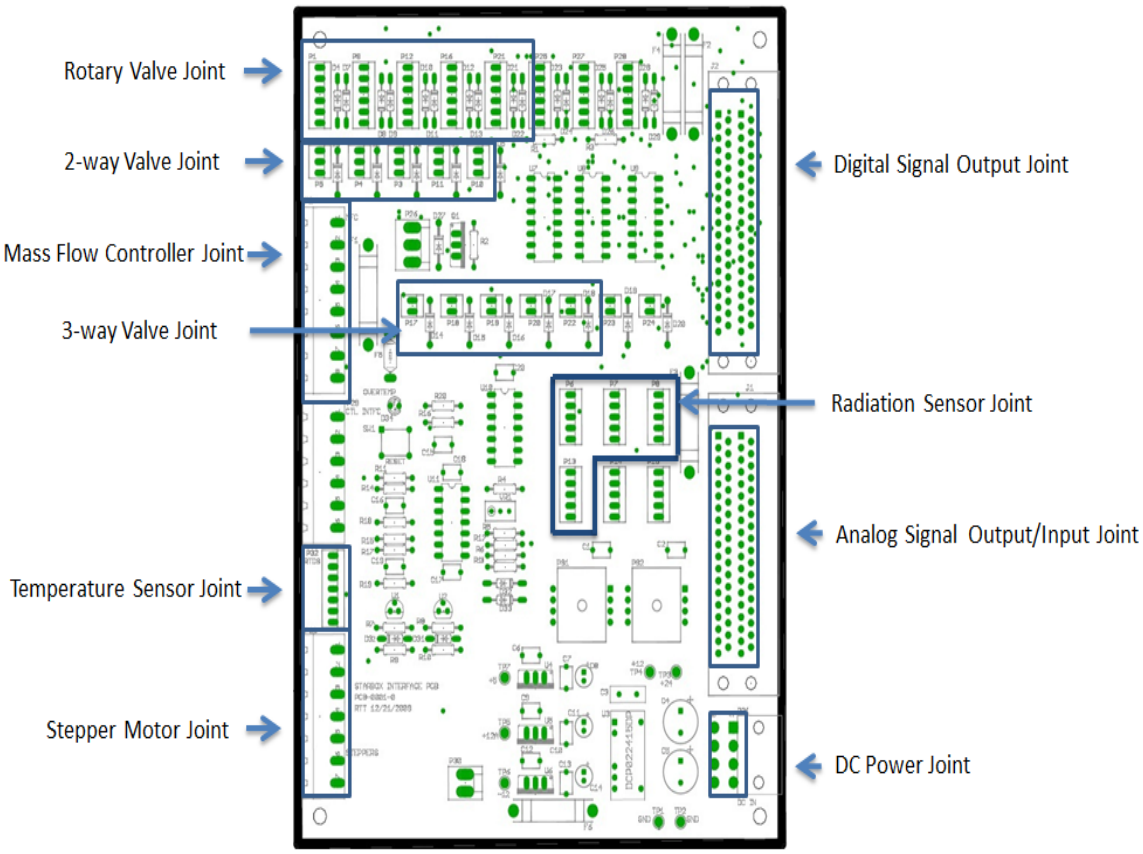

Figure 2.3 The layout of the customized circuit board ??????

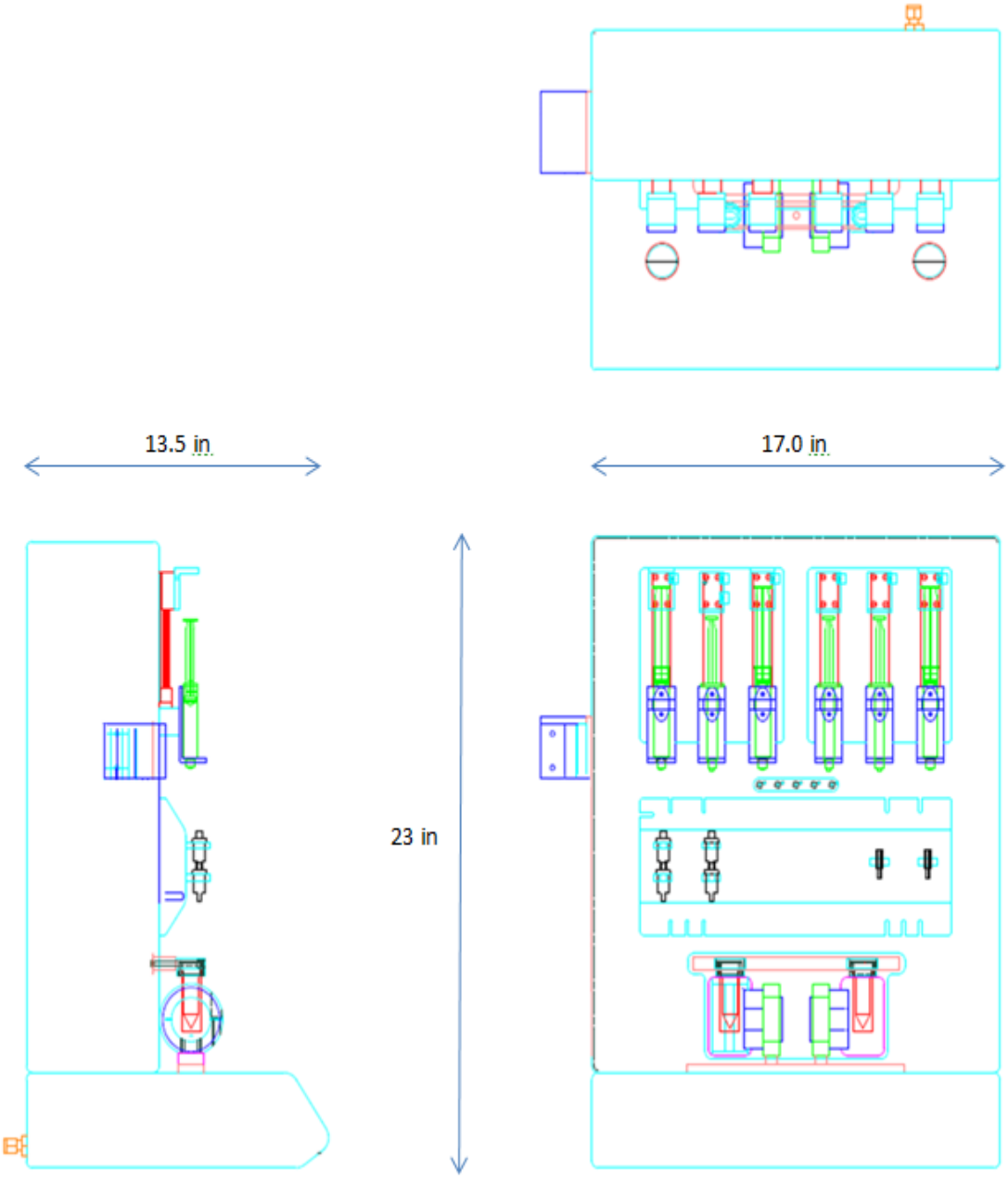

Figure 2.4 The appearance design drawing of this synthesizer

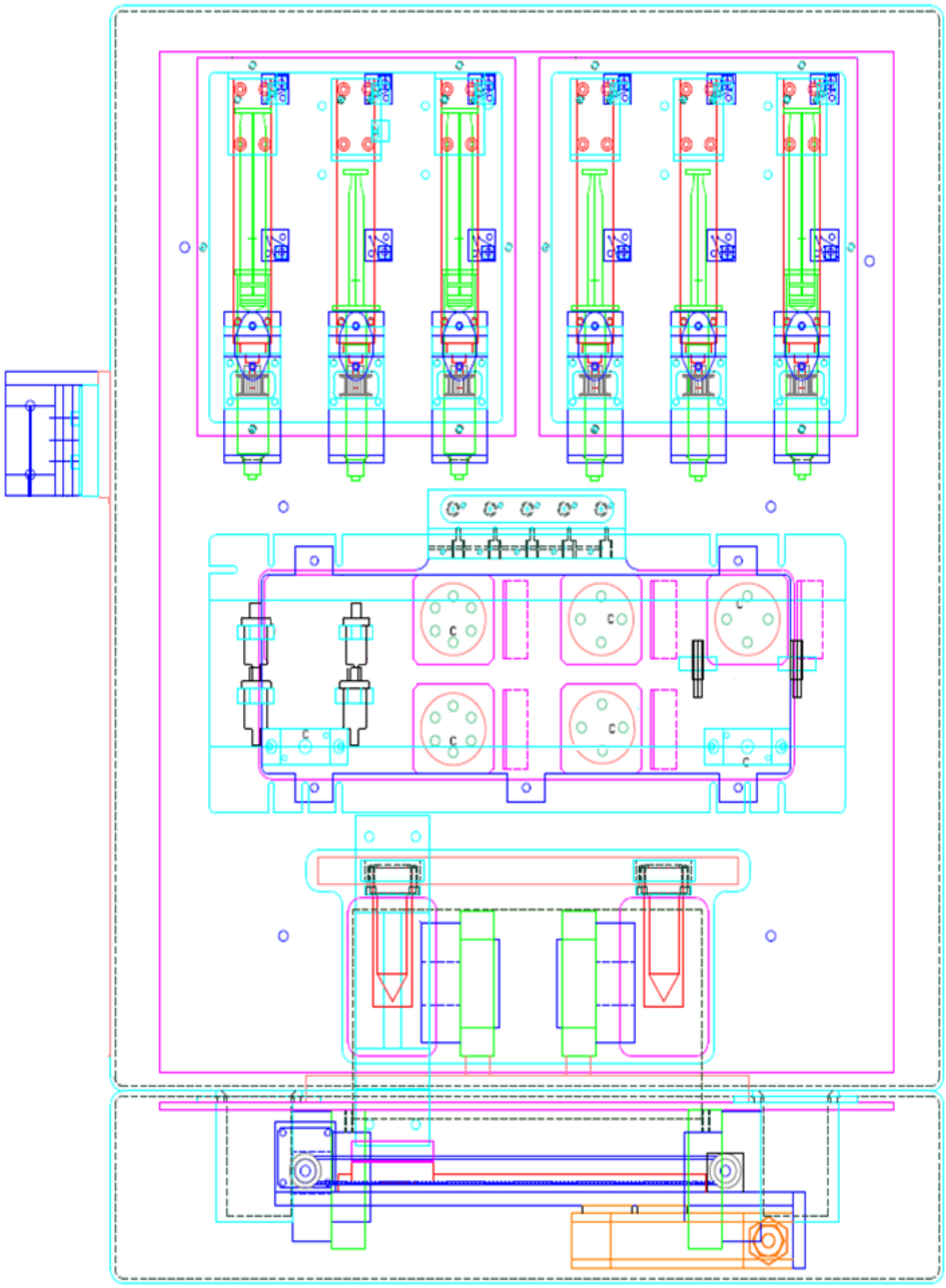

??Figure 2.5 The detail appearance design drawing of this synthesizer: Front View

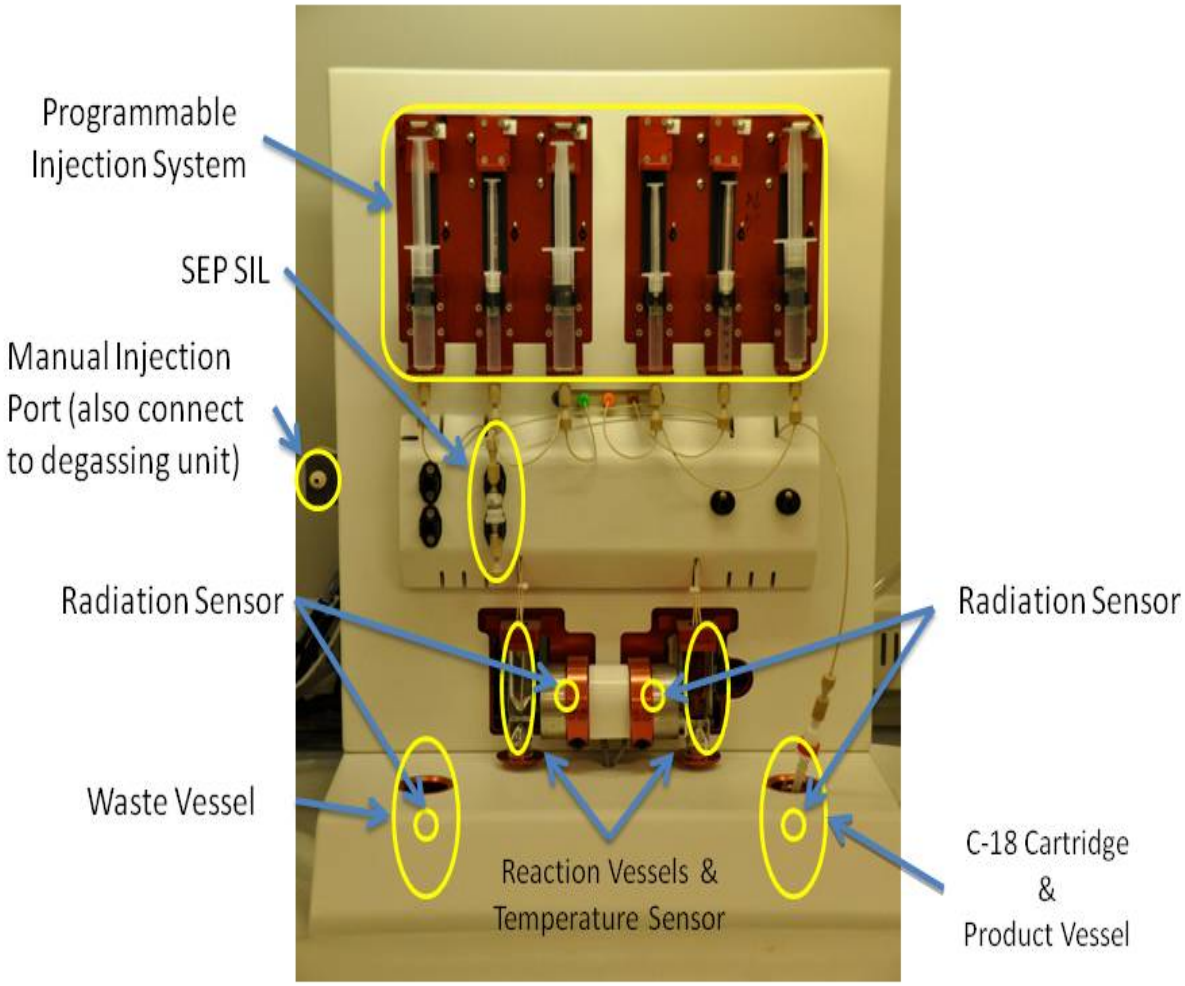

??

Figure 2.6The front view picture of the synthesizer

3 Chapter 3 Software Design and Setup

In the chapter 2, appropriate components are selected to provide essential functions for this automated synthesis module. In this chapter, procedures to set up the connection between the synthesizer and the laptop through the control module, the controlling principle for each component of this automated synthesis module, the important operational codes, and the operational methods of the user interface are discribed. The software of this multi-purpose automated synthesis is developed by LabVIEW 2009 which is a visual programming language of National Instruments for programmable logic controller, and this program provide the software debug. The basic program of LabVIEW 2009 is called virtual instrument (VI).

3.1 Steps for initializing the connection between hardware and software

After connecting the ethernet cable from the control box to the laptop, the software, Measurement & Automation Explorer (National Instruments, Austin, TX, USA) was initialized. Through this software, a physical IP address for NI cFP-1804 in the control box (Figure 3.1) can be assigned. Then, each channel of input/output modules can be controlled. By turning on/off the signal of these modules (Figure 3.2), the basic operation of each component, and debug the connections of hardware components can be tested.

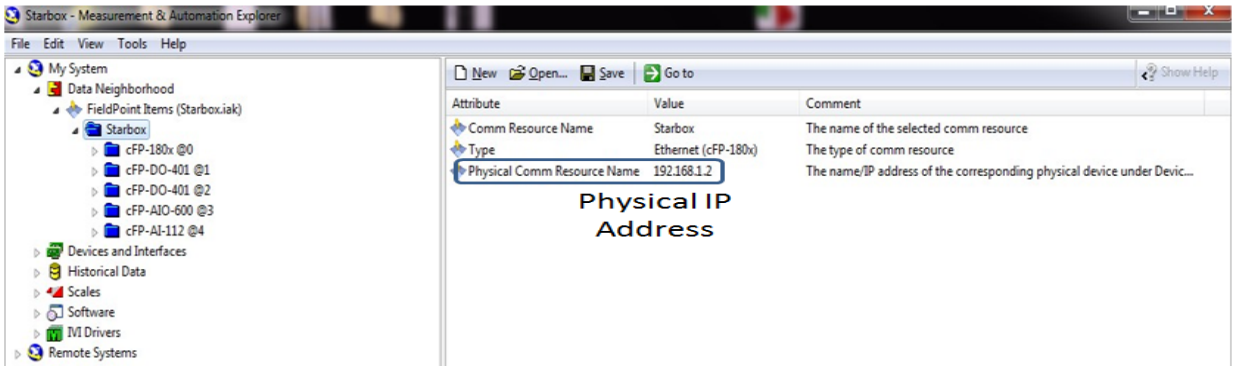

Figure 3.1 IP Assignment of the control box through MAX

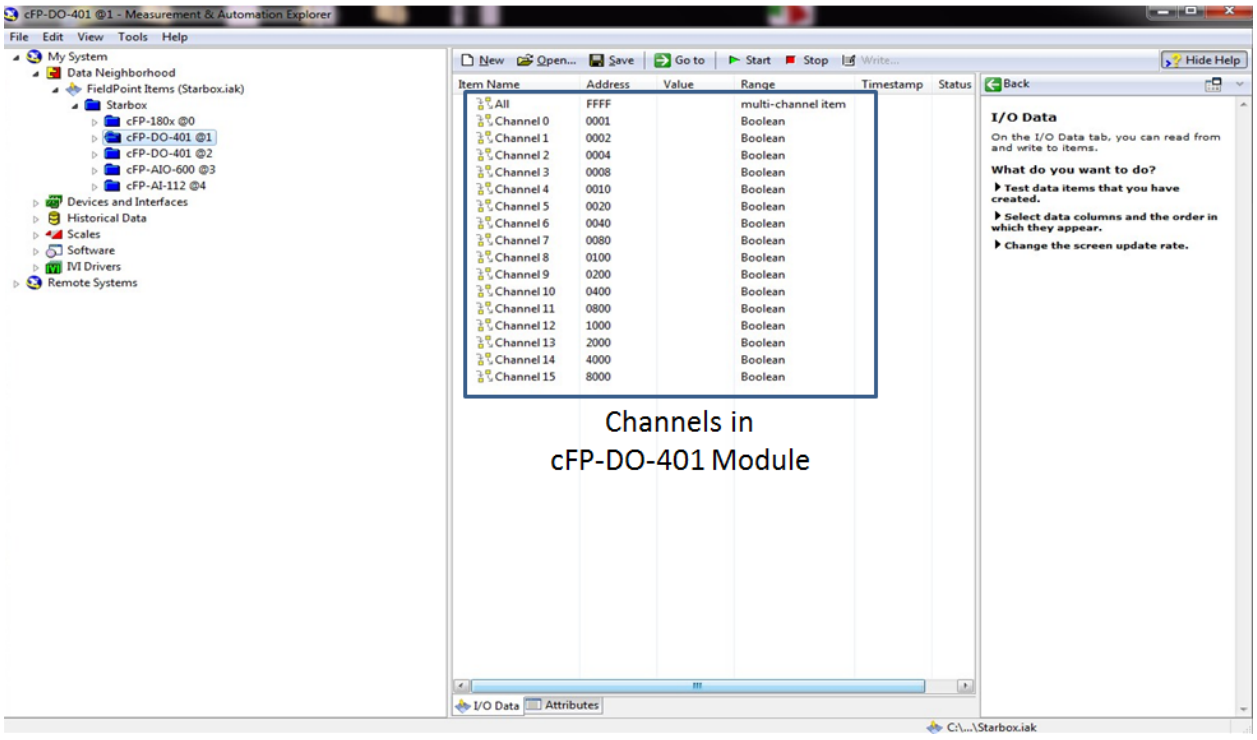

Figure 3.2 Controllable channels in cFP-DO-401 module

3.2 Overall scheme of the software design

Based on the definition of the basic actions of this synthesizer in chapter 2, these functions allow to complete the automated synthesis process. In addition to prove the

concept of multi-purpose automated synthesis comprehensively, there are more features of this customized operational software, such as user-friendliness, safety, and modifiability.

3.2.1 User-friendliness

The software user interface is performed in a graphical user interface (GUI) which can be easily utilized and understood for laboratory personnel with typical training and experience in this field.

3.2.2 Safety

The software is able to check the connection between the components, the control box and the laptop. Flow pressure and heating temperature are restricted in a range for safety operation. In addition, a user can pause or stop the current step during the emergency. After trouble shooting, the user can resume the synthesis process.

3.2.3 Modifiability

The parameters in basic actions and the total synthesis recipe will be modifiable based on the user's demands without difficulty or confusion.

3.3 The controlling principle for each component of this automated synthesis module

Stepper motors are controlled by HyperTerminal codes through the usb to rs485 converter, and other hardware components are controlled by current or voltage changes in each channel of NI modules. In LabVIEW 2009, “global variable” is used to describe these changes which can indicate the current property of the hardware component. I have created “cFP comm handler” VI to control or receive each channel of analog/digital signal modules.

3.3.1 Solenoid Valve

Five different channels in the cFP-DO-401 module can deliver 12 V to trigger five 2-way valves individually; other five channels in the same module can deliver 12 V to trigger five 3-way valves individually.

3.3.2 Rotary Valve

Each rotary valve is controlled by two digital channels in the other cFP-DO-401 module. Triggering one channel is to move the rotor back to the default position of the rotary valve, and triggering another channel is to moves the rotor in a counterclockwise direction to next position. If the default position of 6-way rotary valve 1 is position 1, it would have to trigger 3 times for switch the position 1 of the rotary valve to position 4. If it is necessary to switch the rotor from position 4 to position 2, it would have to trigger 4 times. In order to complete this task, I created the “rotary position calculator”

VI. In this VI, each rotary valve has its own case structure from the commands of Labview 2009. Here, the rotary number 1 is selected as a working example. After sending new position of the rotary valve 1, there will be two conditions. If the new position number is more than or equal to the previous position number, the calculation shows the Figure 3.3. If the new position number is less than the previous position number, the calculation shows in the Figure 3.4. After calculation, these information including active rotary valves, and number of triggers, are sent to “execution” VI.

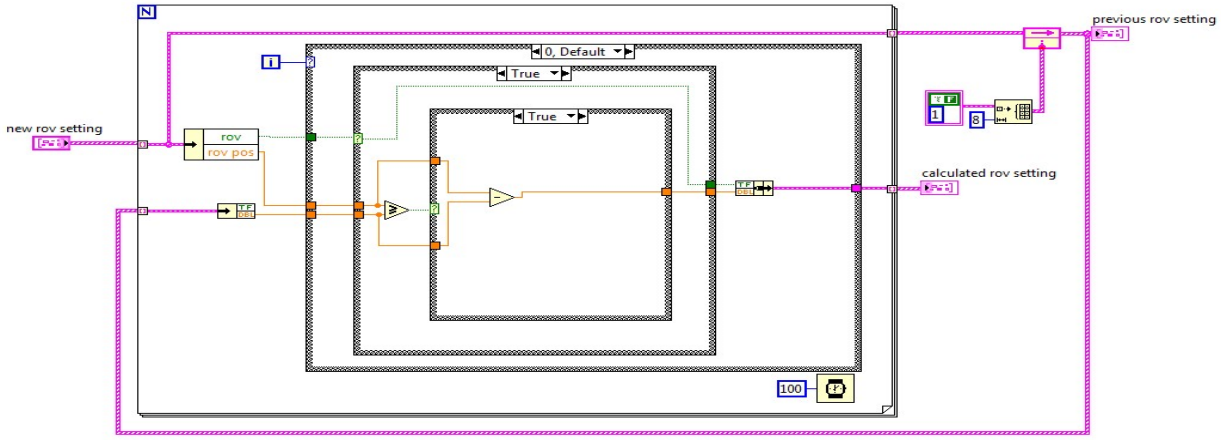

Figure 3.3 “rotary position calculator” VI_ Case 1

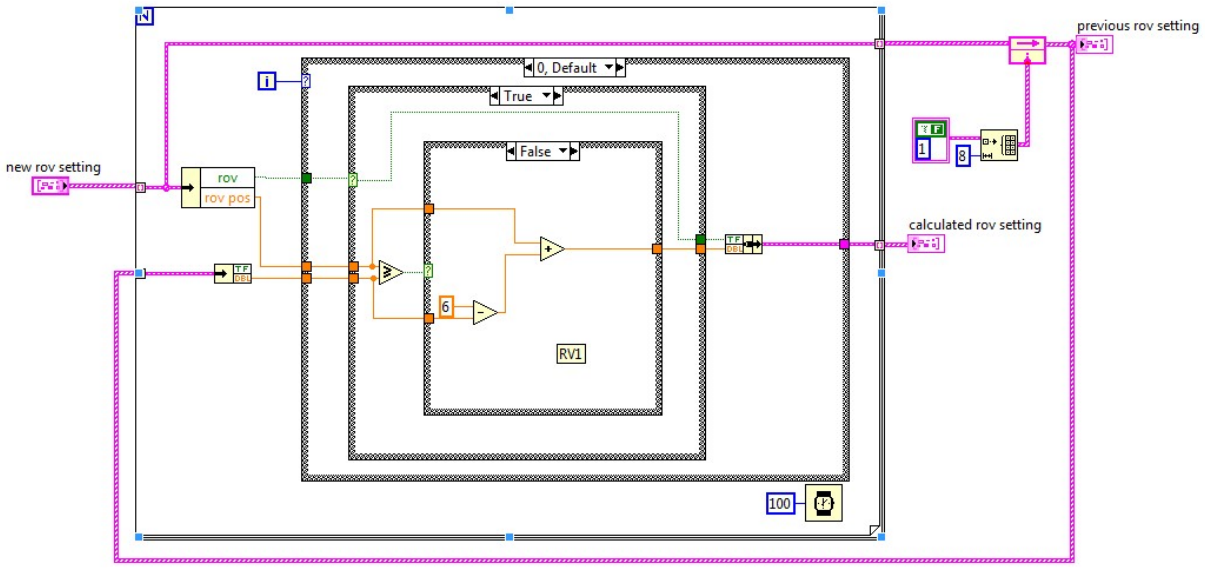

Figure 3.4 “rotary position calculator” VI_ Case 2

3.3.3 Mass Flow Controller

The functions of this mass flow controller are to monitor and control nitrogen flow rate by one input channel and one output channel in the cFP-AIO-600 module, respectively. “cFP comm handler” VI can provide two functions, “I read” and “I set”, which are detailed in section 3.4.1.. Determined by the calibration chart from the manufacture, we can know the relationship between current and the flow rate.

3.3.4 Infrared Heater

The infrared heater is controlled by one analog input channel in the cFP-AIO-600 module, and “I set” in the “cFP common handler” VI can be used to set different current for controlling heating rate. In chemical reactions, an ideal heater should provide fast

heating, but doesn't have the occurrence of overheating. In order to avoid overheating, I created the proportional-integral-derivative (PID) controller which can send different current based on the temperature in the reaction vial.

3.3.5 Temperature Sensor & Radiation Sensor

Each sensor is able to send current to one analog input in the cFP-AIO-600 module. In order to calculate the relationship between temperature in the reaction vial and current, after infrared heater turned on, I set various currents and recorded different temperature in the vials which is measured by a thermo couple thermometer. Then, I have the relationship equation which is established for temperature monitoring (Figure 3.5).

$$(V-T_{offset})*T_{gain}=Temperature$$

$*T1_{offset}=1.1239$, $T1_{gain}=475.05$

$*$ $T2_{offset}=1.1178$, $T2_{gain}=430.00$

T1: Temperature in Vial 1

T2: Temperature in Vial 2

Figure 3.5 The relationship of measured voltage and vial temperature

The radiation sensor uses a small CsI scintillator to detect X-ray energy, and its size is very small. Therefore, it can't be used as real radiation counter. However, it can

provide the relative information of radiation which can indicate the radiation solution in what location.

3.3.6 Vacuum Pump

The vacuum pump is controlled by one voltage output channel in the cFP-DO-401 module.

3.3.7 Stepper Motor

Through an usb to rs485 converter, these stepper motor controllers can connect to PC or laptop. Instead of creating “global variable”, I have to use NI Virtual Instrument Software Architecture (NI VISA) to communicate with these controllers by HyperTerminal codes.

3.4 Important operational VIs

In previous sections, the relationship between hardware components of the synthesizer, the modules in the control box, and some Vis were described. In this section, the functions of important operational VIs in details are described.

3.4.1 cFP comm handler VI

This VI can send and receive the signal between NI modules and the hardware components. There are six functions in this VI, “digital set all”, “digital set”, “set rov”, “I set”, “I read”, and “V16 read”.

3.4.1.1 “digital set all”

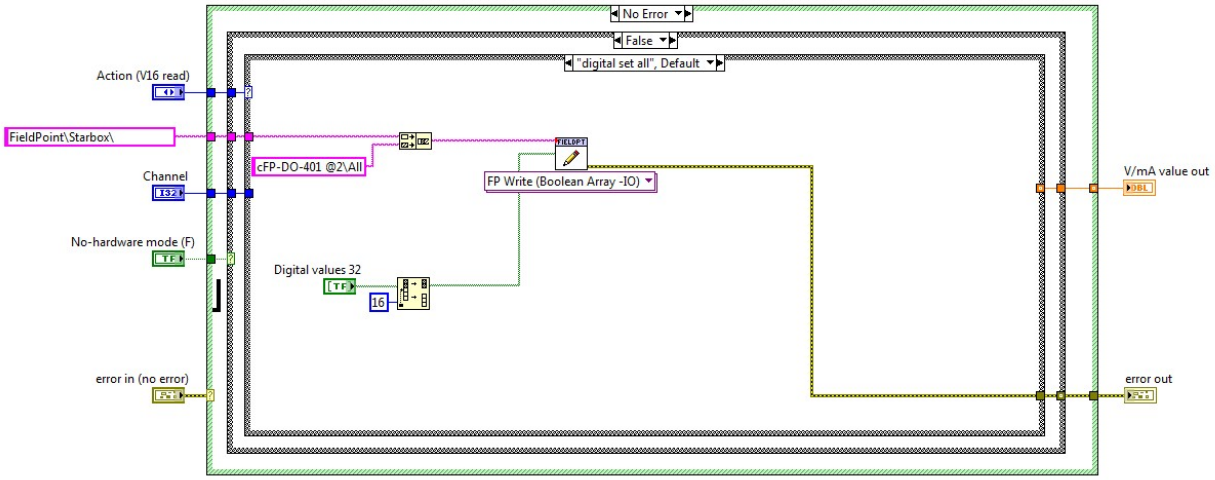

Figure 3.6 The code of ““digital set all” of “cFP comm handler” VI

When the software initialize, this default function of this VI (figure can set default value to each channel in the second digital module (cFP-DO-401).

3.4.1.2 “digital set”

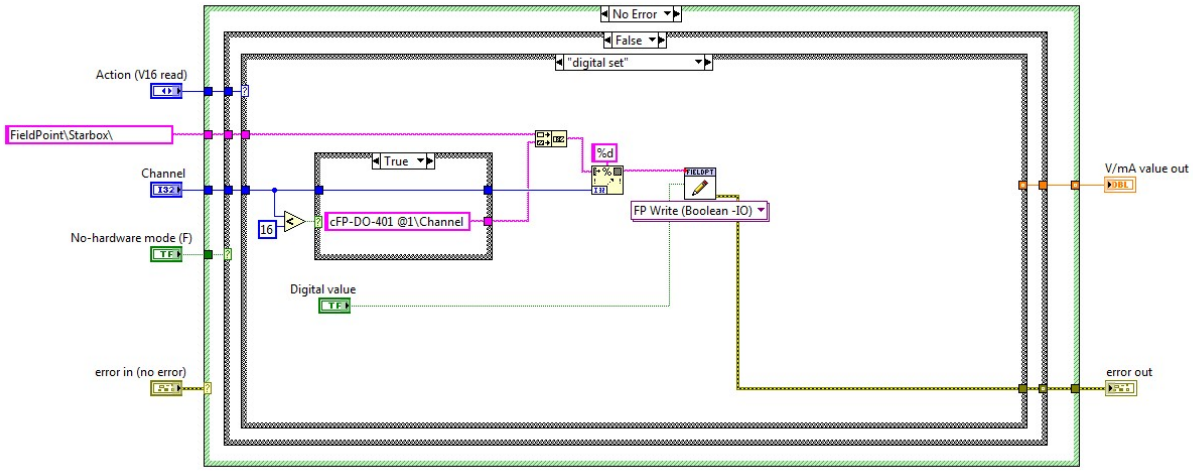

Figure 3.7 The code of “digital set” of “cFP comm handler” VI for digital module 1

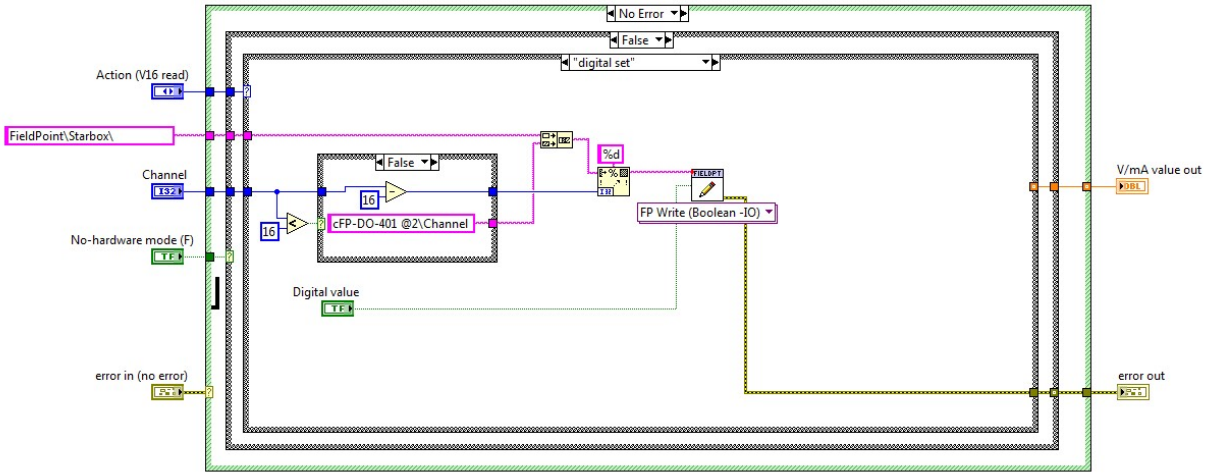

Figure 3.8 The code of “digital set” of “cFP comm handler” VI for digital module 2

This function is to send the signal to the assigned channel of the specific digital module. In this software, each module has 16 channels. I name the channels in module 1 from number 1 to number 16 (Figure 3.7), and the channels in module 2 from number

17 to number 32 (Figure 3.8) are named. The function “digital set” is sufficient for voltage-actived components, such as solenoid valves, and the vacuum pump.

3.4.1.3 “set rov”

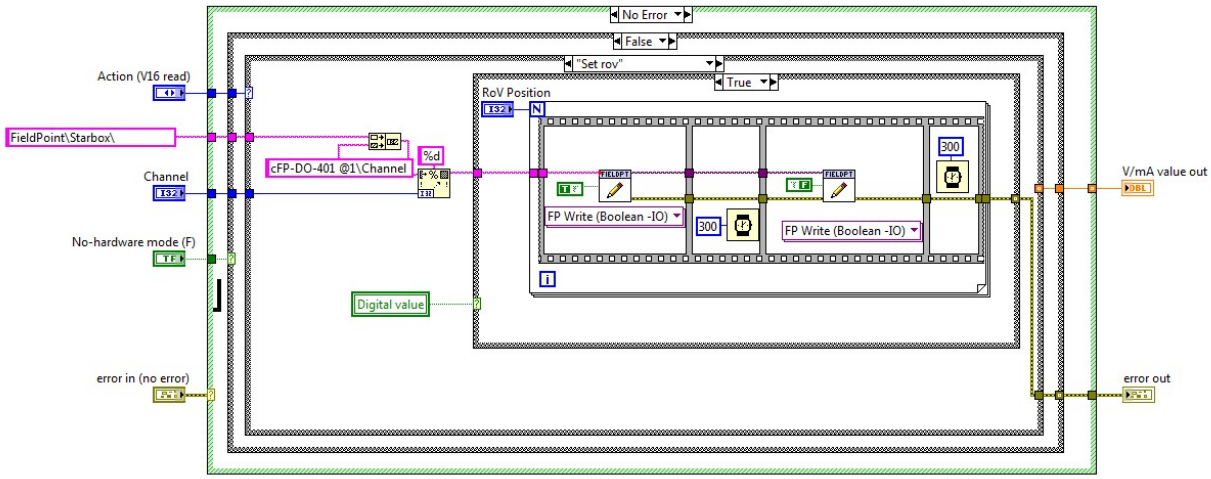

Figure 3.9 The code of “set rov” of “cFP comm handler” VI

The operation method of the rotary valve is its rotor can move to next position when receiving two triggers, one is to turn on the channel, and another is to turn off the channel. The digital module and the rotary valve need a short time to process between two consecutive triggers. Therefore, I put two delays in this function to provide a sufficient time period for the communication of the rotary valve controller and the digital module.

3.4.1.4 “I set”

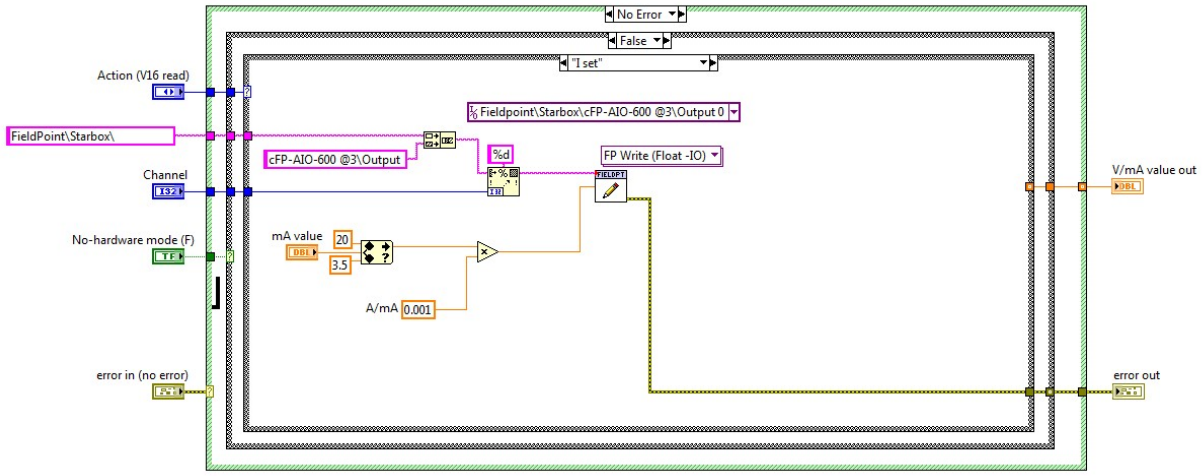

Figure 3.10 The code of “I set” of “cFP comm handler” VI

The function “I set” can send various current through the analog module to control the mass flow controller and the infrared heater. Because these components only work properly in a certain range of current, I put a logic option to control the current under the safe range which is between 3.5 to 20 mA.

3.4.1.5 “I read”

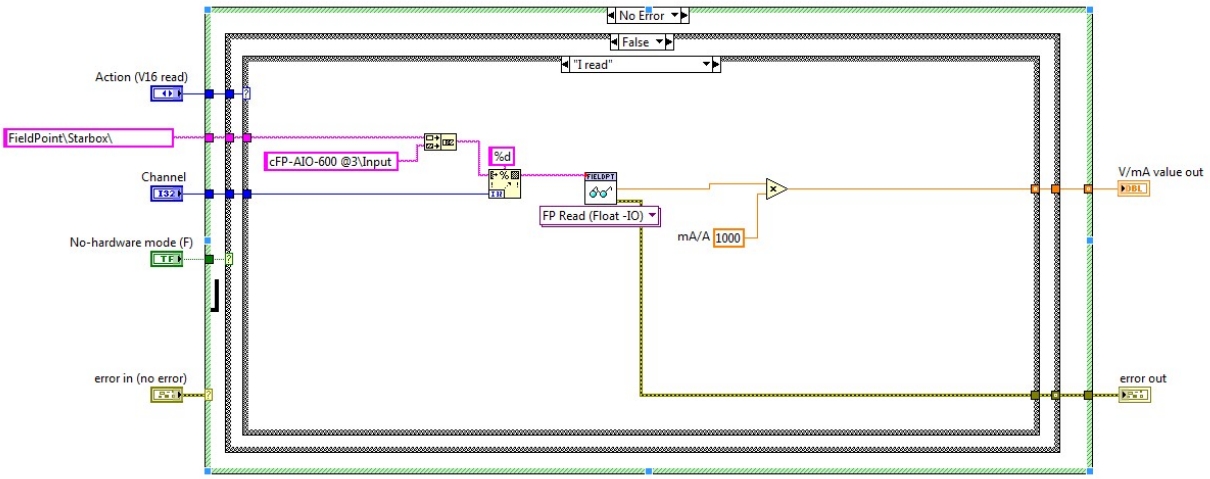

Figure 3.11 The code of “I read” of “cFP comm handler” VI

The function “I read” is to receive the data from the radiation sensors and temperature sensors through the analog module.

3.4.1.6 “V16 read”

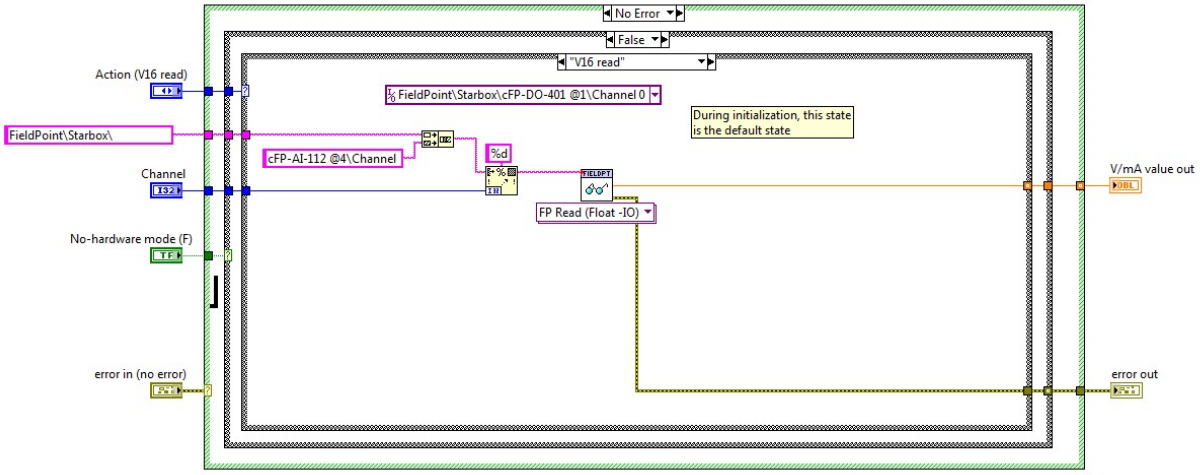

Figure 3.12 The code of “V16 read” of “cFP comm handler” VI

This function “V16 read” is to check the connection status of the digital modules, and it only works when initialing the software.

3.4.2 Execution VI

We can use the previous VI to control the components or receive the signal from sensors. “Execution” VI is to execute the combination of these commands to complete one single basic function. Each basic functions includes several parameters, such as valves, vacuum, syringe, injection volume, injection rate, N_2 flow rate, heating temperature, rotary valve position, and heater position. Depended on the features of the basic function, assigned parameters are executed in the sequence in this VI. First, the status of each valve is determined (Figure3.13).

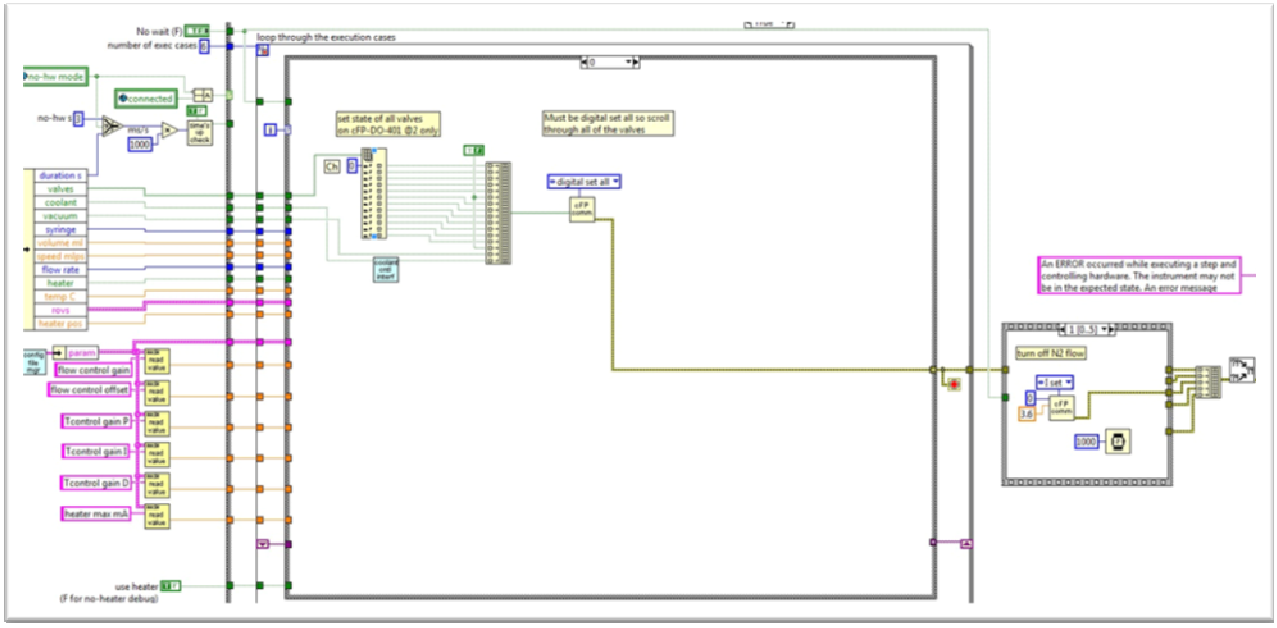

Figure 3.13 "Execution" VI_Step 1

After that, the position of each rotary valve is determined (Figure 3.14).

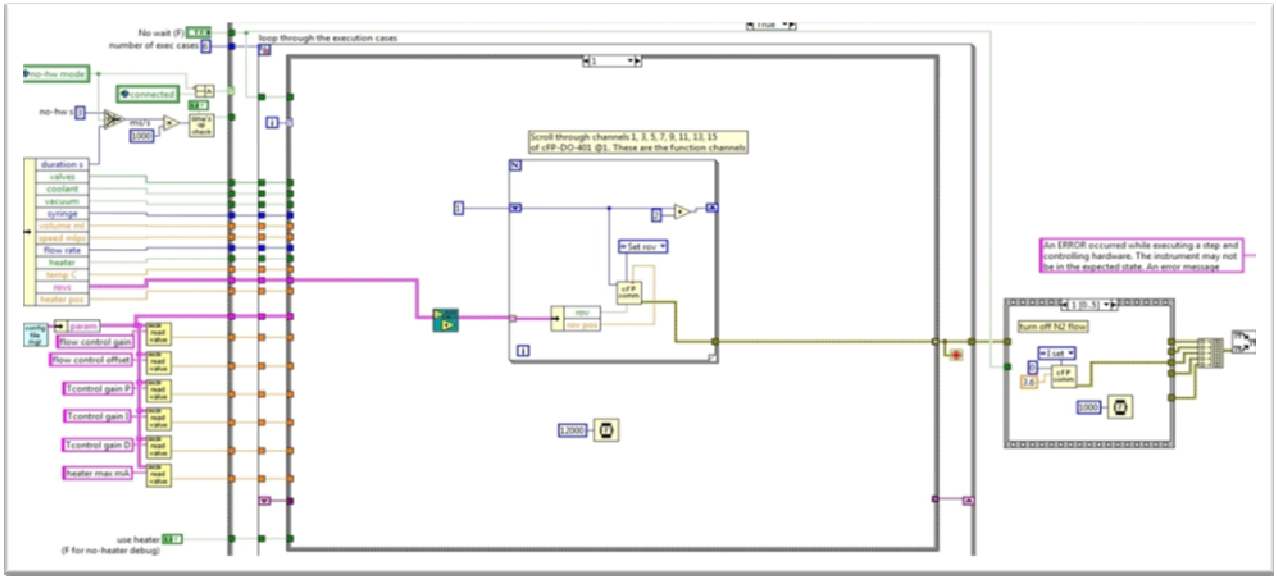

Figure 3.14 "Execution" VI_Step 2

Right now, the flow path is set up. The third step can turn on mass flow controller to allow N_2 flow into this synthesizer for transfer solution to another location (Figure 3.15).

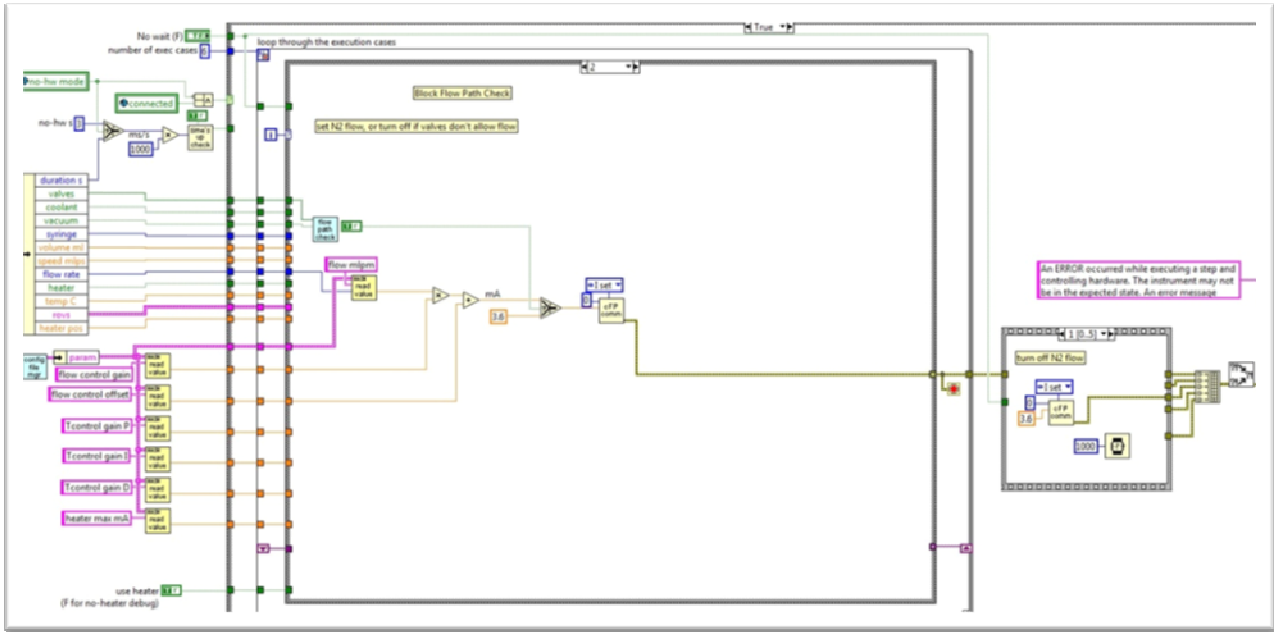

Figure 3.15 "Execution" VI_Step 3

The fourth step can control the stepper motor to inject the chemical in the different speed (Figure 3.16).

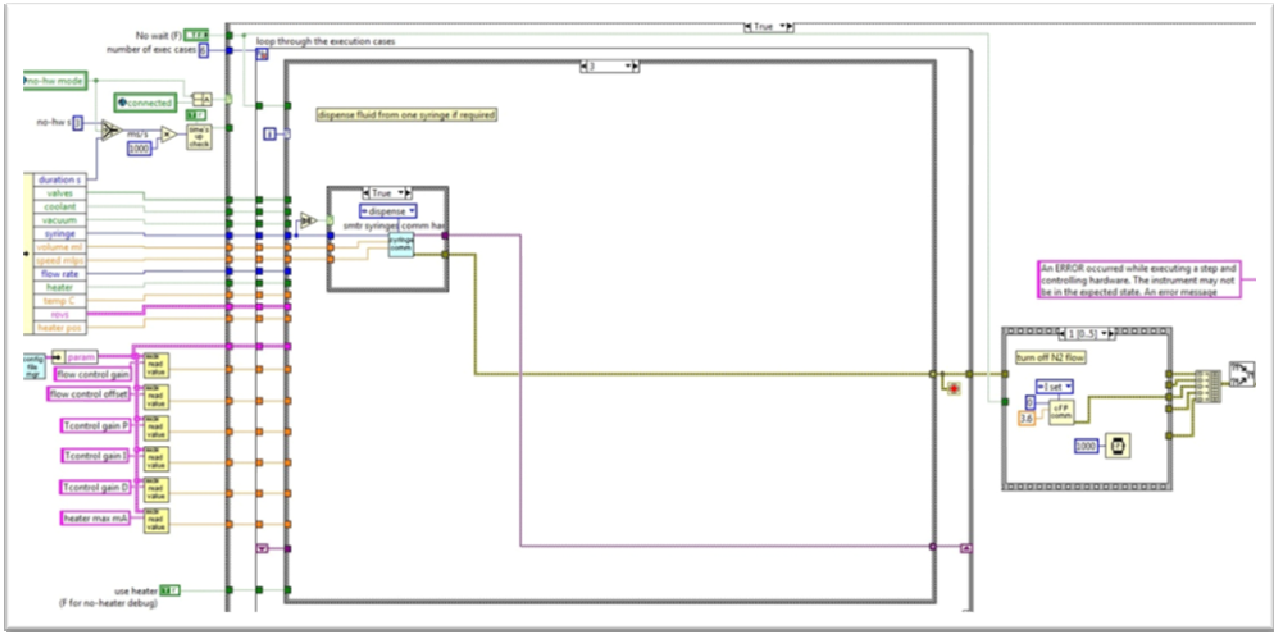

Figure 3.16 “Execution” VI_Step 4

The last step can control the position of the heater and adjust the heating temperature (Figure 3.17).

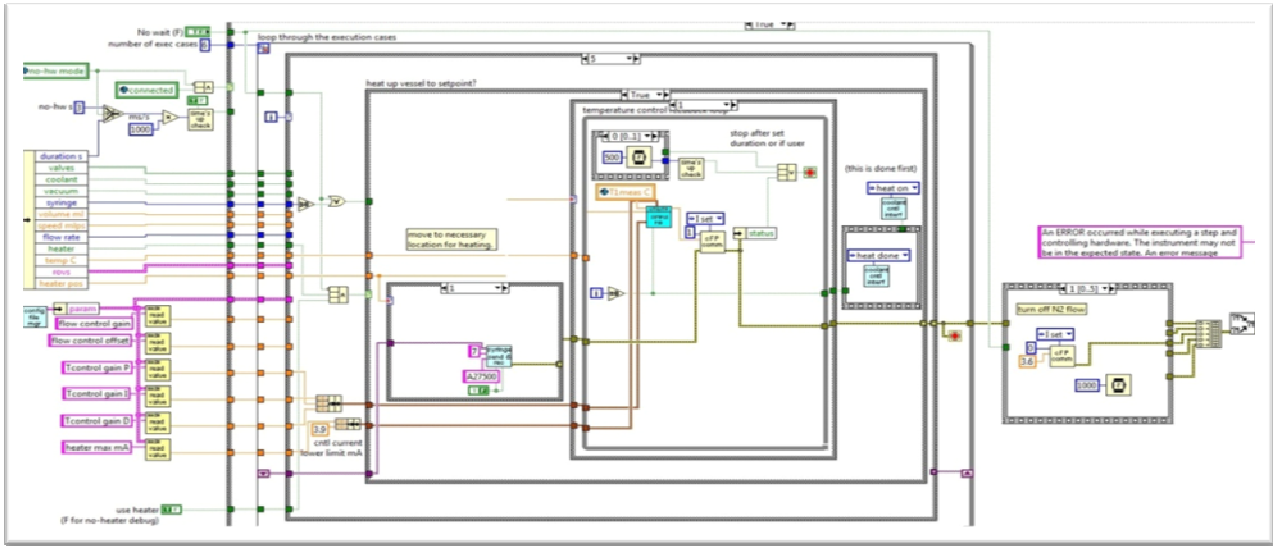

Figure 3.17 "Execution" VI_Step 5

After the duration ends, there are another sequence of commends which can set components to the default condition, except stepper motors. The default condition of flow path is suitable to release the pressure in the vials and channels, and can avoid the unexpected damage.

3.5 Operation of Software

3.5.1 Starting the Application

To start up the application, the user should double-click the customized icon on your desktop that was placed there by the installer.

3.5.2 Panels of the Application Window

3.5.2.1 Main control panel

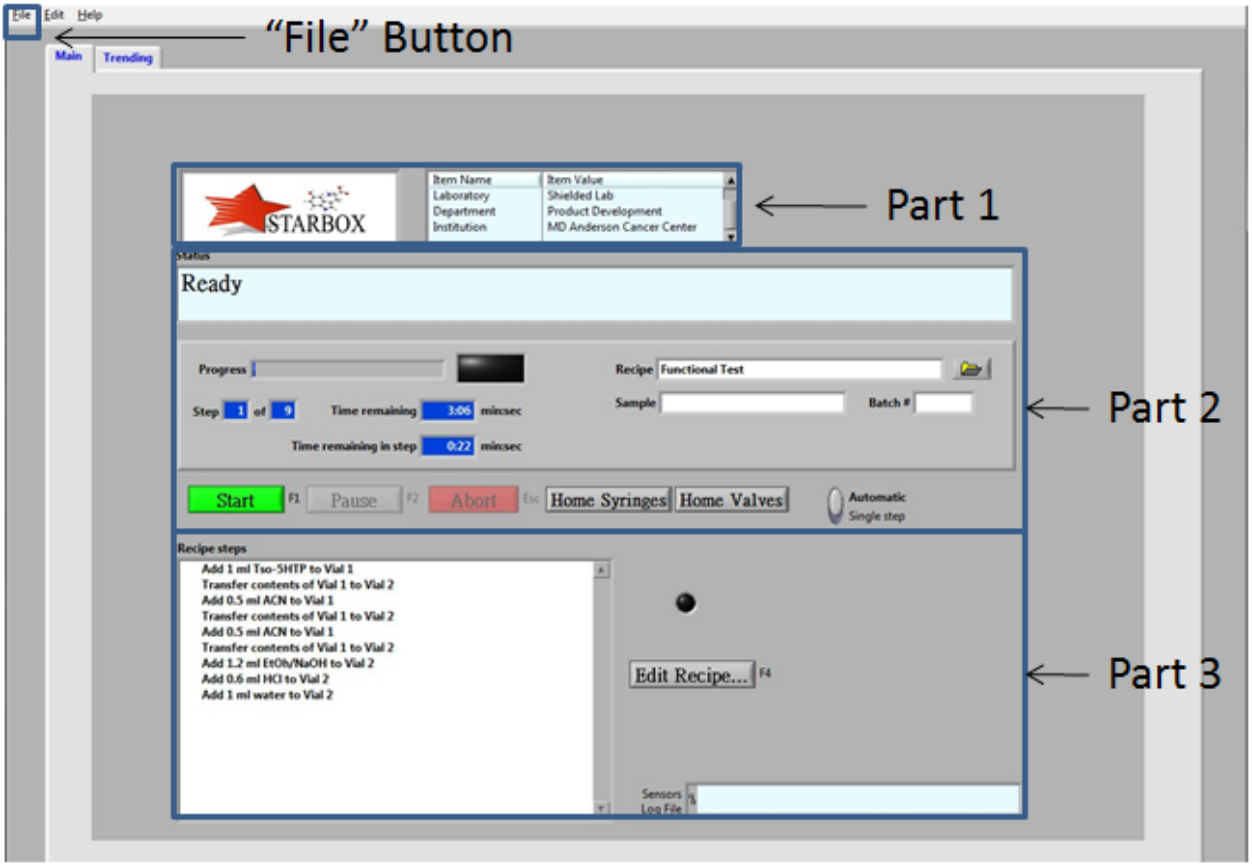

Figure 3.18 Main control panel

This is the overview of the main control panel (Figure 3.18). This panel is divided by three parts, and the function of each part is described in the following paragraph. Every time the user begins a new synthesis recipe, he should click the file button in the upper left of this panel, and choose the reagent setup function.

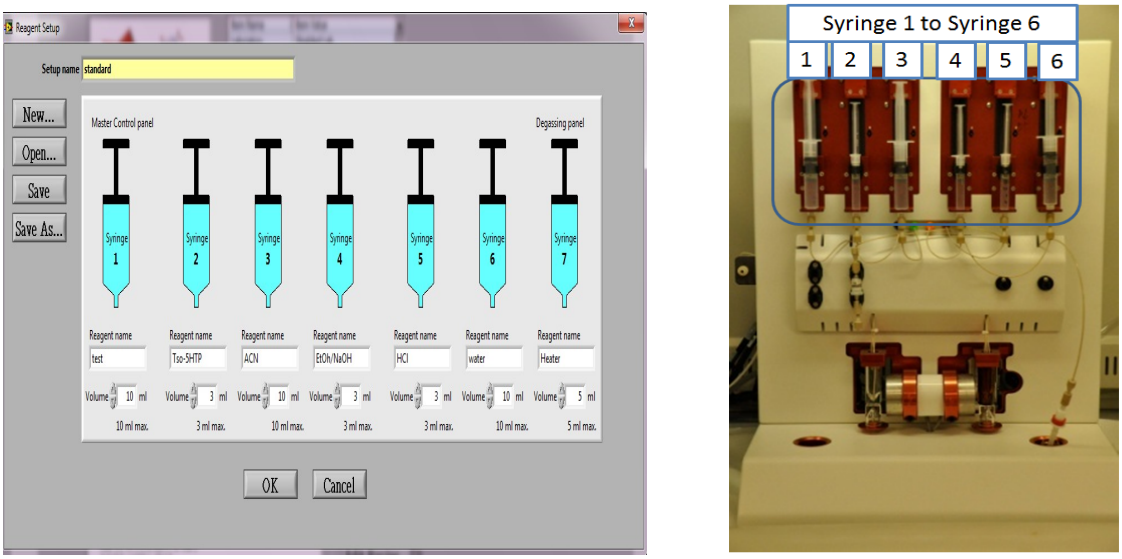

Figure 3.19 Reagent setup panel and its correspondent components in the synthesizer

In the reagent setup (figure 3.19), the user can type the information of syringes in the synthesizer which includes the chemical name, and its initial volume. Based on different synthesis recipes, there would be different reagent setup. The user also can create new a reagent setup, open a previous reagent setup, edit the current reagent setup, or save a new reagent setup via this user interface. Without this step, the automated synthesis can't process correctly.

Main control panel _ part 1

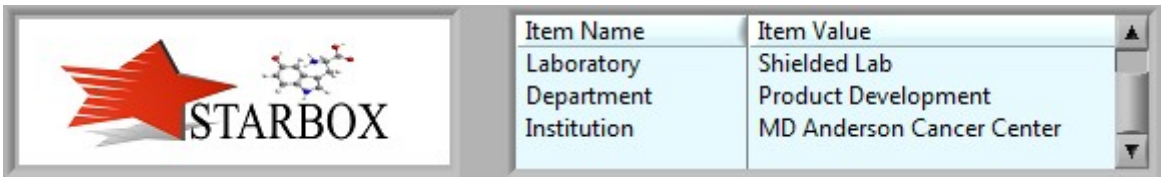

Figure 3.20 Main control panel _ part 1

This is the general information of this module, including its temporary logo, location, facility.

Main control panel _ part 2

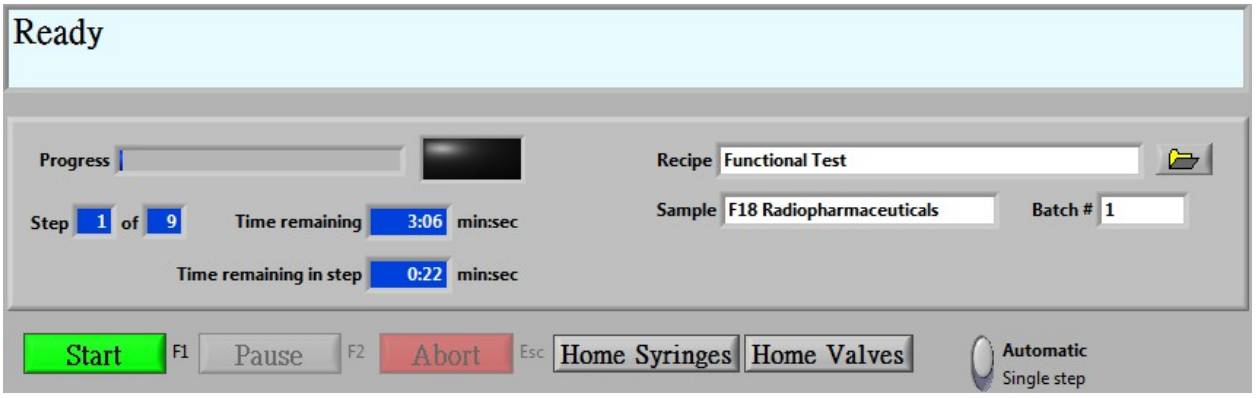

Figure 3.21 Main Control Panel _ Part 2

This upper part of this picture is a dialogue window, and the user can know the current process in this synthesizer. The middle left part of this picture is the information of total synthesis process, including the step of process, the total synthesis time, and the remaining time. The middle right part of this picture can allow users to choose the recipe by clicking the file icon. Under the recipe dialogue, it's the user-defined sample information, and the user-defined number of batch. The bottom part of this picture are the action buttons, including Start, Pause, Abort, Home Syringes, Home Valves, and Automatic/Single step. Once the recipe and its parameters are determined, user should click "Home Syringes", and "Home Valves" buttons to set hardware into the default condition. After that, depending on the demands, user can choose run this recipe automatically or step by step. Right now, the user can click "Start" button to begin the

synthesis process. During the process, the user can click “Pause” or “Abort” to stop the current process or terminate the synthesis.

Main control panel _ part 3

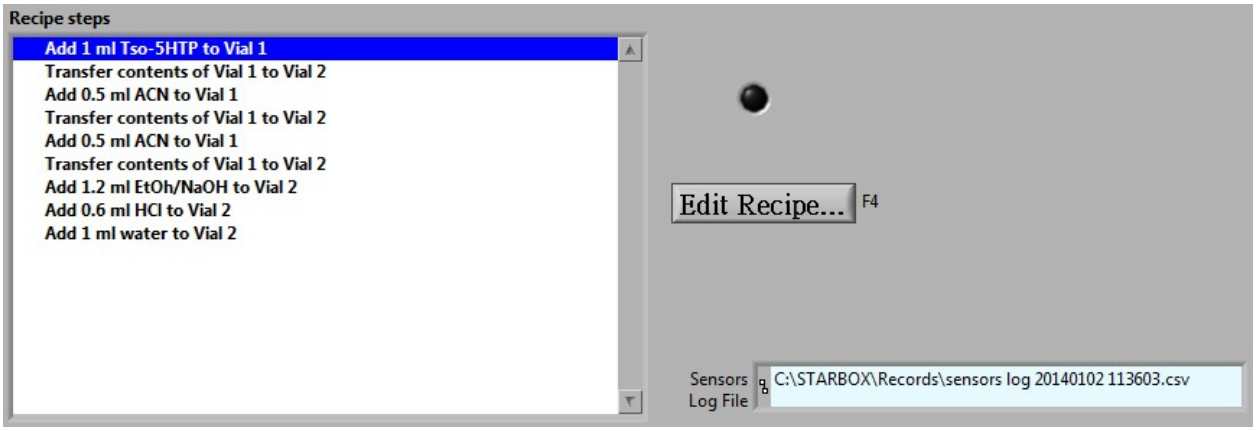

Figure 3.22 Main control panel _ part 3

The button of the main control panel can show the each process of this recipe, allow users to edit the recipe, and show the sensor log file. After the user click “Edit Recipe…” button, the user can edit the recipe in the recipe editor.

3.5.2.2 Recipe edit panel

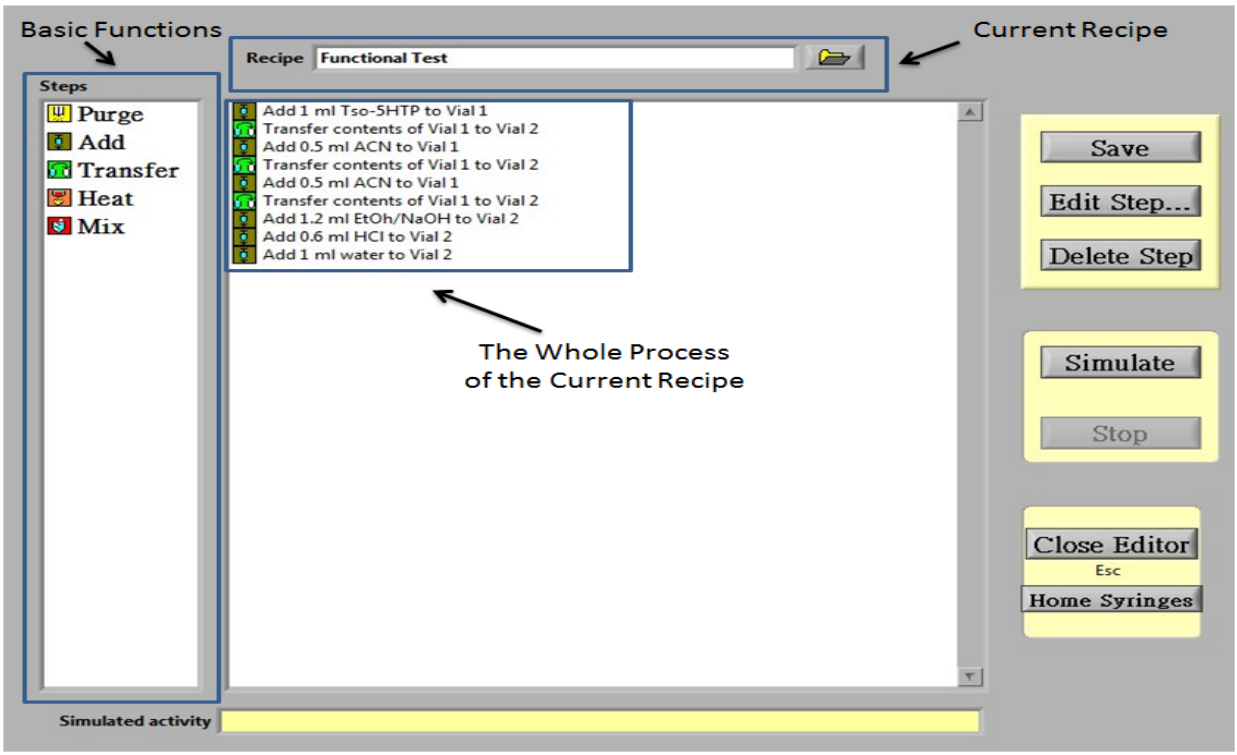

Figure 3.23 Recipe edit panel

The top window shows the current recipe, and the user can change the recipe by clicking “file” icon. The left window shows the five basic function of this automated synthesizer. The middle window shows the whole process of the current recipe. The left parts are the icons, which can save the recipe, edit the step, delete step, simulate the recipe, close the recipe editor, and home syringes.

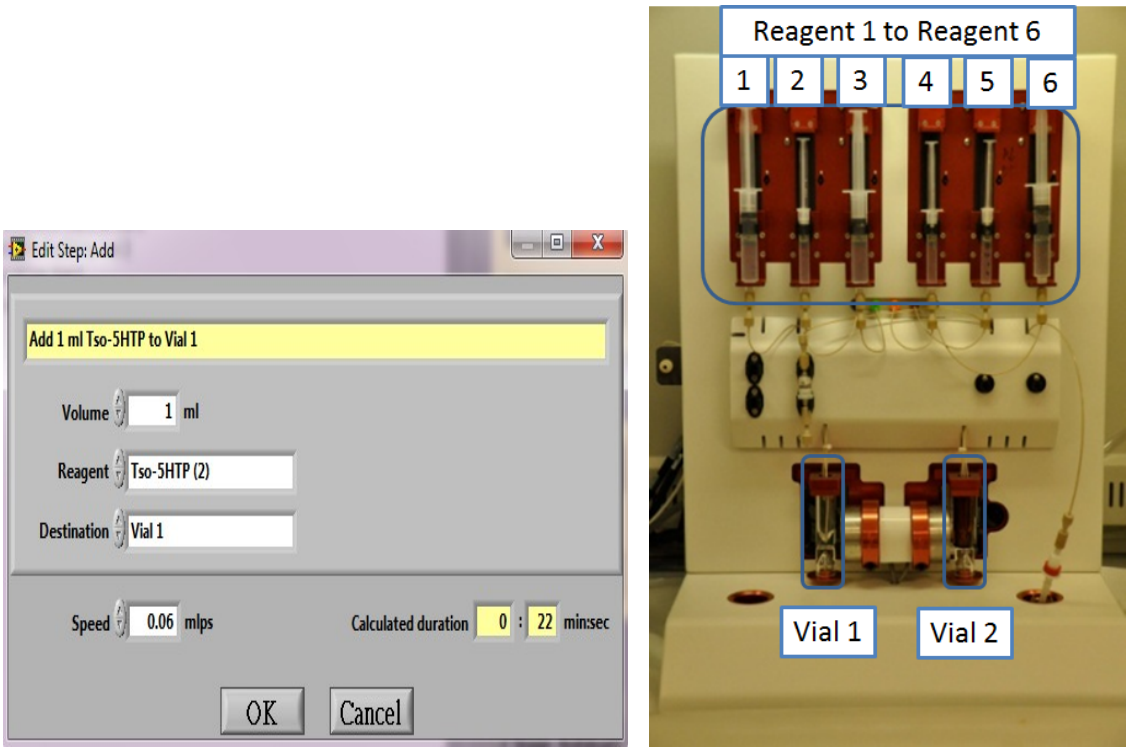

Figure 3.24 "Add" panel and its correspondent components

This basic function, "add" is to transfer the reagent from the syringe to the vial with different flow rates. In this user interface, the user can control four different parameter, injection volume, reagent source, destination, and injection speed. The injection volume and regents would be restricted by initial setting in the reagent setup. The displayed number in the reagent window indicates the actual syringe in this synthesizer. The injection speed is between 0.01 to 0.1 (ml/sec). Based on the speed, the duration can be calculated in this panel.

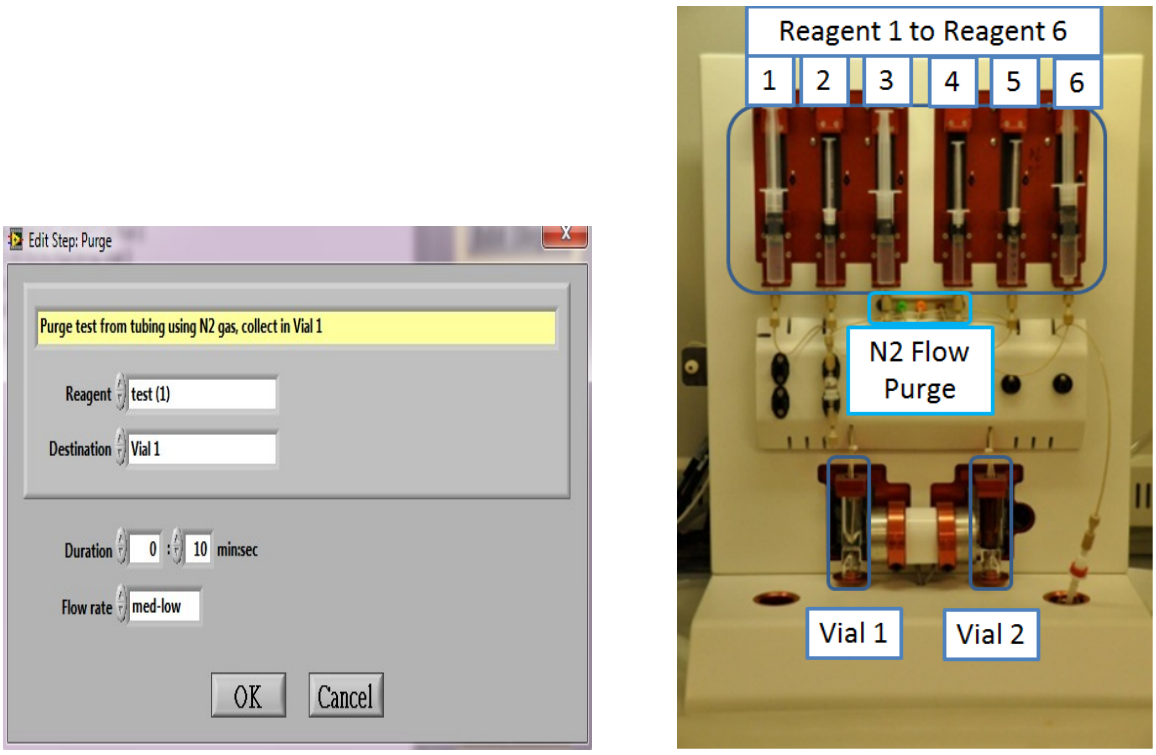

Figure 3.25 "Purge" panel and its correspondent components

After the reagent injected into the vial by the syringe, there are some residual solution in the flow channel. The function, "Purge", can use N_2 flow in different speed to take these residuals into the vial. In this user interface, the user can control four parameters, reagent source, destination, duration, and flow rate. The options of the reagent and the destination in this function are identical to the "add" function. The user can set the suitable duration of "purge", and different N2 flow rate, such as high (200 ml/sec), med-high (180 ml/sec), med(140 ml/sec), med-low(100 ml/sec), and low(50 ml/sec).

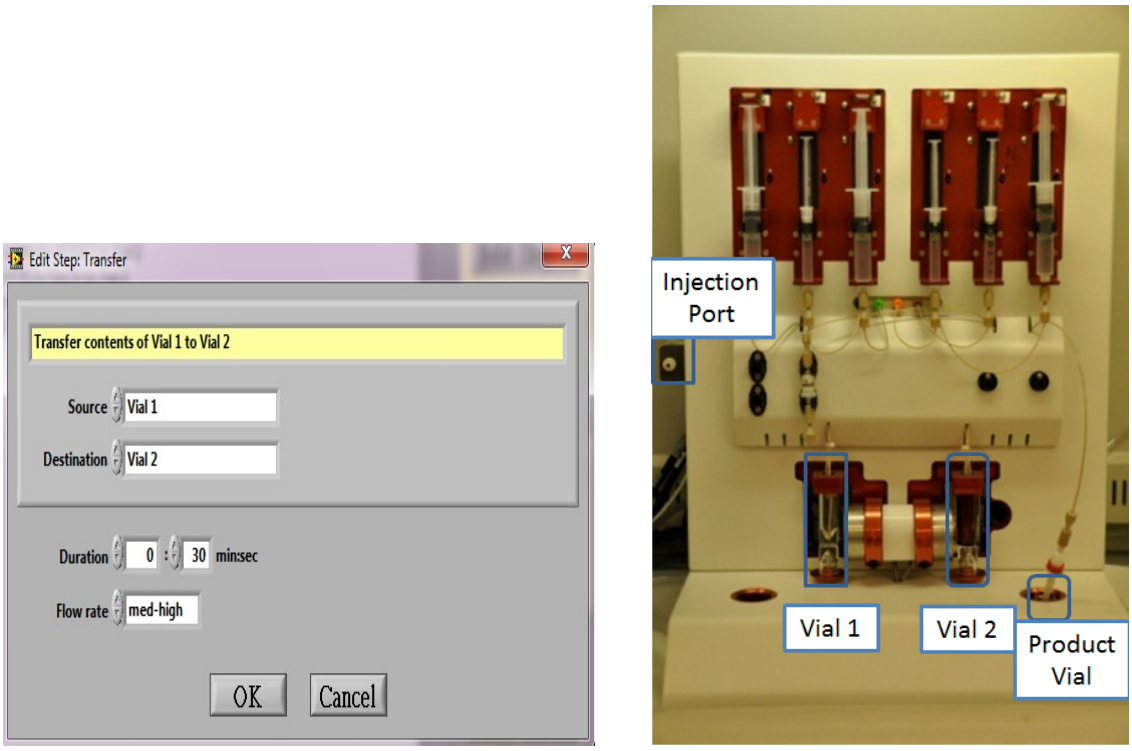

Figure 3.26 "Transfer" panel and its correspondent components

Based on the source and the destination, there are three different options of "transfer" step, from injection port to vial 1, from vial 1 to vial 2, and from vial 2 to product vial. The user can optimize the performance of "transfer" by changing the parameters, duration and flow rate.

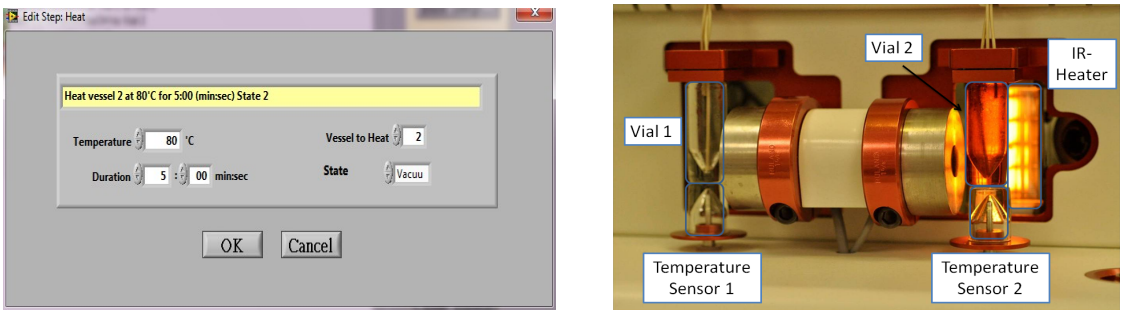

Figure 3.27 "Heat" panel and its correspondent components

There are four parameters of this “heat” function, heating temperature, heated vial, heating duration and addition states. Currently, the working temperature is adjusted from 65°C to 85°C. Two reaction vials, Vial 1 and Vial 2, can be heated by the IR-heater which is installed on the horizontal stepper motor, and this stepper motor can move this IR-heater to different locations on this synthesizer. Based on the different conditions of reactions, users can change the heating duration for the optimization of the end of synthesis radiation yield. There are three different conditions of “state”, vacuum, vent, and off. The “vacuum” can turn the vacuum pump to evaporate the solvents. The “vent” can cause the one channel of the vial open to the outside, and this aspect is used to maintain the pressure balance inside the vial when the vial is heated at high temperature or for longer heating duration. The “off” can maintain the solvent volume inside the vial when the vial is under heating.

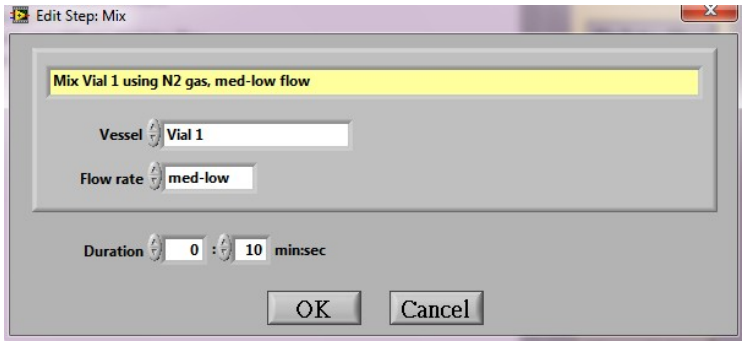

Figure 3.28 “Mix” panel

There are three parameters in “Mix” function, vial, flow rate, and duration. The user can choose the selected vial with different flow rates and different durations for optimization of the synthesis process.

3.5.2.3 Trending panel

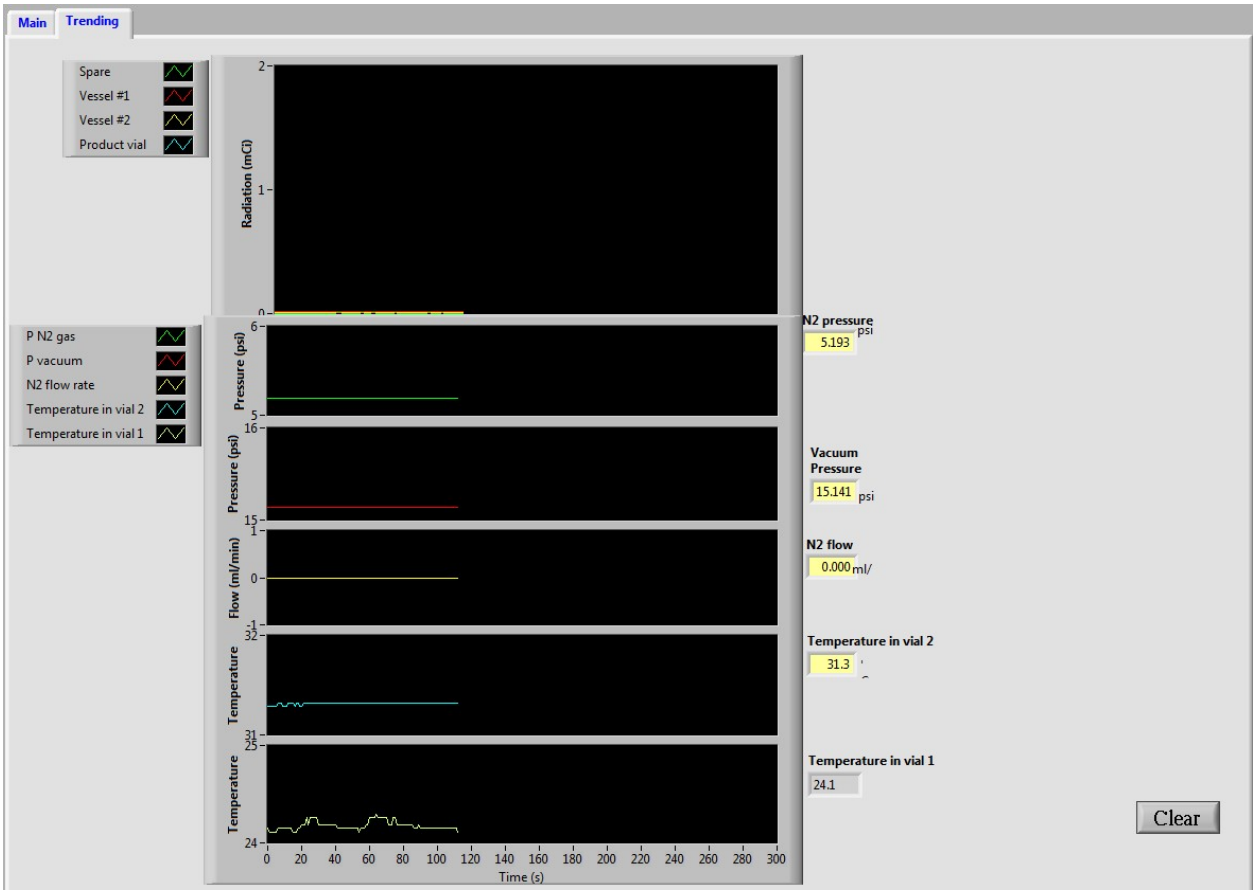

Figure 3.29 Treading panel

The Trending panel displays real-time graphic data from the radiation sensors, vacuum pump pressure, nitrogen flow, and reaction vial temperature, and these data are sampled in every five seconds. When the user begin the automated synthesis, these information could automated saved into an excel file.

4 Chapter 4 Validation of this multi-purpose synthesis module

4.1 Overview of this chapter

Molecular imaging can detect the cellular changes before these changes cause malformed tissue structures. Furthermore, molecular imaging can provide the information about not only tumor localization, but also tumor characterization (79). The most common radiotracer for staging tumors is ^{18}F-FDG (80). Diagnosis of cancers by ^{18}F-FDG PET is based on the observation on the difference of ^{18}F-FDG accumulation between normal and abnormal tissues caused by irregular glucose metabolism including overexpression of glucose transporter 1 and/or enhanced type 2 hexokinase activities (81). However, ^{18}F-FDG PET has several limitations that give rise to false positive/negative results. Therefore, it is amenable to develop different radiotracers as alternatives for better differentiation in tumor imaging. Overexpression of glucose transporter 1 glycosylation and large amino transporter 1 are discovered in various progressive cancers (82, 83). In this study, a glucose analog, glucosamine, and large amino acids, alpha-methyl-p-tyrosine and tryptophan, are selected to be radiolabeled.

The hardware and the software of this automated multi-purpose synthesis module were described in previous chapters. In this chapter, the manual synthesis of reference compounds of these three different radiopharmaceuticals, ^{68}Ga-ECG, ^{18}F-FPAMT, and ^{18}F-FTP, were determined and qualitative analyses of reference compounds were confirmed. After that, manual radiosynthesis recipes of the radiopharmaceuticals were

established, and the radiochemical purity were determined. Then, this automated multi-purpose synthesis module was validated by production of these three radiopharmaceuticals.

4.2 Synthesis of $^{68/69}$Ga-ECG

4.2.1 Synthesis of ECG

The total synthesis scheme of $^{68/69}$Ga-ECG is shown in Figure 4.1. To a solution of thiazolidine-4-carboxylic acid (T) (2.6 g, 0.02 mol) in DMF (20 mL) and 5.0 mL trimethylamine, 1-hydroxybenzotriazole hydrate (2.7 g, 0.02 mol) was added. After 30 min, 1,3,4,6-tetra-O-acetyl-2-amino-α-D-glucopyranose hydrochloride (G-$(Ac)_4$) (7.7 g, 0.02 mol), N,N-di-cyclohexylcarbodiimide (DCC, 4.2 g, 0.02 mol), and 4-dimethylaminopyridine (DMAP, 1.2 g, 0.01 mol) were added to the mixture and stirred for overnight at room temperature. The solution was evaporated to dryness at high vacuum. Dichloromethane (50 mL) was added to the residual and kept at 4°C for overnight, then filtered. The product was purified with silica gel by eluting with CH_2Cl_2/MeOH (95:5, v/v) to yield white product T-G-$(Ac)_4$ 4.08 g (44.2%). NMR and mass spectrometry were used to confirm the structure of T-G-$(Ac)_4$. Sodium was added piece

by piece to a solution of T-G-$(Ac)_4$ (4.08 g, 8.8 mmol) in liquid ammonia (170 g). The color of the solution was slowly changed to dark blue. After 30 minutes, a little of ammonium chloride was added. The liquid ammonia was removed by reduced pressure. The residual solid was triturated with methanol (100 mL). The solid was then filtered and washed with additional methanol (50 mL) to yield crude product 4.16 g. To obtain analytical pure ethylenedicysteine-glucosamine (ECG), the crude product (0.1 g) was dissolved in HCl (0.1 N, 1.0 mL) and purified with a sephadex column by eluting with H_2O. The aqueous fractions were combined and lyophilized to yield ECG (0.029 g, 46.7%). HPLC shows that purity is over 82%. NMR and HPLC were used to confirm the structure

and the purity of ECG. HPLC of cold ECG was in Figure 4.2. 1H NMR (D_2O,): 3.15–3.20

(m, 4H), 3.78–4.05 (m, 6H), 4.08–4.15 (m, 8H), 4.2-4.3 (d, 2H), 4.68–4.73 (d, 2H), 5.19–5.21 (d, 2H).

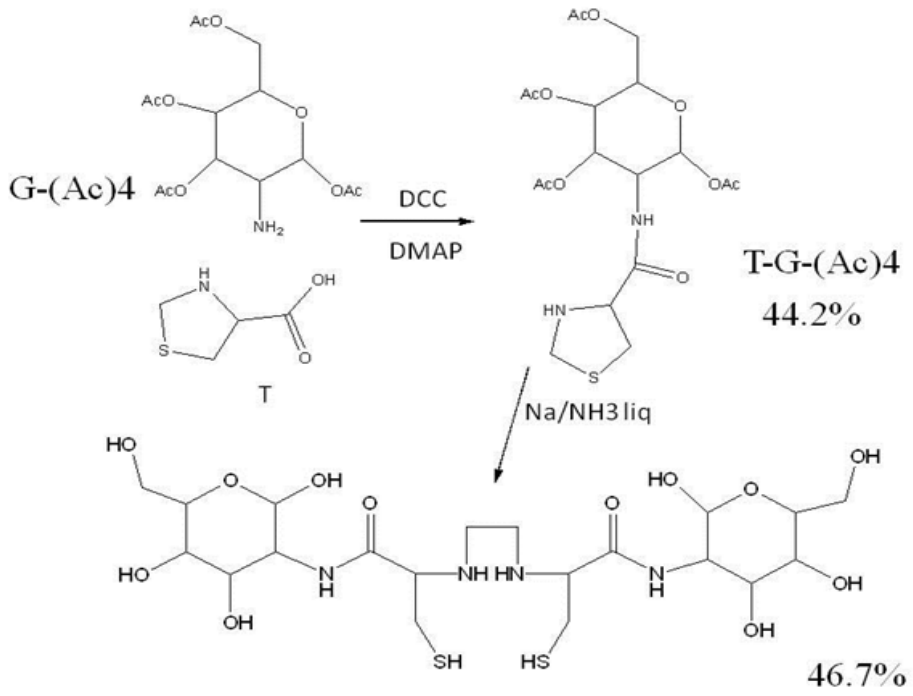

Figure 4.1 Synthesis scheme of ECG

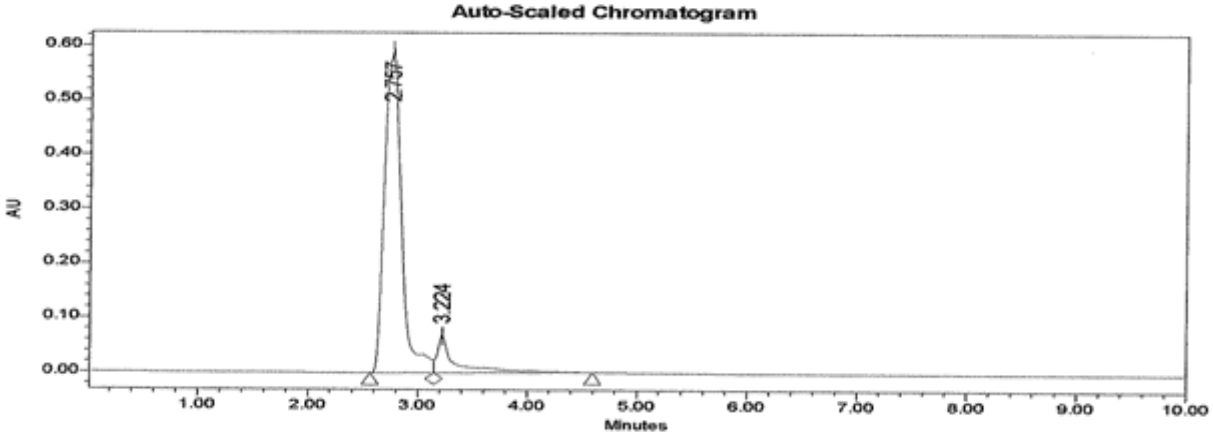

Figure 4.2 HPLC analysis of ECG

4.2.2 Synthesis of ^{69}Ga-ECG

$^{69}GaCl_3$ (20 mg, 0.11mmol) in H_2O (0.2 mL) was added to a solution of ECG (60mg, 0.1mmol) in H_2O (0.5 mL). The pH value was adjusted to 4-5 with NaOH (0.1N, 50 µl). The solution was heated for 30 min at 60°C. The product was purified by a sephadex column eluting with H_2O to yield ^{69}Ga-ECG. After lyophilization, ^{69}Ga-ECG was obtained as white solid (52mg, 78.1%). NMR, and HPLC were used to confirm the structure and the purity of ^{69}Ga-ECG. NMR of cold ^{69}Ga-ECG was in Figure 4.3. 1H NMR (D2O, □): 2.94–3.38 (m, 8H), 3.43–3.65 (m, 4H), 3.50–3.80 (m, 10H), 3.92–4.02 (t, 2H), 4.23–4.34 (d, 2H), 5.15–5.34 (d, 2H).

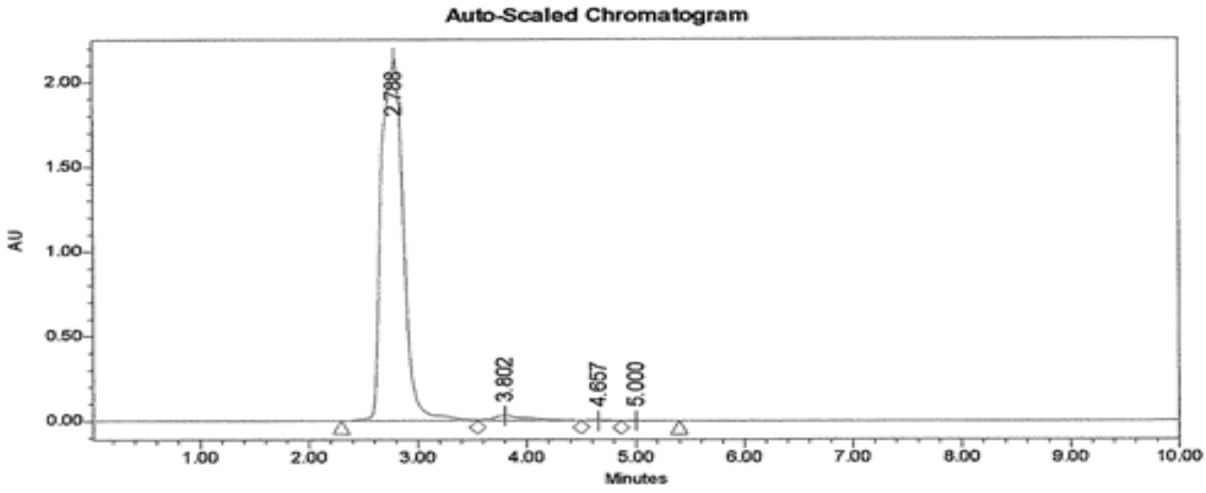

Figure 4.3 HPLC analysis of ^{69}Ga-ECG

4.2.3 Manually synthesis of ^{68}Ga-ECG

$^{68}GaCl_3$ was obtained from a $^{68}Ge/^{68}Ga$ generator (Eckert Ziegler, Valencia, CA) eluted with 0.1 N HCl. $^{68}GaCl_3$ (120 μL, 300 μCi) was added to the solution of ECG (1.2 mg) in H_2O (0.1 mL), and pH value was adjusted to 4-5 with $NaHCO_3$ (40 μL, 0.1 N). The solution was heated at 65°C for 15 min. Radio-TLC analysis of the purity of ^{68}Ga-ECG was > 90% (Figure 4.3).

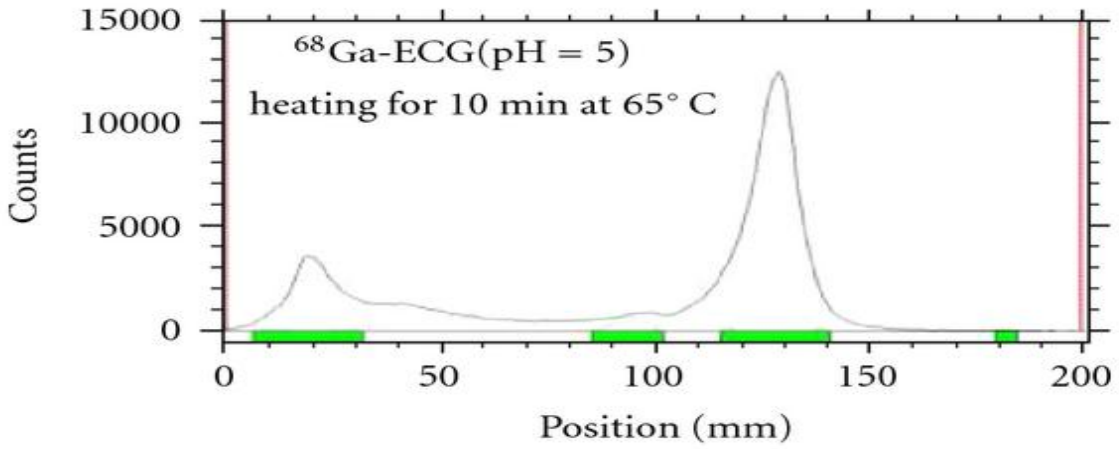

Figure 4.4 Radio-TLC analysis of ^{68}Ga-ECG by manual synthesis

4.2.4 Automated Synthesis method of ^{68}Ga-ECG

ECG (1.3mg) was preload into the reaction vial 1 (RV1) of the automated module, and $^{68}GaCl_3$ (1mL, 5.40 mCi) was loaded into the RV1 from manual injection port. Then, the solution of $NaHCO_3$ (200 µL) injected into the reaction vial 1 from the injection panel, and pH value was adjusted to 4-5. After that, the RV1 was heated at 70°C for 15 minutes. The final step was to transfer the solution in the RV1 to the final product vial. The automated recipe of ^{68}Ga-ECG synthesis is shown in Figure 4.4. Radio-TLC analysis of the purity of ^{68}Ga-ECG was > 90% (Figure 4.5).

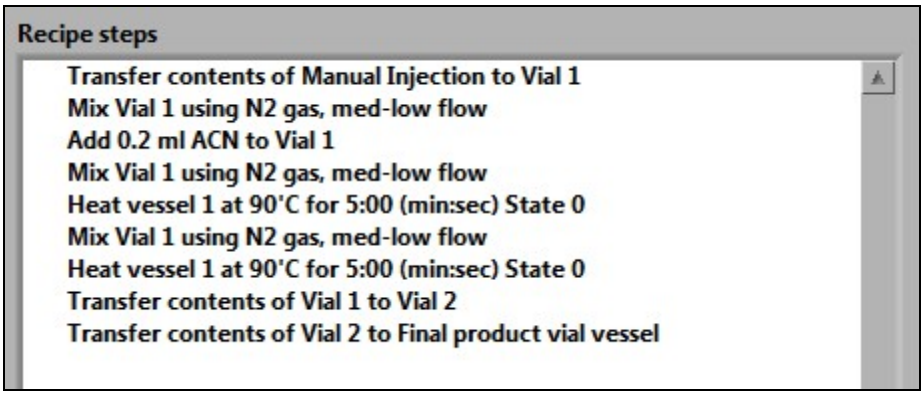

Figure 4.5 Automated synthesis recipe of ^{68}Ga-ECG

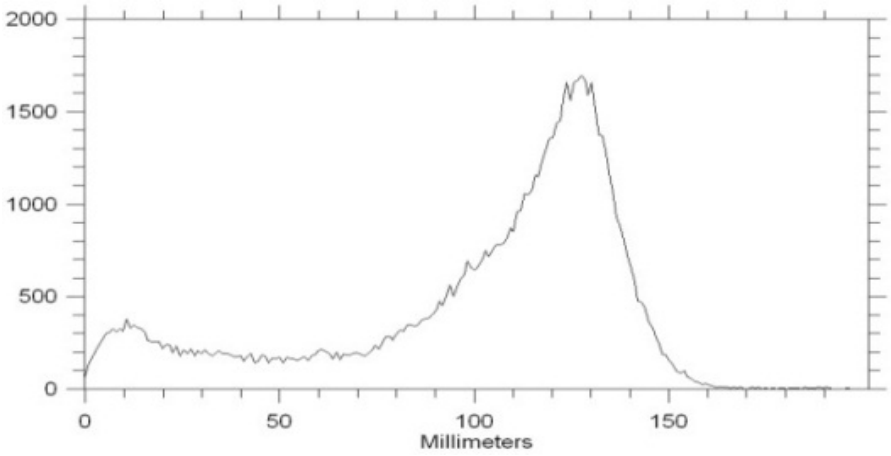

Figure 4.6 Radio-TLC analysis of ^{68}Ga-ECG by automated synthesis

4.3 Synthesis of $^{18/19}$F-FPAMT

4.3.1 Synthesis method of ^{19}F-FPAMT

N-t-butoxycarbonyl-O-[3-hydroxypropyl]-α-methyl tyrosine ethyl ester (490 mg; 1.28 mmol) in anhydrous pyridine (32 mL) was cooled to 0°C. Paratoluenesulfonyl chloride (1015 mg; 5.32 mmol) was added to this solution, and the solution was stirred for 30 min. After it filtered, the filtrate was poured into iced water and extracted with diethyl ether. The ethereal solvent was washed with 30 mL of hydrochloric acid and water (1 : 1, v/v) to remove pyridine, and the solvent was dried over anhydrous $MgSO_4$. After filtration and solvent evaporation, N-t-butoxycarbonyl-O-[3-tosylpropyl]-α-methyl tyrosine ethyl ester (Tso-PAMT/BOC/Ester) was purified by column chromatography using a silica gel column and eluted with hexane and ethyl acetate (2 : 1, v/v) to yield 430 mg (62.5%). NMR, and Mass Spectrum were used to confirm the structure and the purity of Tso-PAMT/BOC/Ester shown in Figure 4.6 and Figure 4.7. ^{1}H NMR ($CDCl_3$) δ=7.78 (d, 2H, J=8.10 Hz), 7.28 (d, 2H, J=5.70 Hz), 7.00 (d, 2H, J=8.70), 6.70 (D, 2H, J=8.70), 4.24 (dd, 2H, J=5.70), 4.17 (t, 2H, J=21.3), 3.96 (t, 2H, J= 11.70), 3.17 (d, 2H, J=13.8), 2.41 (s, 3H), 2.13 (dd, H, J=12.00). 1.56 (s, 3H), 1.49 (s , 9H) 1.33, (t, 3H, J=21.9 Hz) ppm.

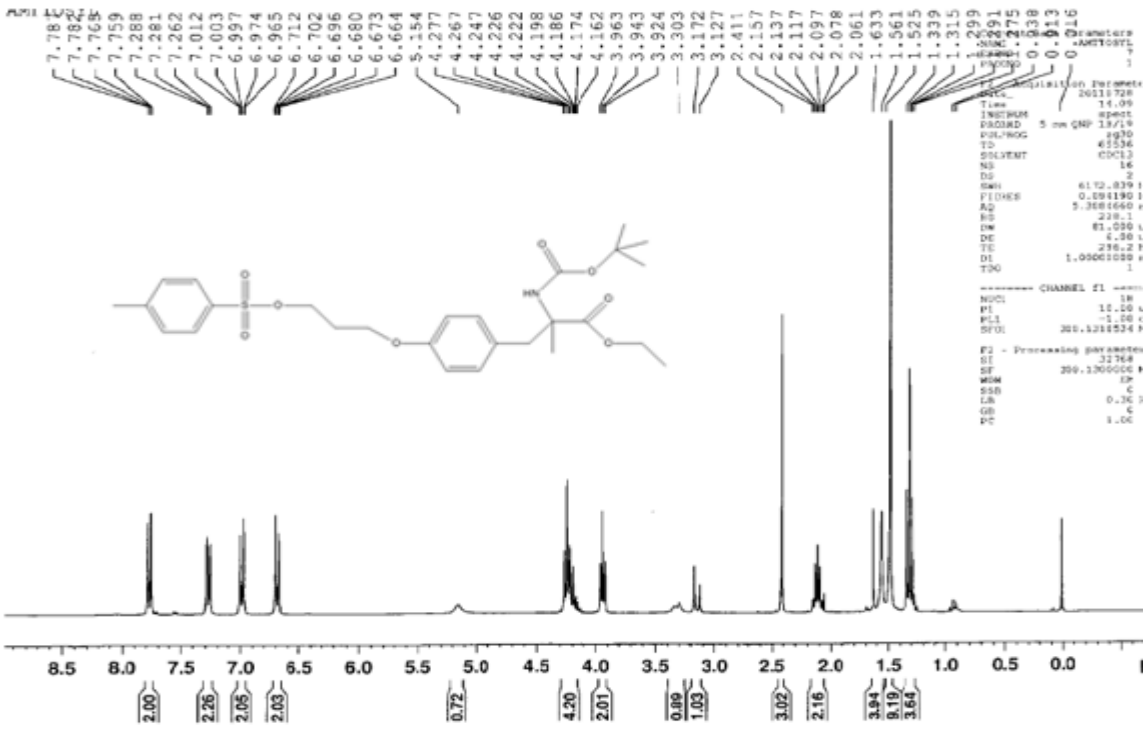

Figure 4.7 NMR of Tso-PAMT/BOC/Ester

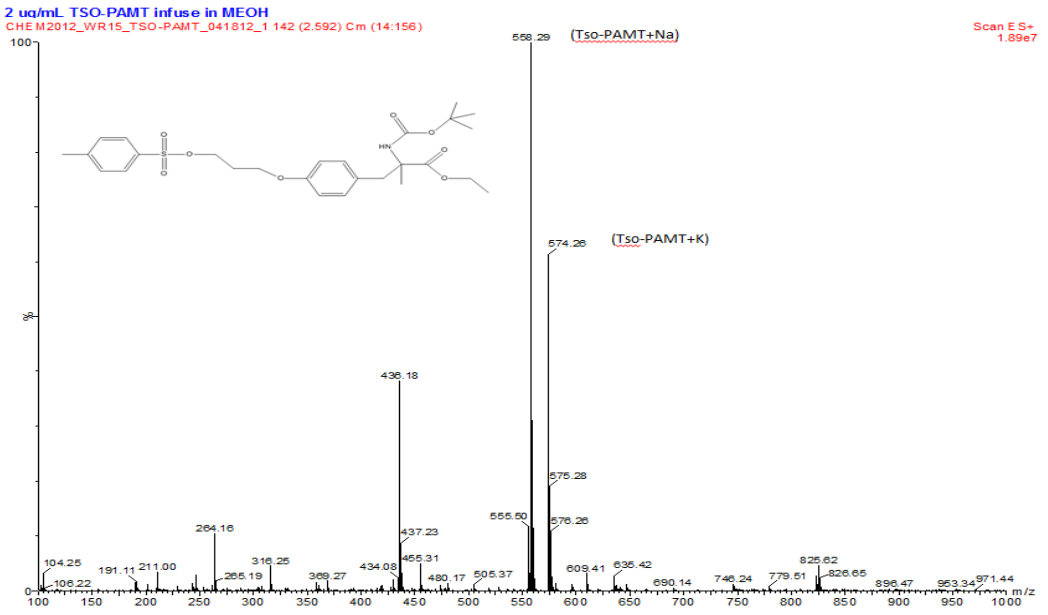

Figure 4.8 Mass spectrum of Tso-PAMT/BOC/Ester

Synthesis of ^{19}F-FPAMT was carried out by three steps (Figure 4.8). The displacement reaction is the first step. Kryptofix 222 (253.9 mg; 0.67 mmol) and K^{19}F (40.5 mg; 0.69 mmol) were added to a vial containing N-t-butoxycarbonyl-O-[3-tosylpropyl]-α-methyl tyrosine ethyl ester (compound 1; 390 mg; 0.75 mmol) in acetonitrile (1 mL). The reaction vial was heated under reflux at 90°C for 40 min. After heating, the solution was evaporated to dryness. The mixture was reconstituted in ethyl acetate (0.5 mL). N-t-butoxycarbonyl-O-[3-^{19}F-fluoropropyl]-α-methyl tyrosine ethyl ester (compound 2) was purified by column chromatography using a silica gel column and eluted with hexane and ethyl acetate (4 : 1, v/v) to yield 120.0 mg of the compound. The second step was to deprotect butoxycarbonyl (BOC), and the third step was to remove ethyl ester groups. O-[3-^{19}F-fluoropropyl]-α-methyl tyrosine ethyl ester (compound 3) was synthesized by reacting N-t-butoxycarbonyl-O-[3-^{19}F-fluoropropyl]-α-methyl tyrosine ethyl ester (compound 2; 82.3 mg; 0.30 mmol) with trifluoroacetate (0.7 mL) in dichloromethane (2.0 mL) at room temperature for 50 min. After the solvent was evaporated to dryness, sodium hydroxide (1 N; 1.0 mL) in methanol (1.0 mL) was added, and the mixture was heated at 90°C for 15 min to remove ethyl ester group. The mixture was passed through a 0.22 μM filter to yield ^{19}F-FPAMT (compound 4). NMR, and Mass Spectrum were used to confirm the structure and the purity of ^{19}F-FPAMT in Figure 4.9 and Figure 4.10.

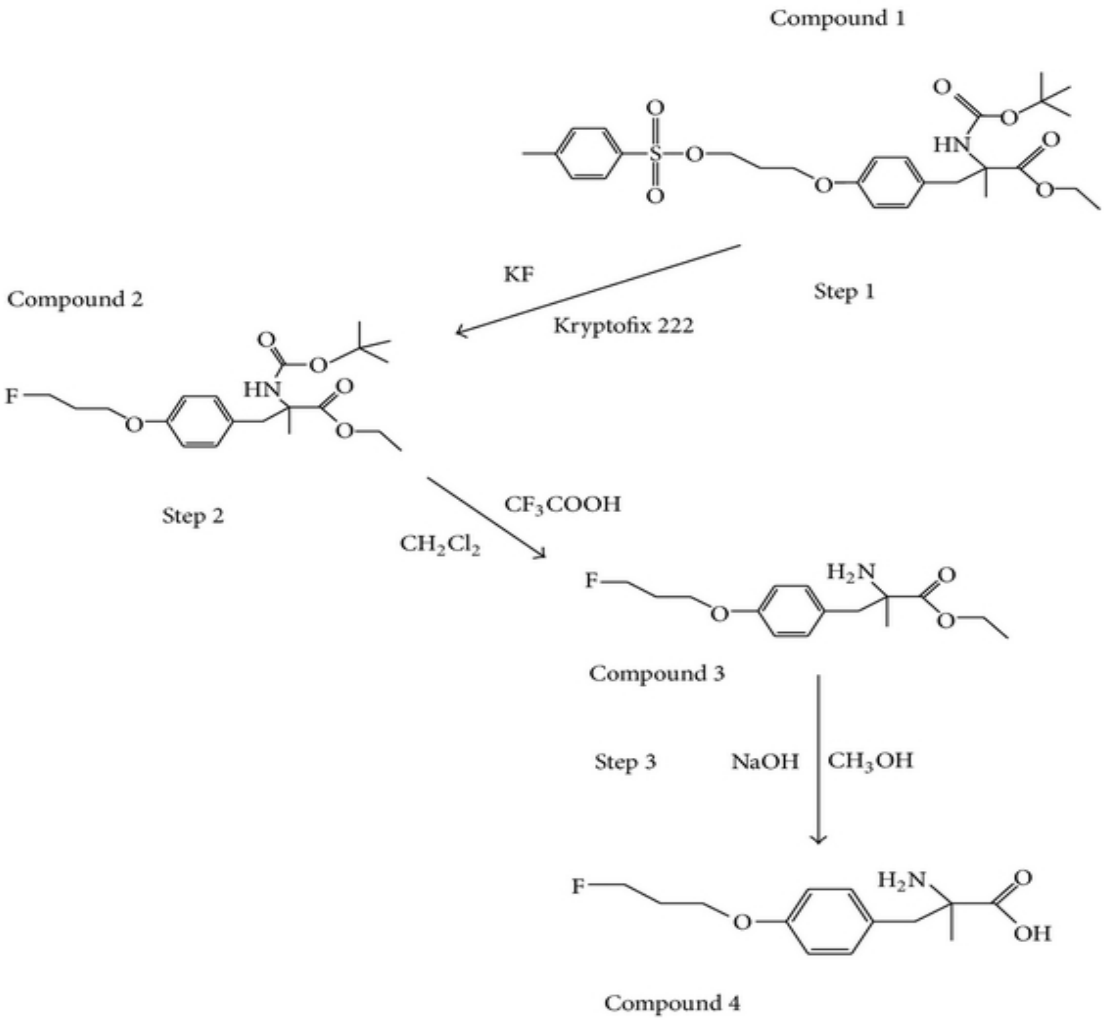

Figure 4.9 Synthesis scheme of $^{18/19}$F-FPAMT

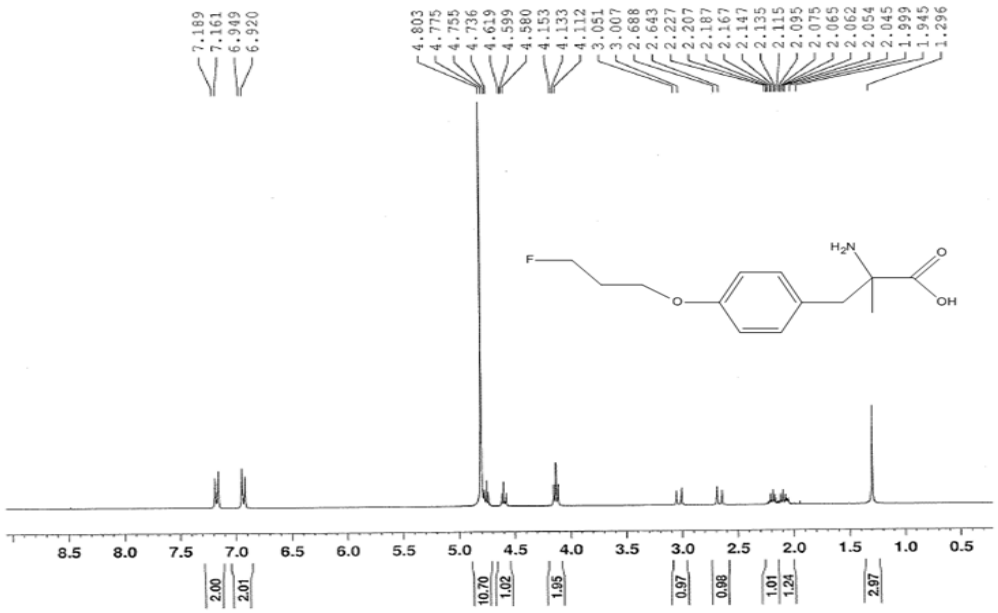

Figure 4.10 NMR analysis of ^{19}F-FPAMT

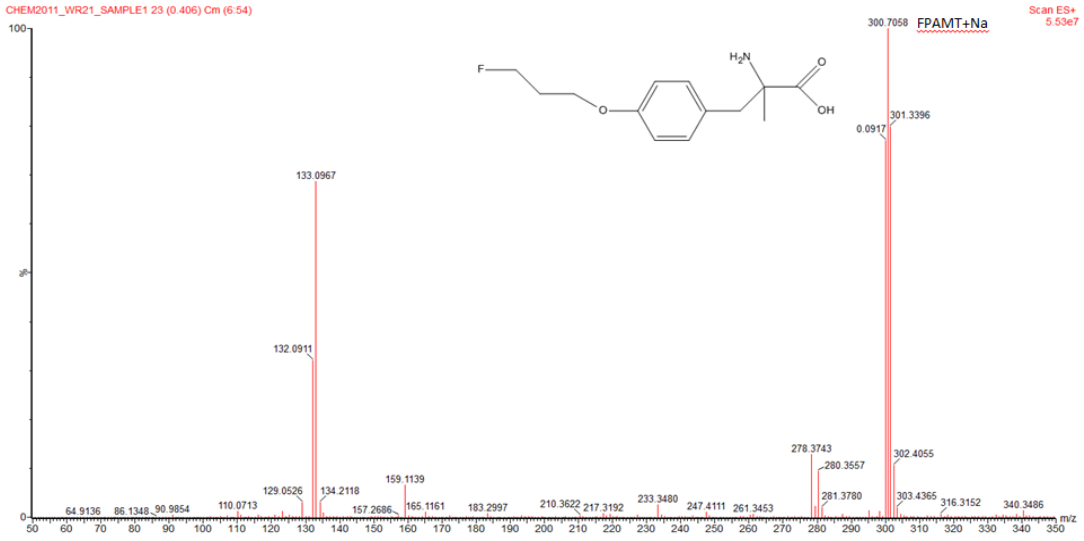

Figure 4.11 Mass spectrum of ^{19}F-FPAMT

4.3.2 Manually synthesis of ^{18}F-FPAMT

[^{18}F]Fluoride in kryptofix complex (100 mCi in 0.3 mL acetonitrile) was purchased from the cyclotron facility of Cyclotope (Houston, TX, USA). N-t-butoxycarbonyl-O-[3-tosylpropyl]-α-methyl tyrosine ethyl ester (2.0 mg; 3.83 µmol) dissolved in acetonitrile (0.1 mL) was added to the [^{18}F]fluoride-kryptofix complex (51.5 mCi). The reaction mixture was heated at 90°C for 15 min to allow the displacement to occur. After the reaction mixture cooled, it was passed through a 500 mg silica gel packed SPE column (Whatman Lab., Clifton, NJ, USA) and eluted with acetonitrile (2.0 mL). The acetonitrile was then evaporated in vacuo at 85°C. The resulting mixture was hydrolyzed with trifluoroacetate (0.2 mL) in dichloromethane (0.2 mL) at room temperature for 10 min to deprotect BOC. After the solvent was evaporated to dryness in vacuo, sodium hydroxide (1 N; 0.2 mL) in methanol (0.2 mL) was added and heated at 90°C for 15 min to remove ethyl ester group. After methanol evaporated, hydrochloric acid (0.1 N; 0.2 mL) was used to adjust the pH of the final product to 6.5. Radio-TLC was performed to assure the radiochemical purity of ^{18}F-FPAMT (Figure 4.11).

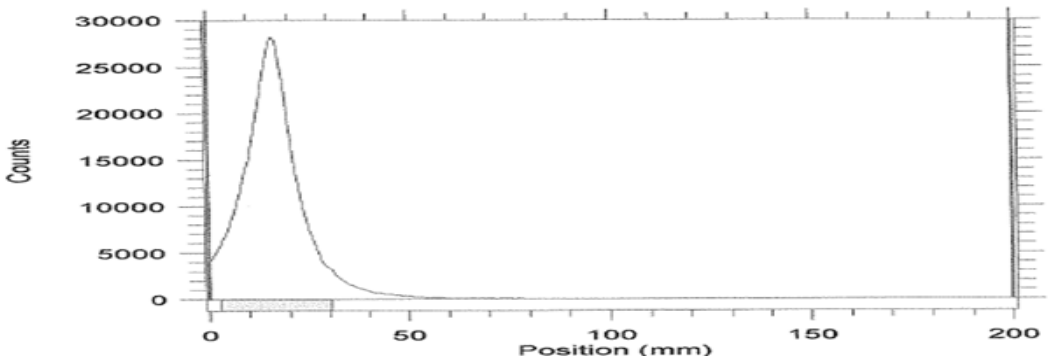

Figure 4.12 Radio-TLC analysis of ^{18}F-FPAMT by manually synthesis

4.3.3 Automated synthesis of ^{18}F-FPAMT

The automated radiosynthesis of ^{18}F-FPAMT was achieved by our customized automated module and its total synthesis recipe is shown in Figure 4.12. The automated radiosynthesis consisted of three steps: nucleophilic substitution, deprotection of BOC, and deesterification. Before radiosynthesis was completed, the reaction vial 1 (RV1) was preloaded with N-t-butoxycarbonyl-O-[3-tosylpropyl]-α-methyl tyrosine ethyl ester (6.2 mg; 11.8 μmol), and three syringes were loaded with different solutions: acetonitrile (3.0 mL), trifluoroacetate in dichloromethane (2.5 mL; 1 : 1, v/v), and 1N sodium hydroxide in ethyl alcohol (3.0 mL; 1 : 2, v/v). For the nucleophilic substitution, [^{18}F]fluoride-kryptofix complex (29.36 mCi, 0.2 mL) was manually injected into the RV1 through the injection hole, and additional acetonitrile (0.35 mL) was manually injected into the RV1 to flush the residual [^{18}F]fluoride-kryptofix complex inside the flow channel. Following this step, the infrared (IR) heater automatically heated the RV1 at 90°C for 15 min. For free fluoride separation, the mixture in the RV1 was automatically passed through a 500 mg silica gel packed SPE column (Whatman Lab., Clifton, NJ, USA) to the reaction vial 2 (RV2) via nitrogen flow. Additional acetonitrile (2.0 mL) was then added to RV1, and the residual mixture was filtered through a SPE column to remove the free fluoride. The solution inside RV2 was evaporated in *vacuo* at 90°C for 15 min before deprotection of BOC was performed. Trifluoroacetate in dichloromethane (0.4 mL; 1:1, v/v) was loaded into RV2, and the solution was set under room temperature for 10 min

to allow the reaction to finish. The solvent was then evaporated to dryness in *vacuo* for 15 min. For deesterification, 1N sodium hydroxide in methanol (0.6 mL; 1:1, v/v) was loaded into RV2. The reaction mixture in RV2 was heated at 90°C for 15 min. Once deesterification was completed, the solvent in RV2 was evaporated in *vacuo*, and the radioactivities of the solvent in the column, RV1, and RV2 were measured upon the completion of ^{18}F-FPAMT. Radio-TLC was performed to assure the radiochemical purity of ^{18}F-FPAMT (Figure 4.13).

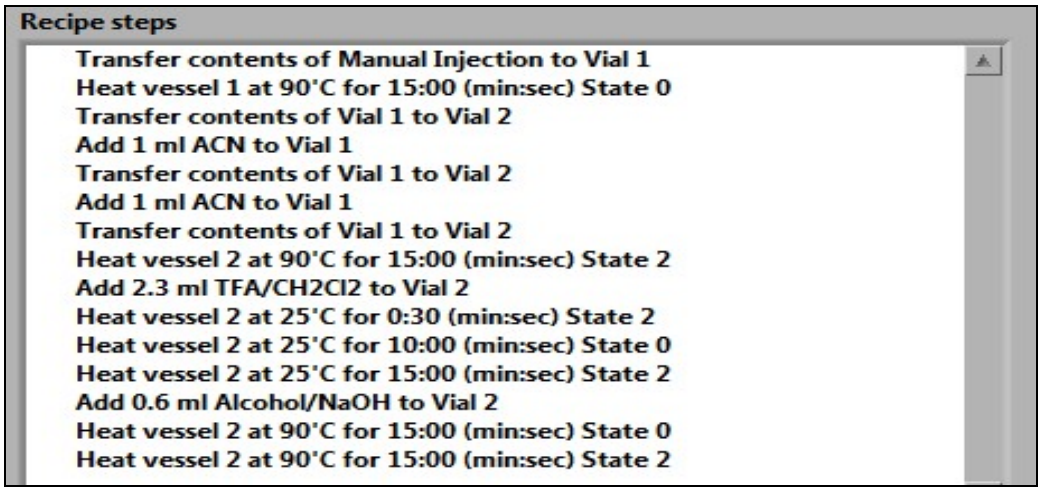

Figure 4.13 Automated synthesis recipe of ^{18}F-FPAMT

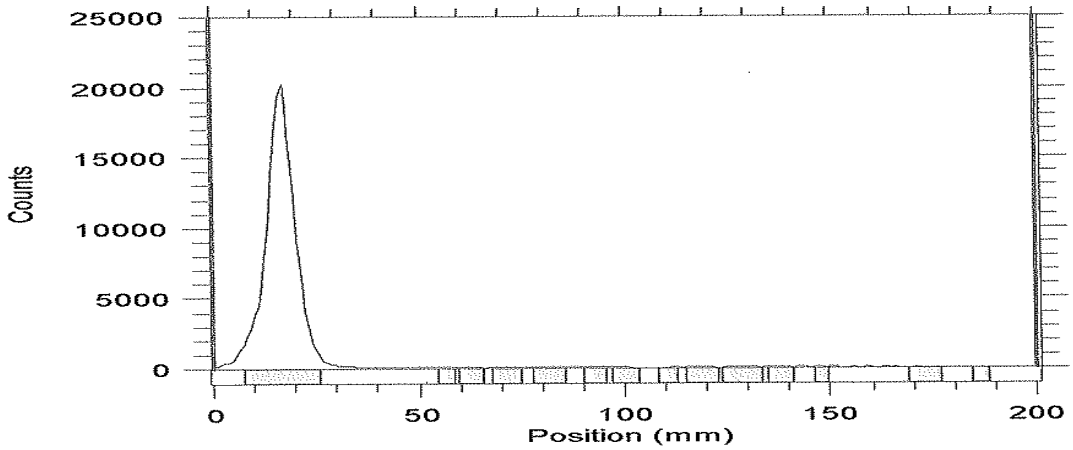

Figure 4.14 Radio-TLC analysis of ^{18}F-FPAMT by automated synthesis

4.4 Synthesis of $^{18/19}$F-FTP

4.4.1 Synthesis of ^{19}F- FTP

The synthetic scheme of [$^{18/19}$F]fluoropropoxytryptophan ($^{18/19}$F-FTP) is shown in Figure 4.14. Three steps were involved in the synthesis. In step 1, thionyl chloride ($SOCl_2$, 2.4 ml, 34 mmol) was dissolved in anhydrous methanol (100 ml) and cooled to 0°C. 5-Hydroxytryptophan (5.00 g, 22.7 mmol) was added in portions. After temperature returned to room temperature, the mixture was refluxed overnight. The solvent was evaporated, followed by silica-gel packed column chromatographic purification using ethyl acetate/hexane (4:1, v/v) as an eluent to yield 5-hydroxytryptophan methyl ester hydrochloride 5.18 g (84% yield). ^{1}H-NMR (300MHz, $CDCl_3$): 7.23 (d, J=8.7Hz, 1H), 7.15 (s, 1H), 6.91 (d, J=2.1Hz, 1H), 6.73 (dxd, J=8.7, J'= 2.3Hz, 1H), 4.29 (t, J=6.3, 1H), 3.83 (s, 3H),

3.26-3.42 (m, 2H). 13C-NMR (300MHz, $CDCl_3$): 169.8, 150.8, 132.2, 127.9, 125.4, 112.2, 112.1, 105.6, 102.1, 53.5, 52.7, 26.7.

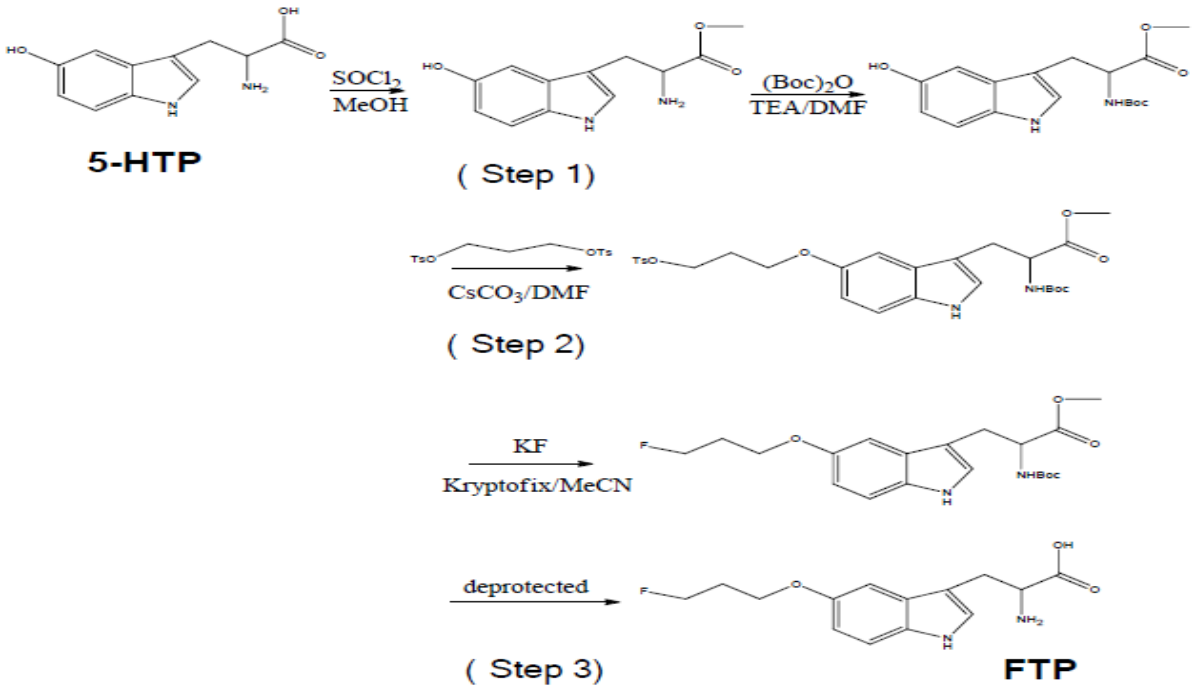

Figure 4.15 Synthesis scheme of $^{18/19}$F-FTP

Subsequently, 5-hydroxytryptophan methyl ester (2.4 g, 10 mmol) was dissolved in anhydrous dimethylformamide (DMF, 100 mL). Anhydrous triethyl amine (TEA, 4 ml, 30 mmol) was added while stirring. Ditertbutyl dicarbonate ($(Boc)_2O$, 2.6 g, 12 mmol) was then added to the solution. The mixture was stirred and heated at 60°C overnight. The reaction mixture was evaporated under reduced pressure and was reconstituted in ethyl acetate. The crude product solution was loaded on a silica gel column and eluted with ethyl acetate/hexane (from 1:3 to 2:3, v/v). N-Boc-5-Hydroxytryptophan methyl ester was collected after solvent evaporation to yield 3.08 g (92% yield). 1H-NMR

(300MHz, $CDCl_3$): 7.05 (d, J=8.7Hz, 1H), 6.90 (s, 1H), 6.84 (d, J=2.1Hz, 1H), 6.56 (dxd, J=8.7, J'= 2.3Hz, 1H), 4.30 (t, J=6.3, 1H), 3.56 (s, 3H), 2.90-3.10 (m, 2H), 1.29 (s, 9H).

In step 2, an aliphatic tosyl chain was to be added at phenolic hydroxyl group of N-Boc-5-hydroxytryptophan methyl ester. Cesium carbonate ($CsCO_3$, 3.9 g, 12 mmol) was added to N-Boc-5-hydroxytryptophan methyl ester (3.4 g, 10 mmol) in 60 ml of anhydrous DMF while stirring under nitrogen atmosphere. 1,3-ditosyl-propanol (6.2 g, 16 mmol) was added to the solution. The mixture was stirred for overnight at 60°C. The reaction mixture was evaporated under reduced pressure and was reconstituted in ethyl acetate. The crude product solution was loaded on a silica gel column and eluted with ethylacetate /hexane (from 1:3 to 2:3, v/v) to yield 4.6 g (84% yield) of N-Boc-tosylpropoxytryptophan methyl ester (Tso-TP/Boc/Ester). NMR was used to confirm the structure of Tso-TP/Boc/Ester (Figure 4.15). 1H-NMR (300MHz, $CDCl_3$): 7.77 (d, J=8.3Hz, 2H), 7.24 (d, J=8.8Hz, 1H), 7.19 (d, J=8.3Hz, 2H), 6.97 (s, 1H), 6.91 (d, J=2.4Hz, 1H), 6.70 (dxd, J=8.8, J'= 2.4Hz, 1H), 4.53 (m, 1H), 4.28 (t, J=6.3Hz, 2H), 4.00 (t, J=5.8Hz, 2H), 3.67 (s, 3H), 3.21 (d, J=5.2, 2H), 2.34 (s, 3H), 2.13 (quintet, H=6.0Hz, 2H), 1.41 (s, 9H). Mass spectrometry (M+): 545.5 (100%), 445.4 (5%), 171.2 (10%), 105.2 (10%).

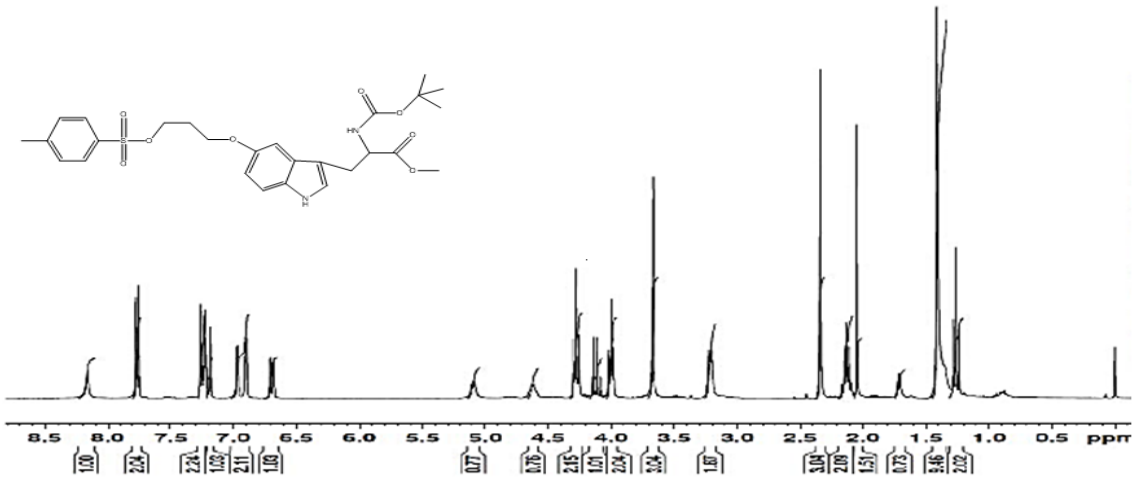

Figure 4.16 NMR Analysis of Tso-TP/Boc/Ester

In step 3, N-Boc-tosylpropoxytryptophan methyl ester was reacted with potassium fluoride in 2,2,2-kryptofix, followed by de-protection. N-Boc-tosylpropoxytryptophan methyl ester (50 mg, 0.09 mmol), potassium fluoride (10.5 mg, 0.18 mmol) and 2,2,2-kryptofix (34 mg, 0.09 mmol) were dissolved in anhydrous acetonitrile (5 mL) while stirring under nitrogen atmosphere and was refluxed for 4 hrs. The reaction mixture was evaporated under reduced pressure and reconstituted in ethyl acetate (0.5 ml), and purified with column chromatography using hexane in ethyl acetate (1:1, v/v) to obtain 15 mg (43% yield) of N-Boc-fluoropropoxytryptophan methyl ester (FTP/Boc/Ester). NMR and Mass Spectrum was used to confirm the structure of FTP/Boc/Ester (Figure 4.16 & Figure 4.17). 1H-NMR (300MHz, $CDCl_3$): 7.16 (d, J=8.8HJz, 1H), 6.95 (s, 1H), 6.91 (d, J=2.3Hz, 1H), 6.78 (dxd, J=8.8, J'= 2.3Hz, 1H), 5.02 (d, 2H), 4.69 (t, J=5.9Hz, 1H), 4.53 (t, J=5.9Hz, 1H), 4.07 (d, J=5.1Hz, 2H), 3.61 (s, 3H), 3.21 (d, J=5.1,

2H), 2.17 (quintet, H=6.0Hz, 1H), 2.08 (quintet, H=6.0Hz, 1H), 1.35 (s, 9H). Mass spectrometry (M+): 393.3 (50%), 248.8 (10%), 172.8 (20%), 140.8 (30%), 112.6 (100%).

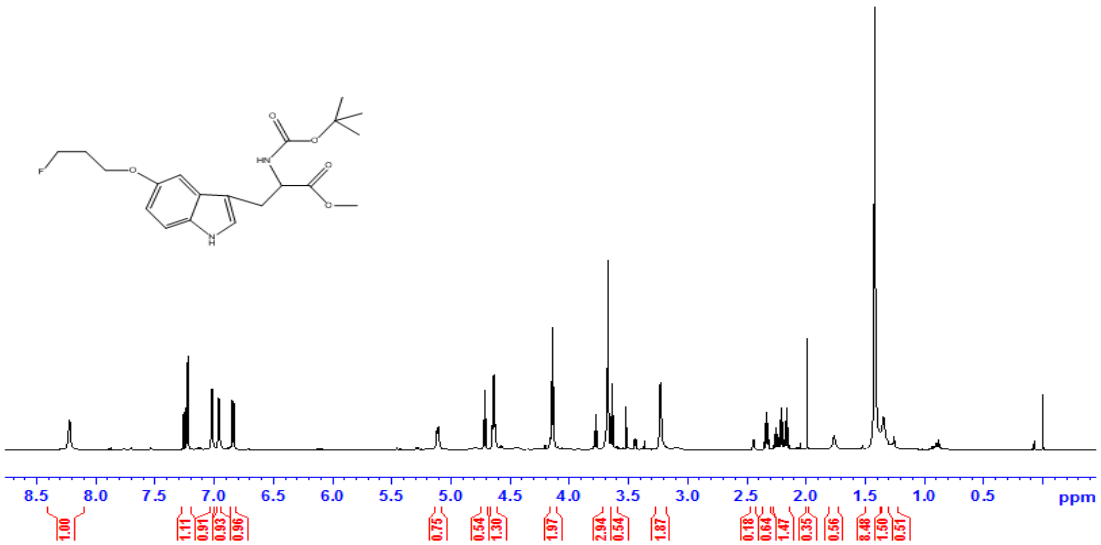

Figure 4.17 NMR analysis of ^{19}F-FTP/Boc/Ester

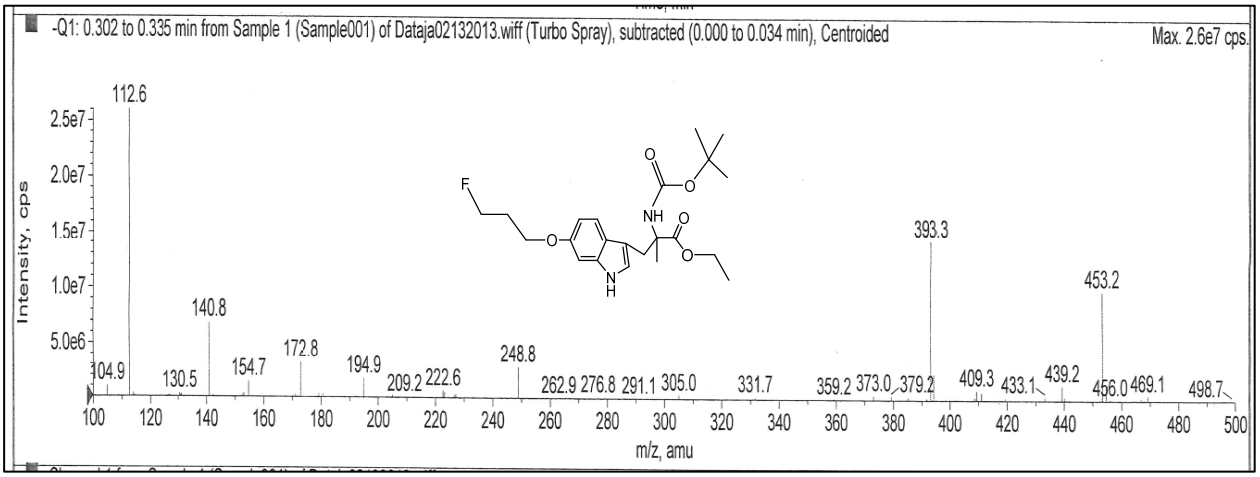

Figure 4.18 Mass spectrum of ^{19}F-FTP/Boc/Ester

To de-protect amino and ester groups, N-Boc-fluoropropoxytryptophan methyl ester (15 mg, 0.038 mmol) was dissolved in the mixture of dichloromethane and anhydrous trifluoroacetic acid (0.5ml; 1:1, v/v). The mixture was stirred for 60 min. After solvent evaporation, NaOH (1N 0.5ml) was added to the residue. The reaction mixture was heated at 85°C for 60min. The product was purified by prep-TLC (1 mm) using MeOH: EtOAC (1:3, v:v) to yield fluoropropoxytryptophan (FTP, 5.5 mg, 44%). NMR and HPLC were used to confirm the structure of ^{19}F-FTP (Figure 4.18 & Figure 4.19). ^{1}H-NMR (300MHz, $CDCl_3$): 6.97 (s, 1H), 6.91 (d, J=2.4Hz, 1H), 6.70 (dxd, J=8.8, J'= 2.4Hz, 1H), 4.53 (m, 1H), 4.28 (t, J=6.3Hz, 2H), 4.00 (t, J=5.8Hz, 2H), 3.67 (s, 3H), 3.21 (d, J=5.2, 2H), 2.13 (quintet, H=6.0Hz, 2H).

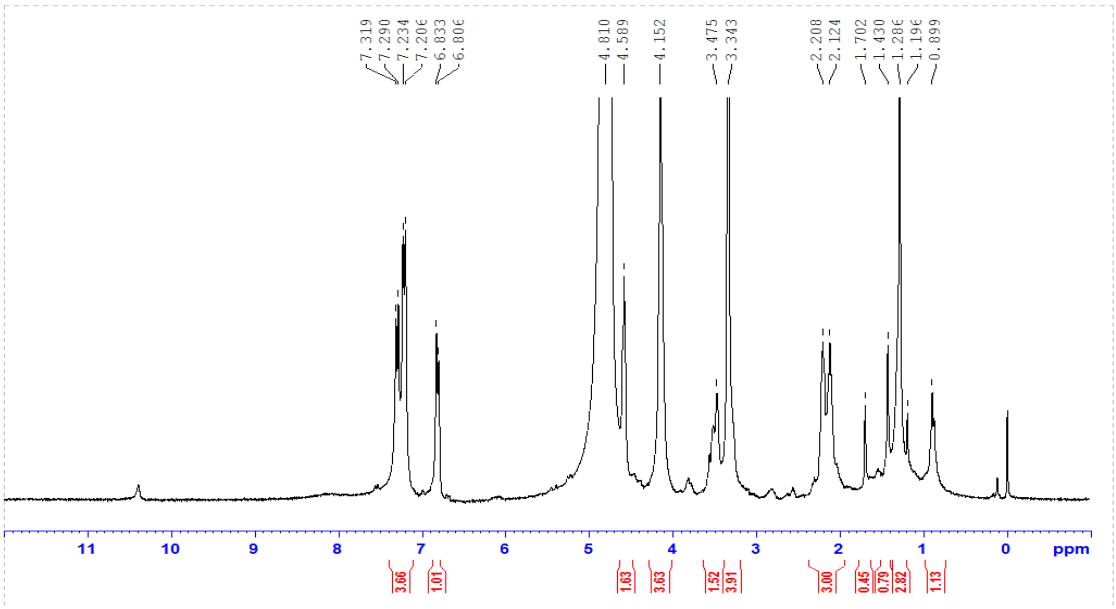

Figure 4.19 NMR analysis of ^{19}F-FTP

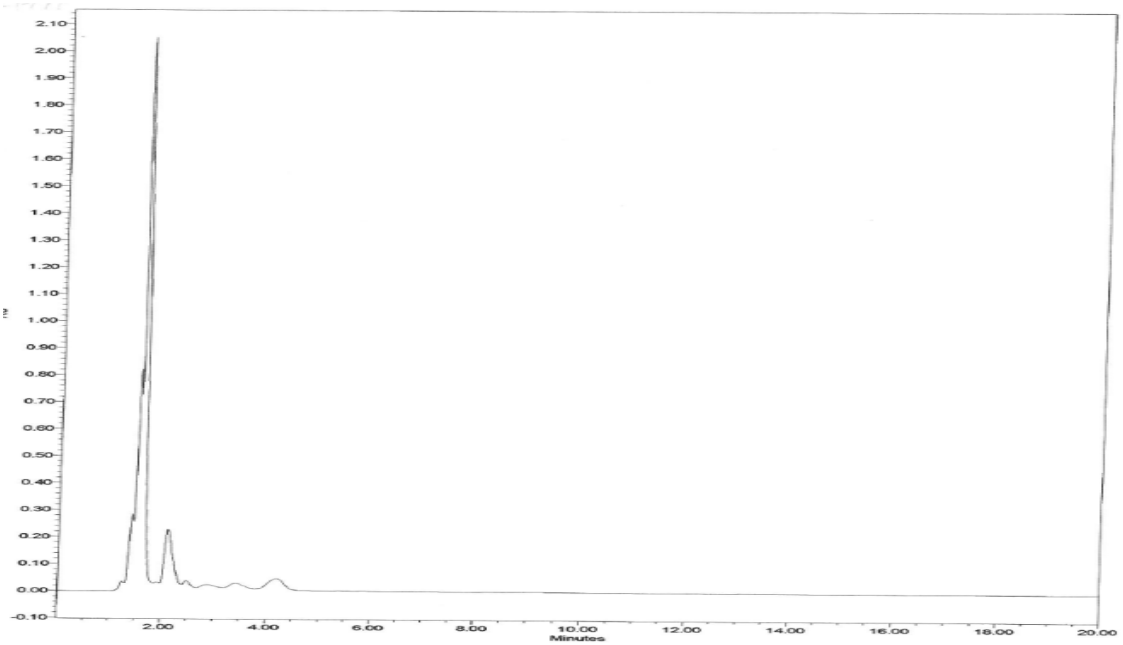

Figure 4.20 HPLC analysis of ^{19}F-FTP

4.4.2 Manually synthesis method of ^{18}F- FTP

[^{18}F]Fluoride in kryptofix complex (110 mCi in 0.3 mL acetonitrile) was purchased from the cyclotron facility of Cyclotope (Houston, TX, USA). N-Boc-tosylpropoxytryptophan methyl ester (3.3 mg; 6.16 µmol) dissolved in acetonitrile (0.1 mL) was added to the [^{18}F]fluoride-kryptofix complex (97.4 mCi). The reaction mixture was heated at 85°C for 20 min to allow the displacement to occur. After the reaction mixture cooled, it was passed through a 500 mg silica gel packed SPE column (Whatman Lab., Clifton, NJ, USA) and eluted with acetonitrile (2 mL). The acetonitrile was then evaporated in *vacuo* at 85°C. The resulting mixture was hydrolyzed with trifluoroacetate (0.5 mL) in dichloromethane (0.5 mL) at room temperature for 10 min to deprotect BOC. After the solvent was evaporated to dryness in *vacuo*, sodium hydroxide (1 N; 0.25 mL) in methanol (0.25 mL) was added and heated at 85°C for 15 min to remove ethyl ester group. After methanol evaporated, hydrochloric acid (0.1 N, 0.2 mL) was used to adjust the pH of the final product to 6.5. HPLC were performed to assure the purity and identity of the product (Figure 4.20). The ^{18}F- FTP radioactivity at the end of synthesis is 17.2 mCi, and the radiochemical yield at end of synthesis is 31.17%.

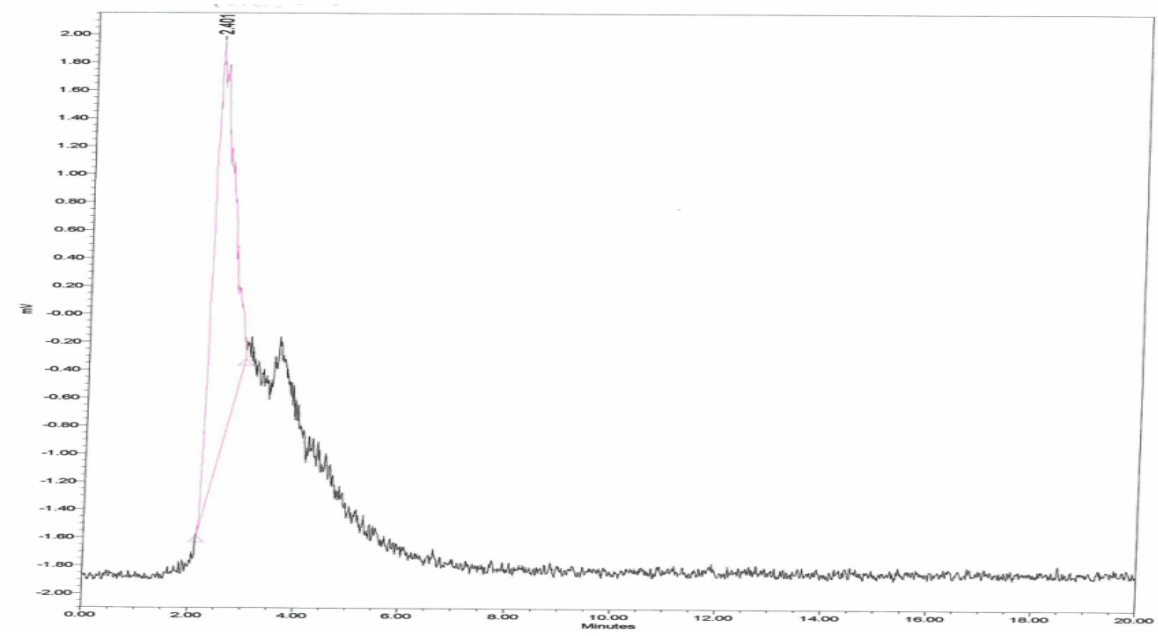

Figure 4.21 Radio-HPLC analysis of ^{18}F-FTP by manual synthesis

4.4.3 Automated synthesis method of ^{18}F- FTP

The synthetic scheme is the same as that of cold FTP (Figure 4.14). [^{18}F]Fluoride was produced by proton irradiation of enriched [^{18}O]-water (Sigma Chemical Company, St. Louis, MO) in a small-volume silver target. Aliquots containing 120 mCi of ^{18}F activity were combined with 26 mg kryptofix-2,2,2 and 4.6 mg anhydrous potassium carbonate, heated under reduced pressure to remove the excess [^{18}O]-water, and dried by azeotropic distillation with acetonitrile (3 x 1.5 mL). K^{18}F/kryptofix complex was reconstituted in acetonitrile (0.3 mL). The automated synthesis recipe of 18F-FTP is shown in Figure 4.21. N-Boc-tosylpropoxytryptophan methyl ester (5 mg) was preloaded in the reaction vial (RV1) of this module, and an aliquot of K^{18}F/kryptofix in acetonitrile

(16.7 mCi, 0.1 mL) was then administered to the RV1 via the external injection port. The IR heater automatically warmed the RV1 at 90°C for 15 min. The mixture in the RV1 was passed through a 500mg silica gel packed SPE column (Whatman Lab, Clifton, NJ) and eluted with ethyl acetate (1.0 mL) to the reaction vial 2 (RV2) under nitrogen flow to remove free fluoride. Before de-BOC, the solution inside the RV2 was evaporated under vacuum at 90°C for 15 min. After that, trifluoroacetate (0.2 mL) in dichloromethane (0.4 mL) was loaded into the RV2 to deprotect amino group. The solution was set under room temperature for 10 minutes to allow for the reaction to complete and then the solvent was evaporated to dryness under vacuum for 15 minutes. For de-esterfication, ethyl alcohol (0.4 mL) and 1N NaOH (0.2 mL) were added into RV2. The hydrolysis of the ester group was performed at 90°C for 15min. The solution in RV2 was evaporated under reduced pressure. ^{18}F-FTP was reconstituted in water (1.2 mL) and filtered through a 0.22 µm-filter. The activities of column, RV1 and RV2 were counted upon completion of the synthesis. HPLC were performed to assure the purity and identity of the product (Figure 4.22). The ^{18}F- FTP radioactivity at the end of synthesis is 3.85 mCi, and the radiochemical yield at end of synthesis is 22.37%.

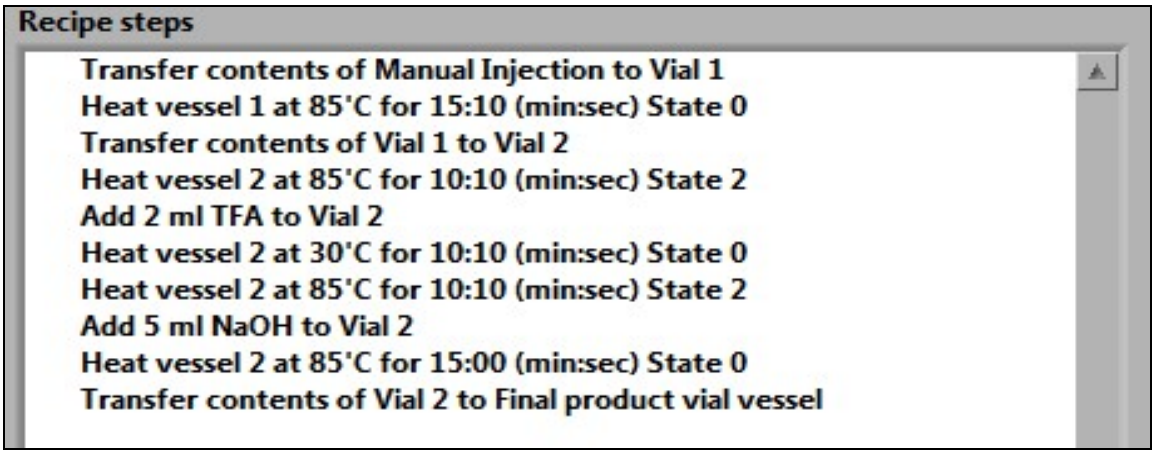

Figure 4.22 Automated synthesis recipe of ^{18}F-FTP

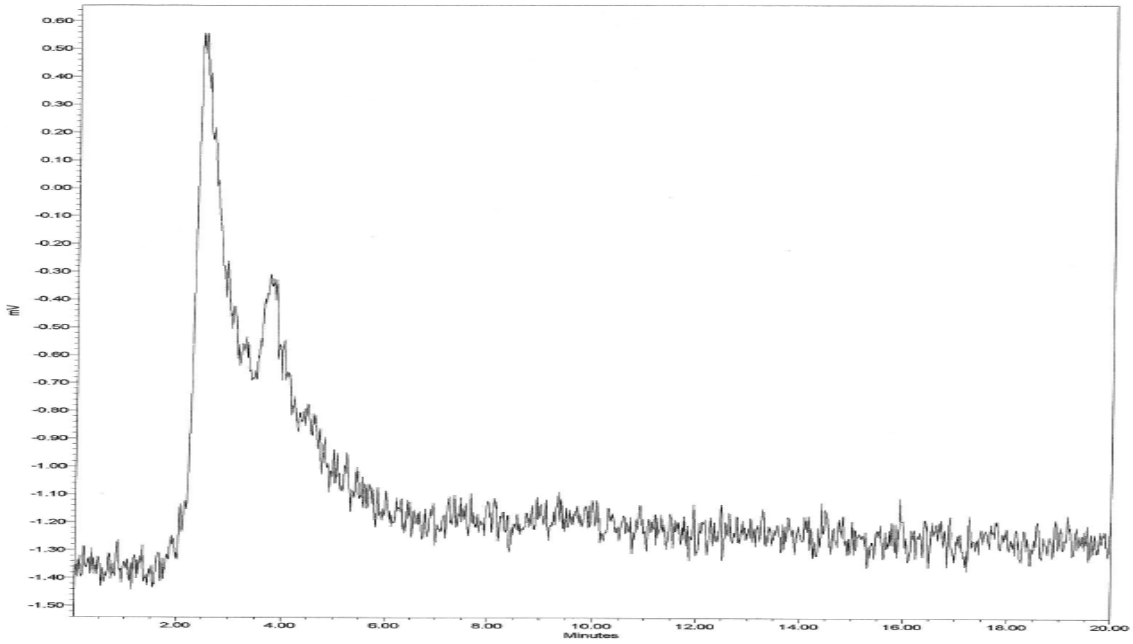

Figure 4.23 Radio-HPLC analysis of ^{18}F-FTP by automated synthesis

4.5 Discussion

4.5.1 Discussion of synthesis of ^{68}Ga-ECG

^{68}Ge/^{68}Ga generator can provide $^{68}Ga^{3+}$ in 0.1M HCl, and the free hydrated Ga^{3+} ion is stable only under acidic conditions. When the pH in this solution changes to 3-7, Ga^{3+} forms insoluble gallium hydroxide. That condition was observed during synthesis of ^{68}Ga-ECG w. Initially, Ga^{3+} elution was added into the vials containing ECG, and the vial was heated to stabilize ^{68}Ga-ECG. Then $NaHCO_3$ was added into the vial to adjust the pH to 5-6 value after heating. The radiochemical purity of ^{68}Ga-ECG in this method only reached 30% (Figure 4.23). To solve this problem, $NaHCO_3$ was added into the vial before the vial was heated. Finally, this method provided high radiochemical purity of ^{68}Ga-ECG, and can be easily practiced on this automated synthesis module.

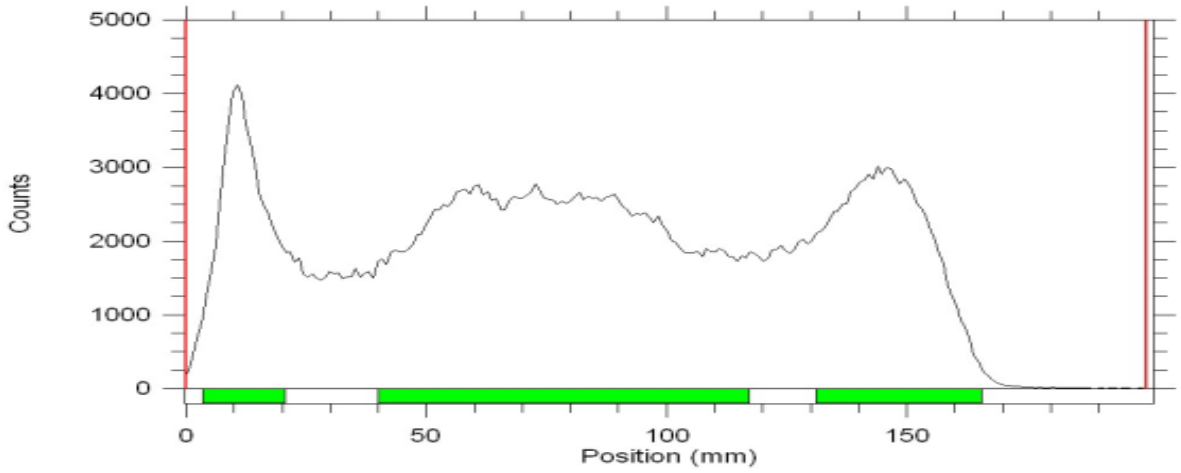

Figure 4.24 Radio-TLC analysis of ^{68}Ga-ECG with gallium hydroxide

4.5.2 Discussion of synthesis of ^{18}F-FPAMT & ^{18}F-FTP

The traditional method for the synthesis of ^{18}F-labeled tyrosine analogs such as ^{18}F-FET and ^{18}F-FAMT was through the electrophilic substitution reaction which provides low yield (84, 85). Besides, the reaction uses ^{18}F-F_2 gas, and HPLC separation makes it even difficult to apply this method in automated modules. Although a nucleophilic reaction could result in a high yield of ^{18}F-FET, this method still requires HPLC for purification (86). Thus, it is not ideal to use this synthesis method in automated synthesis modules. In this study, we obtained ^{18}F-FPAMT and ^{18}F-FTP by nucleophilic reactions without HPLC purification. Therefore, our method for the synthesis of ^{18}F-FPAMT and ^{18}F-FTP can be applied to the multi-purposed automated synthesis module.

Table4.1 shows the result comparisons between the manual synthesis and the automated synthesis of ^{18}F-FPAMT; Table 4.2 shows the result comparisons between the manual synthesis and the automated synthesis of ^{18}F-FTP. The pH value and radiochemical yield of each radiopharmaceutical by manual and automated syntheses were similar. However, the yield, the specific activity, and the synthesis time of these two drugs made by the manual synthesis were different from the automated synthesis. For the specific activity issue of these two radiopharmaceuticals, the amount of starting material of the manual synthesis was less than automated synthesis, but the radioactivity of K^{18}F/kryptofix in automated synthesis was less than in manual synthesis. Therefore, the specific activity of the automated synthesis was lower than manual

synthesis. For manual syntheses of radiopharmaceuticals, the shorter synthesis time often demonstrates higher yield. But the automated synthesis results of ^{18}F-FPAMT and ^{18}F-FTP showed low yields no matter how soon the synthesis completed. The reason for the low yield is that residues of ^{18}F-FPAMT & ^{18}F-FTP were trapped inside the SPE columns. The columns were designed only to absorb unreacted K^{18}F/krytofix mixtures. To reduce this problem, an optimization process is designed for adjustment of the solution retention time inside the SPE column which is influenced by N_2 flow rate. Instead of the current steady pressure flow, the stepwise profile of N2 flow rate should be the key point to increase the yield by automated synthesis.

	Manual synthesis	Automated Synthesis
pH value	5~6	5~6
Radiochemical Purity	>90%	>90%
Yield (Decay Corrected)	10.05 mCi (34%)	2.21 mCi (15%)
Specific Activity	32 μCi/mol	16 μCi/mol
Synthesis Time	88min	109min

Table 4.1 ^{18}F-FPAMT Result comparisons between manual synthesis and automated synthesis

	Manual synthesis	Automated Synthesis
pH value	5~6	5~6
Radiochemical Purity	>90%	>90%
Yield (Decay Corrected)	17.2 mCi (31.2%)	1.36 mCi (8%)
Specific Activity	38 Ci/μmol	20 Ci/μmol
Synthesis Time	91min	69min

Table 4.2 ^{18}F-FTP Result comparisons between manual synthesis and automated synthesis

5 Chapter 5 Discussion

On March 10, 2000, FDA announced ^{18}F-FDG to be a safe and effective PET drug for certain indications when it produced in a qualified condition(87). The qualified condition is followed by current Good Manufacturing Practice (cGMP) regulations (88), and an automated synthesis module with validated specifications is to produce certified ^{18}F-FDG. In addition, ^{18}F-FDG produced by an automated synthesis module is housed in a hot cell that reduces the radiation exposure of employees. Though, ^{18}F-FDG PET is useful in disease detection. However, it has the limitations in tumor diagnosis, such as differentiations between tumors and inflammatory tissue (89-91), and the differentiation of low-grade gliomas (92-94). As a result, there are strong clinical demands to use other radioactive drugs to overcome these limitations or to be employed in other clinical applications (19, 95-100). In order to achieve clinical demands, the design of an automated synthesis module can not only serve for a special synthesis recipe which is used to produce one special drug, such as ^{18}F-FDG (101). Therefore, the novel automated multi-purpose synthesis module is proposed and validated by production of three different PET radiopharmaceuticals which provides the possibilities to make up for the deficiency of ^{18}F-FDG.

5.1 Future work for hardware improvement

After validation of the automated synthesis module, there are three hardware aspects which could be improved in the future, the design for easy maintenance, the design for upgrading, and the dead volume issue.

5.1.1 The design for easy maintenance

Our initial hardware design concept of this module is straightforward, and this concept is that the components of the hardware can provide the functions to replace the manual synthesis of radiopharmaceuticals. However, the current feature of design doesn't include the easy maintenance. The maintenance process is very time-consuming because of the fixed outer shell and the compact configuration of inside components. In order to solve this problem, the physical appearance of this module can be constituted by several removable sheets instead of the fixed outer shell, and the new design of the inner configurations of this module should provide engineers more accessibility of the hardware components.

5.1.2 The design for upgrading

The current design of this module is a proof of concept for the automated synthesis of three different radiopharmaceuticals. In order to synthesize other radiopharmaceuticals with complicated recipes or to improve the synthesis performance in the future, it is necessary that the hardware design is cable of upgrading. The upgrading of this module should provide the users extra functions or better performance of the existing functions. The one possible extra function is to use the webcam for monitoring this module during the synthesis, and the dynamic video can be

transformed to serious grey-scale pictures which can be compared to the images of the standard processes. Therefore, this function can provide extra safety control. For existing functions, different types of IR heaters and mass flow controllers can be selected to increase the performance of this module. Other than upgrading the functions of this module, it is also important to upgrade the injection panel. For this current module, radiochemists can perfect its synthesis result by modifications of the parameters, and transfer this final recipe for clinical usages. However, it is better to design a dual-use replaceable panel which not only keeps the current syringe-type panel for optimization of the synthesis recipe but also can be replaced to a kit-type panel for clinical usages. In addition, this dual-use panel can provide radiochemists incentives to practice the new synthesis recipes on this module because the process of optimization for synthesis can help them produce the synthesis kits for different radiopharmaceuticals.

5.1.3 The dead volume issue

Comparisons of the results of automated synthesis and manual synthesis, it demonstrates the radiochemical yield of automated synthesis is lower than manual synthesis. The major reason is the dead volume issue, and some solutions were stuck inside the automated module. Multiple tests were to determine the effect of dead volume issue. First, the radioactivity of ^{99m}Tc-pertechnetate (1 mL) was measured, and injected into this module through the injection port. Then, this solution was

automatically transferred to the final product vial through RV1, and RV2, and flow channels. The average radioactivity of the final product vial was 90% of the initial radioactivity. The approximately 100 µl solution can be trapped inside the automated module even if N_2 gas was used to purge the flow channels. For next generation of this automated synthesis module, less passages of flow channels can ameliorate this problem to improve the radiochemical yield.

5.2 Future work for software improvement

The software improvement includes the increase the stability, the software development for hardware upgrade and the new design of the user interface.

5.2.1 Increase the stability

The stability of this automated synthesis module includes two aspects, the stability of the software, and the stability of the interaction between hardware and software. In addition, the stability of the hardware of this module depends on assurance of its individual component which is described in its specifications.

For traditional programming language, such as C, the compiling order is from the first line to the last line. However, the labview is a graphic-based programming language. The compiling order of labview is based on the character of sub-programs, and the graphic position. Therefore, the wrong sequence of sub-programs compiling produces the “racing” event which causes the software unstable or CPU overdrive.

The other reason causes the software unstable is the interaction between hardware and software. The compiling time for sub-programs often takes microseconds, but scanning frequency of the sensors or movable components takes milliseconds. The difference will cause the system unstable. A “time-delay” sub-program can slow down the speed of software processing, and reorder the sequence of sub-programs compiling. The solution can allow the programs response functionally after receiving all the signals from hardware components.

5.2.2 The software development for hardware upgrade and the new design of the user interface.

In section 5.1, the new injection panel and a webcam are the possible direction of the hardware upgrade. This hardware upgrade must be accomplished with the software upgrade for increase the performance of the next generation module. The new user interface of the next generation module should provide the user the real-time imaging of the module. In addition, a diagram of this module will be completed and this diagram should be animated for visualization of the synthesis process.

5.3 Conclusion

Initially, radiochemists synthesize the radiopharmaceuticals for translational and preclinical usages occasionally. After FDA approval for the specific radiopharmaceutical in clinics, the demand of this radiopharmaceutical is increased. However, this high

demand might cause radiochemists with the high risk of radiation overexposure. In addition, most PET radiopharmaceuticals are made by organic syntheses which take longer synthesis time than traditional SPECT radiopharmaceuticals. An automated synthesis module is the solution for high demands of FDA-approved PET radiopharmaceuticals. Currently, there are 46 FDA-approved radiopharmaceuticals, and only 6 radiopharmaceuticals are used in PET applications. Most commercialized automated synthesis modules were designed to synthesize these FDA-approved PET radiopharmaceuticals, and it is difficult for researchers to modify these modules to synthesize its own radiopharmaceuticals. Here, we designed an automated multi-purposes synthesis module which can provide the essential synthesis functions to researchers who is used to synthesizing radiopharmaceuticals manually, and allow researchers to optimize the synthesis recipes by this module. Moreover, this module also can provide clinical services by modification its software.

^{68}Ga-ECG, ^{18}F-FPAMT, and ^{18}F-FTP were selected to validate the concept of automated multi-purposes synthesis module. Nonradioactive manual synthesis of these three compounds were processed, and the structure analyses of ^{69}Ga-ECG, ^{19}F-FPAMT, and ^{19}F-FTP were demonstrated. After that, ^{68}Ga-ECG, ^{18}F-FPAMT, and ^{18}F-FTP were synthesized manually and automatically. The results showed the radiochemical purity of these compounds made from automated syntheses was identical as the manual syntheses. However, the yield of automated syntheses were lower than those of manual synthesis because of the dead volume issue.

Bibliography

1. Herschman, H. R. 2003. Molecular Imaging: Looking at Problems, Seeing Solutions. Science 302:605-608.
2. Strauss, L. G., and P. S. Conti. 1991. The applications of PET in clinical oncology. J Nucl Med 32:623-648; discussion 649-650.
3. Antonini, A., and I. U. Isaias. 2008. Single photon-emission computed tomography imaging in early Parkinson's disease. Expert review of neurotherapeutics 8:1853-1864.
4. Berman, D. S., R. Hachamovitch, H. Kiat, I. Cohen, J. A. Cabico, F. P. Wang, J. D. Friedman, G. Germano, K. Van Train, and G. A. Diamond. 1995. Incremental value of prognostic testing in patients with known or suspected ischemic heart disease: a basis for optimal utilization of exercise technetium-99m sestamibi myocardial perfusion single-photon emission computed tomography. Journal of the American College of Cardiology 26:639-647.
5. Spencer, S. S., W. H. Theodore, and S. F. Berkovic. 1995. Clinical applications: MRI, SPECT, and PET. Magnetic resonance imaging 13:1119-1124.
6. Fenster, A., and D. B. Downey. 2000. Three-dimensional ultrasound imaging. Annual review of biomedical engineering 2:457-475.
7. Garvey, C. J., and R. Hanlon. 2002. Computed tomography in clinical practice. Bmj 324:1077-1080.

8. Livieratos, L. 2012. Basic Principles of SPECT and PET Imaging. In Radionuclide and Hybrid Bone Imaging. I. Fogelman, G. Gnanasegaran, and H. Wall, editors. Springer Berlin Heidelberg. 345-359.

9. Saha, G. B. 2005. Basics of PET imaging physics, chemistry, and regulations. Springer, New York, NY. 1 online resource (xv, 206 p.).

10. Keidar, Z., O. Israel, and Y. Krausz. 2003. SPECT/CT in tumor imaging: Technical aspects and clinical applications. Seminars in nuclear medicine 33:205-218.

11. Del Vecchio, S., A. Zannetti, R. Fonti, F. Iommelli, L. M. Pizzuti, A. Lettieri, and M. Salvatore. 2010. PET/CT in cancer research: from preclinical to clinical applications. Contrast media & molecular imaging 5:190-200.

12. Been, L. B., A. J. Suurmeijer, D. C. Cobben, P. L. Jager, H. J. Hoekstra, and P. H. Elsinga. 2004. [18F]FLT-PET in oncology: current status and opportunities. European journal of nuclear medicine and molecular imaging 31:1659-1672.

13. Torizuka, T., N. Tamaki, T. Inokuma, Y. Magata, S. Sasayama, Y. Yonekura, A. Tanaka, Y. Yamaoka, K. Yamamoto, and J. Konishi. 1995. In vivo assessment of glucose metabolism in hepatocellular carcinoma with FDG-PET. J Nucl Med 36:1811-1817.

14. Cai, W., K. Chen, K. A. Mohamedali, Q. Cao, S. S. Gambhir, M. G. Rosenblum, and X. Chen. 2006. PET of vascular endothelial growth factor receptor expression. J Nucl Med 47:2048-2056.

15. Eschmann, S. M., F. Paulsen, M. Reimold, H. Dittmann, S. Welz, G. Reischl, H. J. Machulla, and R. Bares. 2005. Prognostic impact of hypoxia imaging with 18F-

misonidazole PET in non-small cell lung cancer and head and neck cancer before radiotherapy. J Nucl Med 46:253-260.

16. Niu, G., and X. Chen. 2009. PET Imaging of Angiogenesis. PET clinics 4:17-38.

17. Adonai, N., K. N. Nguyen, J. Walsh, M. Iyer, T. Toyokuni, M. E. Phelps, T. McCarthy, D. W. McCarthy, and S. S. Gambhir. 2002. Ex vivo cell labeling with 64Cu-pyruvaldehyde-bis(N4-methylthiosemicarbazone) for imaging cell trafficking in mice with positron-emission tomography. Proceedings of the National Academy of Sciences of the United States of America 99:3030-3035.

18. Welch, M. J., C. S. Redvanly, and NetLibrary Inc. 2003. Handbook of radiopharmaceuticals radiochemistry and applications. J. Wiley, New York. xiv, 848 p.

19. Jacobson, M., R. Steichen, and P. Peller. 2012. PET Radiochemistry and Radiopharmacy. In PET-CT and PET-MRI in Oncology. P. Peller, R. Subramaniam, and A. Guermazi, editors. Springer Berlin Heidelberg. 19-30.

20. Bessell, E. M., and P. Thomas. 1973. The deoxyfluoro-D-glucopyranose 6-phosphates and their effect on yeast glucose phosphate isomerase. Biochem J 131:77-82.

21. Urdang, L. 1975. The Random House College Dictionary - Stein,J. Verbatim 2:11-12.

22. Myers, R. L. 2003. The basics of chemistry. Greenwood Press, Westport, Conn.

23. Chirakal, R., G. Firnau, M. Adams, G. J. Schrobilgen, G. Coates, G. T. Bida, and E. S. Garnett. 1995. Routine Production of [18F]F2 from 11 MeV Proton-Only

Cyclotron and Its Use for the Synthesis of 18F-Tracers for Heart and Brain. In Chemists' Views of Imaging Centers. A. Emran, editor. Springer US. 425-429.

24. AGENCY, I. A. E. 2008. CYCLOTRON PRODUCED RADIONUCLIDES : PRINCIPLES AND PRACTICE

25. Dawood, K. M. 2004. Electrolytic fluorination of organic compounds. Tetrahedron 60:1435-1451.

26. Kirk, K. L. 2008. Fluorination in medicinal chemistry: Methods, strategies, and recent developments. Org Process Res Dev 12:305-321.

27. Sood, S., G. Firnau, and E. S. Garnett. 1983. Radiofluorination with xenon difluoride: a new high yield synthesis of [18F]2-fluro-2-deoxy-D-glucose. The International journal of applied radiation and isotopes 34:743-745.

28. Jewett, D. M., J. F. Potocki, and R. E. Ehrenkaufer. 1984. A Gas Solid-Phase Microchemical Method for the Synthesis of Acetyl Hypofluorite. J Fluorine Chem 24:477-484.

29. Adam, M. J., T. J. Ruth, J. R. Grierson, B. Abeysekera, and B. D. Pate. 1986. Routine synthesis of L-[18F]6-fluorodopa with fluorine-18 acetyl hypofluorite. J Nucl Med 27:1462-1466.

30. Cen, Y., and A. A. Sauve. 2009. Diastereocontrolled Electrophilic Fluorinations of 2-Deoxyribonolactone: Syntheses of All Corresponding 2-Deoxy-2-fluorolactones and 2 '-Deoxy-2 '-fluoro-NAD(+)s. Journal of Organic Chemistry 74:5779-5789.

31. Kasbollah, A., P. Eu, S. Cowell, and P. Deb. 2013. Review on production of 89Zr in a medical cyclotron for PET radiopharmaceuticals. Journal of nuclear medicine technology 41:35-41.

32. Lasne, M.-C., C. Perrio, J. Rouden, L. Barré, D. Roeda, F. Dolle, and C. Crouzel. 2002. Chemistry of β +-Emitting Compounds Based on Fluorine-18. In Contrast Agents II. W. Krause, editor. Springer Berlin Heidelberg. 201-258.

33. Gona, K. B., V. Gomez-Vallejo, D. Padro, and J. Llop. 2013. [18F]fluorination of o-carborane via nucleophilic substitution: towards a versatile platform for the preparation of 18F-labelled BNCT drug candidates. Chemical communications 49:11491-11493.

34. Guo, N., D. Alagille, G. Tamagnan, R. R. Price, and R. M. Baldwin. 2008. Microwave-induced nucleophilic [18F]fluorination on aromatic rings: synthesis and effect of halogen on [18F]fluoride substitution of meta-halo (F, Cl, Br, I)-benzonitrile derivatives. Applied radiation and isotopes : including data, instrumentation and methods for use in agriculture, industry and medicine 66:1396-1402.

35. Ross, T. L., J. Ermert, C. Hocke, and H. H. Coenen. 2007. Nucleophilic 18F-fluorination of heteroaromatic iodonium salts with no-carrier-added [18F]fluoride. J Am Chem Soc 129:8018-8025.

36. Lu, S., S. D. Lepore, S. Y. Li, D. Mondal, P. C. Cohn, A. K. Bhunia, and V. W. Pike. 2009. Nucleophile assisting leaving groups: a strategy for aliphatic 18F-fluorination. The Journal of organic chemistry 74:5290-5296.

37. Kim, D., H.-J. Jeong, S. Lim, and M.-H. Sohn. 2010. Recent Trends in the Nucleophilic [18F]-radiolabeling Method with No-carrier-added [18F]fluoride. Nucl Med Mol Imaging 44:25-32.

38. Yu, S. 2006. Review of F-FDG Synthesis and Quality Control. Biomedical imaging and intervention journal 2:e57.

39. Hintermann, L., R. Masuo, and K. Suzuki. 2008. Solvent-Controlled Leaving-Group Selectivity in Aromatic Nucleophilic Substitution. Organic letters 10:4859-4862.

40. Vlasov, V. M. 1993. Fluoride ion as a nucleophile and a leaving group in aromatic nucleophilic substitution reactions. J Fluorine Chem 61:193-216.

41. Hamill, T. G., S. Krause, C. Ryan, C. Bonnefous, S. Govek, T. J. Seiders, N. D. Cosford, J. Roppe, T. Kamenecka, S. Patel, R. E. Gibson, S. Sanabria, K. Riffel, W. Eng, C. King, X. Yang, M. D. Green, S. S. O'Malley, R. Hargreaves, and H. D. Burns. 2005. Synthesis, characterization, and first successful monkey imaging studies of metabotropic glutamate receptor subtype 5 (mGluR5) PET radiotracers. Synapse 56:205-216.

42. Matsumoto, J.-I., T. Miyamoto, A. Minamida, Y. Nishimura, H. Egawa, and H. Nishimura. 1984. Synthesis of fluorinated pyridines by the balz-schiemann reaction. An alternative route to enoxacin, a new antibacterial pyridonecarboxylic acid. J Heterocyclic Chem 21:673-679.

43. Rosch, F. 2013. Past, present and future of 68Ge/68Ga generators. Applied radiation and isotopes : including data, instrumentation and methods for use in agriculture, industry and medicine 76:24-30.

44. Wadas, T. J., E. H. Wong, G. R. Weisman, and C. J. Anderson. 2010. Coordinating radiometals of copper, gallium, indium, yttrium, and zirconium for PET and SPECT imaging of disease. Chemical reviews 110:2858-2902.

45. Brechbiel, M. W. 2008. Bifunctional chelates for metal nuclides. The quarterly journal of nuclear medicine and molecular imaging : official publication of the Italian Association of Nuclear Medicine 52:166-173.

46. Bauwens, M., R. Chekol, H. Vanbilloen, G. Bormans, and A. Verbruggen. 2010. Optimal buffer choice of the radiosynthesis of (68)Ga-Dotatoc for clinical application. Nuclear medicine communications 31:753-758.

47. Koukouraki, S., L. G. Strauss, V. Georgoulias, J. Schuhmacher, U. Haberkorn, N. Karkavitsas, and A. Dimitrakopoulou-Strauss. 2006. Evaluation of the pharmacokinetics of 68Ga-DOTATOC in patients with metastatic neuroendocrine tumours scheduled for 90Y-DOTATOC therapy. European journal of nuclear medicine and molecular imaging 33:460-466.

48. Elgeti, F., H. Amthauer, T. Denecke, I. Steffen, F. Heuck, L. Stelter, and J. Ruf. 2008. Incidental detection of breast cancer by 68Ga-DOTATOC-PET/CT in women suffering from neuroendocrine tumours. Nuklearmedizin. Nuclear medicine 47:261-265.

49. Jindal, T., A. Kumar, R. Kumar, and R. Dutta. 2010. Role of 68Ga-DOTATOC PET/CT in carcinoids. Pathology international 60:143-144.

50. Souvatzoglou, M., T. Maurer, U. Treiber, G. Weirich, B. J. Krause, and M. Essler. 2009. 68Ga-DOTATOC-PET/CT detects neuroendocrine differentiation of prostate cancer metastases. Nuklearmedizin. Nuclear medicine 48:N52-54.

51. Otte, A., E. Jermann, M. Behe, M. Goetze, H. C. Bucher, H. W. Roser, A. Heppeler, J. Mueller-Brand, and H. R. Maecke. 1997. DOTATOC: a powerful new tool for receptor-mediated radionuclide therapy. European journal of nuclear medicine 24:792-795.

52. Buchmann, I., M. Henze, S. Engelbrecht, M. Eisenhut, A. Runz, M. Schafer, T. Schilling, S. Haufe, T. Herrmann, and U. Haberkorn. 2007. Comparison of 68Ga-DOTATOC PET and 111In-DTPAOC (Octreoscan) SPECT in patients with neuroendocrine tumours. European journal of nuclear medicine and molecular imaging 34:1617-1626.

53. Merrifield, R. B., J. M. Stewart, and N. Jernberg. 1966. Instrument for automated synthesis of peptides. Analytical chemistry 38:1905-1914.

54. Ido, T., C. N. Wan, V. Casella, J. S. Fowler, A. P. Wolf, M. Reivich, and D. E. Kuhl. 1978. Labeled 2-Deoxy-D-Glucose Analogs - F-18-Labeled 2-Deoxy-2-Fluoro-D-Glucose, 2-Deoxy-2-Fluoro-D-Mannose and C-14-2-Deoxy-2-Fluoro-D-Glucose. Journal of labelled compounds & radiopharmaceuticals 14:175-183.

55. Barrio, J. R., N. S. Macdonald, G. D. Robinson, A. Najafi, J. S. Cook, and D. E. Kuhl. 1981. Remote, Semiautomated Production of F-18-Labeled 2-Deoxy-2-Fluoro-D-Glucose. J Nucl Med 22:372-375.

56. Hamacher, K., H. H. Coenen, and G. Stocklin. 1986. Stereospecific Synthesis of Nca 2-[F-18]-Fluoro-2-Deoxy-D-Mannose and 2-[F-18]-Fluoro-2-Deoxy-D-Glucose and the Influence of Added Carrier (Kf) on Fdg-Synthesis. Journal of labelled compounds & radiopharmaceuticals 23:1095-1095.

57. Hamacher, K., H. H. Coenen, and G. Stocklin. 1986. Efficient Stereospecific Synthesis of No-Carrier-Added 2-[F-18]-Fluoro-2-Deoxy-D-Glucose Using Aminopolyether Supported Nucleophilic-Substitution. J Nucl Med 27:235-238.

58. Lagrange, J. L., J. Maublant, and J. Darcourt. 1995. Positron Emission Tomography - Role of F-18 Fluorodeoxyglucose ((18)Fdg) Imaging in Oncology. Bulletin du cancer 82:611-622.

59. Conti, P. S., D. L. Lilien, K. Hawley, J. Keppler, S. T. Grafton, and J. R. Bading. 1996. PET and [F-18]-FDG in oncology: A clinical update. Nuclear medicine and biology 23:717-735.

60. Biersack, H. J., H. Bender, J. Ruhlmann, A. Schomburg, and F. Grunwald. 1997. FDG-PET in clinical oncology: Review and evaluation of results of a private clinical PET center. Nucl Med A:1-29.

61. Lewellen, T. K. 2000. PET and oncology - FDG and beyond. Radiology 217:292-292.

62. Czernin, J. 2002. Clinical applications of FDG-PET in oncology. Acta Med Aust 29:162-170.

63. Rahman, O., M. Erlandsson, E. Blom, and B. Langstrom. 2010. Automated synthesis of F-18-labelled analogs of metomidate, vorozole and harmine using

commercial platform. Journal of labelled compounds & radiopharmaceuticals 53:169-171.

64. Sun, L. Q., T. Mori, C. S. Dence, D. E. Ponde, M. J. Welch, T. Furukawa, Y. Yonekura, and Y. Fujibayashi. 2006. New approach to fully automated synthesis of sodium [18F]fluoroacetate -- a simple and fast method using a commercial synthesizer. Nuclear medicine and biology 33:153-158.

65. Paolillo, V., S. Riese, J. G. Gelovani, and M. M. Alauddin. 2009. A fully automated synthesis of [F-18]-FEAU and [F-18]-FMAU using a novel dual reactor radiosynthesis module. Journal of labelled compounds & radiopharmaceuticals 52:553-558.

66. Li-Quan Sun Li-Quan, S., L. Ai-Qin Luo Ai-Qin, and Y. Fujibayashi. 2009. Automated Synthesis of 18F-Fluoroacetate Using Explora FDG4 Module.1-4.

67. Oh, S. J., C. Mosdzianowski, D. Y. Chi, J. Y. Kim, S. H. Kang, J. S. Ryu, J. S. Yeo, and D. H. Moon. 2004. Fully automated synthesis system of 3'-deoxy-3'-[18F]fluorothymidine. Nuclear medicine and biology 31:803-809.

68. Vercouillie, J., C. Prenant, S. Maia, P. Emond, S. Guillouet, J. B. Deloye, L. Barré, and D. Guilloteau. 2010. Automated production of [18F]FDDNP using a TRACERlab MXFDG. Journal of Labelled Compounds and Radiopharmaceuticals 53:208-212.

69. Lodi, F., A. Rizzello, A. Carpinelli, D. Di Pierro, G. Cicoria, V. Mesisca, M. Marengo, and S. Boschi. 2008. Automated Synthesis of [11C]Meta Hydroxyephedrine, a PET

Radiopharmaceutical for Studying Sympathetic Innervation in the Heart. Computers in Cardiology 2008, Vols 1 and 2:341-343.

70. Kiesewetter, D. O., B. K. Vuong, and M. A. Channing. 2003. The automated radiosynthesis of [18F]FP-TZTP. Nuclear medicine and biology 30:73-77.

71. Wang, M., Y. Zhang, Y. Zhang, and H. Yuan. 2009. Automated synthesis of hypoxia imaging agent [18F]FMISO based upon a modified Explora FDG4 module. J Radioanal Nucl Ch 280:149-155.

72. Kersemans, K., J. Mertens, and V. Caveliers. 2010. Radiosynthesis of 4-[18F]fluoromethyl-L-phenylalanine and [18F]FET via a same strategy and automated synthesis module. Journal of Labelled Compounds and Radiopharmaceuticals 53:58-62.

73. Yajima, K., H. Yamazaki, H. Kawashima, S. Ino, N. Hayashi, and Y. Miyake. 1995. Automated synthesis of radiopharmaceuticals for positron emission tomography: an apparatus for [1-C] labeled carboxylic acid. The Journal of automatic chemistry 17:109-114.

74. Cork, D. G., H. Yamato, K. Yajima, N. Hayashi, T. Sugawara, and S. Kato. 1994. Automated synthesis of radiopharmaceuticals for positron emission tomography: an apparatus for labelling with [C] methyl iodide (MIASA). The Journal of automatic chemistry 16:219-230.

75. Oh, S. J., D. H. Moon, W. W. Lee, S. W. Park, M. K. Hong, S. J. Park, D. I. Shin, and H. K. Lee. 2003. Automated preparation of 188Re-labeled radiopharmaceuticals for endovascular radiation therapy. Applied radiation and isotopes : including

data, instrumentation and methods for use in agriculture, industry and medicine 59:225-230.

76. Azhdarinia, A., D. J. Yang, C. Chao, and F. Mourtada. 2007. Infrared-based module for the synthesis of 68Ga-labeled radiotracers. Nuclear medicine and biology 34:121-127.

77. Matarrese, M., P. Bedeschi, R. Scardaoni, F. Sudati, A. Savi, A. Pepe, V. Masiello, S. Todde, L. Gianolli, C. Messa, and F. Fazio. 2010. Automated production of copper radioisotopes and preparation of high specific activity [(64)Cu]Cu-ATSM for PET studies. Applied radiation and isotopes : including data, instrumentation and methods for use in agriculture, industry and medicine 68:5-13.

78. Guette, J. P., N. Crenne, H. Bulliot, J. R. Desmurs, and F. Igersheim. 1988. Automation in the Organic-Chemistry Laboratory - Why - How. Pure Appl Chem 60:1669-1678.

79. Jaffer, F. A., and R. Weissleder. 2005. Molecular imaging in the clinical arena. Jama-J Am Med Assoc 293:855-862.

80. Rohren, E. M., T. G. Turkington, and R. E. Coleman. 2004. Clinical applications of PET in oncology. Radiology 231:305-332.

81. Pauwels, E. K. J., M. J. Ribeiro, J. H. M. B. Stoot, V. R. McCready, M. Bourguignon, and B. Maziere. 1998. FDG accumulation and tumor biology. Nuclear medicine and biology 25:317-322.

82. Hakomori, S. 2002. Glycosylation defining cancer malignancy: New wine in an old bottle. Proceedings of the National Academy of Sciences of the United States of America 99:10231-10233.

83. Fuchs, B. C., and B. P. Bode. 2005. Amino acid transporters ASCT2 and LAT1 in cancer: Partners in crime? Semin Cancer Biol 15:254-266.

84. Inoue, T., K. Tomiyoshi, T. Higuichi, K. Ahmed, M. Sarwar, K. Aoyagi, S. Amano, S. Alyafei, H. Zhang, and K. Endo. 1998. Biodistribution studies on L-3-[fluorine-18]fluoro-alpha-methyl tyrosine: a potential tumor-detecting agent. J Nucl Med 39:663-667.

85. Forsback, S., O. Eskola, J. Bergman, M. Haaparanta, and O. Solin. 2009. Alternative solvents for electrophilic synthesis of 6-[18F]fluoro-L-DOPA. Journal of Labelled Compounds and Radiopharmaceuticals 52:286-288.

86. Zuhayra, M., A. Alfteimi, C. V. Forstner, U. Lutzen, B. Meller, and E. Henze. 2009. New approach for the synthesis of [18F]fluoroethyltyrosine for cancer imaging: simple, fast, and high yielding automated synthesis. Bioorganic & medicinal chemistry 17:7441-7448.

87. Vallabhajosula, S., and Ebooks Corporation Limited. 2009. Molecular Imaging Radiopharmaceuticals for PET and SPECT. Springer, Dordrecht. 1 online resource (386 p.).

88. Hung, J. C. 2002. Comparison of various requirements of the quality assurance procedures for F-18-FDG injection. J Nucl Med 43:1495-1506.

89. Love, C., M. B. Tomas, G. G. Tronco, and C. J. Palestro. 2005. FDG PET of infection and inflammation. Radiographics : a review publication of the Radiological Society of North America, Inc 25:1357-1368.

90. Belohlavek, O., J. Votrubova, M. Spacek, and P. Sebesta. 2007. The role of FDG-PET/CT in the diagnosis of low-grade infection of vascular prosthesis. European journal of nuclear medicine and molecular imaging 34:S155-S155.

91. Adler, L. P., and S. L. Hodder. 1995. Fdg Pet for Imaging Patients with Infection and Fever of Undetermined Origin. Radiology 197:183-183.

92. Chen, W., T. Cloughesy, N. Kamdar, N. Satyamurthy, M. Bergsneider, L. Liau, P. Mischel, J. Czernin, M. E. Phelps, and D. H. Silverman. 2005. Imaging proliferation in brain tumors with 18F-FLT PET: comparison with 18F-FDG. J Nucl Med 46:945-952.

93. Goldman, S., P. Violon, O. Dewitte, M. Levivier, B. Pirotte, P. Damhaut, D. Wikler, E. Stanus, and J. Hildebrand. 1996. PET-FDG in glioma: Relationship to local histology and prognostic value in low grade tumor and early after surgery. J Nucl Med 37:74-74.

94. Seiz, M., A. Dimitrakopoulou-Strauss, J. Tuttenberg, L. G. Strauss, G. A. Schubert, W. Eisenhut, and C. Weinmann. 2008. Bombesin and FDG-PET in patients with low grade glioma: Differentiation between malignant transformation and tumour recurrence. Onkologie 31:114-114.

95. Alauddin, M. M. 2012. Positron emission tomography (PET) imaging with (18)F-based radiotracers. American journal of nuclear medicine and molecular imaging 2:55-76.

96. Holland, J. P., P. Cumming, and N. Vasdev. 2013. PET radiopharmaceuticals for probing enzymes in the brain. American journal of nuclear medicine and molecular imaging 3:194-216.

97. Dunphy, M. P., and J. S. Lewis. 2009. Radiopharmaceuticals in preclinical and clinical development for monitoring of therapy with PET. J Nucl Med 50 Suppl 1:106S-121S.

98. Elsinga, P. H., and R. A. Dierckx. 2013. Small Molecule PET-Radiopharmaceuticals. Current pharmaceutical design.

99. Pascali, G., P. Watts, and P. A. Salvadori. 2013. Microfluidics in radiopharmaceutical chemistry. Nuclear medicine and biology 40:776-787.

100. Gulyas, B., and C. Halldin. 2012. New PET radiopharmaceuticals beyond FDG for brain tumor imaging. Q J Nucl Med Mol Im 56:173-190.

101. Boschi, S., F. Lodi, C. Malizia, G. Cicoria, and M. Marengo. 2013. Automation synthesis modules review. Applied radiation and isotopes : including data, instrumentation and methods for use in agriculture, industry and medicine 76:38-45.

VITA

I Hong Shih was born in Taipei, Taiwan on September 28, 1980, the son of Lin-Lin Hong and Shin-Lin Shih. After completing his work in Taipei Private Yanping High School in 1998, he entered National Tsing Hua University in Hsinchu, Taiwan. He received the degree of Bachelor of Science in engineering and system science in June, 2003. Then, he entered Nationa Chiao Tung University in Hsinchu, Taiwan, and received the degree of Master of Science in mechanical engineering in June, 2005. After that, he served in the army as a mandatory military corporal of management until February, 2007. After completing the military service, he worked in National Health Institute for the research of functional MRI until April, 2008. In September of 2008, he entered The University of Texas Graduate School of Biomedical Sciences at Houston.

Permanent address:

6F, No.2, Lane 3, Tai-an Street, Taipei, Taiwan